MHD GENERATOR DUCT FLOW WITH CROSS STREAM DEPENDENT FLUID PROPERTIES

By

THOMAS ALBERT TROVILLION

A DISSERTATION PRESENTED TO THE GRADUATE COUNCIL OF
THE UNIVERSITY OF FLORIDA
IN PARTIAL FULFILLMENT OF THE REQUIREMENTS FOR THE
DEGREE OF DOCTOR OF PHILOSOPHY

UNIVERSITY OF FLORIDA

1978

Engineering & Physics 10/1/79

Dedicated to my parents, Tom and Dorothy

ACKNOWLEDGMENTS

The author wishes to thank the chairman of his committee, Dr. U. H. Kurzweg, for the valuable assistance and advice in guiding this work to its completion. Also he would like to express his appreciation to Drs. R. E. Elkins and E. R. Lindgren for the many helpful discussions in formulating this problem and their role in starting the project out of which this problem was taken. This work was funded by a grant from the U.S. Navy Office of Naval Research, Power Branch, under contract number N00014-76-C-0410.

TABLE OF CONTENTS

		Page
ACKNOWLEDGMENTS		iii
LIST OF FIGURES		vi
KEY TO SYMBOLS		ix
ABSTRACT		xii
CHAPTER		
I	INTRODUCTION	1
II	FORMULATION OF PROBLEM	11
	Governing Equations	11
	Boundary Conditions	17
III	APPROXIMATIONS TO THE FULL EQUATIONS	25
	Slug Flow Approximation	26
	Hartmann Flow Approximation	28
	Generator Voltage	33
	Efficiency of the Generator	36
	Inviscid Core Approximation	44
IV	FINITE DIFFERENCE SOLUTION	46
	PRADI Solution	46
	Generalized Nodal Spacing	52
	Reasons for the PRADI Method	58
	Selection of Nodal Spacing	60
	Iteration of the B_1 Boundary Condition	73
	Boundary Condition on the Finite Conductivity Electrode	78
	Initial Guess	80
	Convergence Criteria	82
V	NUMERICAL RESULTS	86
	Velocity Contours and Current Streamlines	87
	Variation with Load Factor	94
	Variation with Electrode Conductivity	101
	Insulating Channel Case	108
	Variation with Hartmann Number	109

TABLE OF CONTENTS--Continued

CHAPTER		Page
	Conductivity Variation in the Cross Section	114
	Partitioned Channel	124
	Efficiency of the Generator	136
	Average Velocity of the Fluid	145
	Conductivity Variation	150
	Viscosity Variation	154
VI	CONCLUSIONS	157
APPENDIX: COMPUTER PROGRAM		162
BIBLIOGRAPHY		188
BIOGRAPHICAL SKETCH		192

LIST OF FIGURES

Figure		Page
2-1	Coordinates for Magnetohydrodynamic Channel	12
2-2	Boundary Conditions for the Quadrant	18
3-1	Hartmann Boundary Layer Profile	34
3-2	Hartmann Efficiencies versus Load Factor	42
3-3	Hartmann Efficiences versus Hartmann Number	42
4-1	Quadrant Nodal Spacing	63
4-2	Finite Difference Profile Error	64
4-3	Variable Nodal Spacing within Quadrant	70
5-1	Velocity Contours M=20, K=0.95	88
5-2	Current Streamlines M=20, K=0.95	89
5-3	Velocity Contours M=20, K=0	95
5-4	Current Streamlines M=20, K=0	96
5-5	Velocity Contours M=20, K=0.82	97
5-6	Current Streamlines M=20, K=0.82	98
5-7	Velocity Contours M=20, K=1.0	99
5-8	Current Streamlines M=20, K=1.0	100
5-9	Velocity Contours M=20, K=0.95, K_w=0.5	102
5-10	Current Streamlines M=20, K=0.95, K_w=0.5	103
5-11	Velocity Contours M=20, K=0.95, K_w=0.75	104
5-12	Current Streamlines M=20, K=0.95, K_w=0.75	105

LIST OF FIGURES--Continued

Figure		Page
5-13	Velocity Contours M=20, K=0.95, K_w=1.0	106
5-14	Current Streamlines M=20, K=0.95, K_w=1.0	107
5-15	Velocity Contours in Insulated Channel M=20	110
5-16	Current Streamlines in Insulated Channel M=20	111
5-17	Velocity Contours M=100, K=0.95	112
5-18	Current Streamlines M=100, K=0.95	113
5-19	Velocity Contours in Full Insulated Channel M=100	115
5-20	Current Streamlines in Full Insulated Channel M=100	116
5-21	Velocity Contours with Conductivity Variation σ_c/σ_0=0.25	119
5-22	Current Streamlines with Conductivity Variation σ_c/σ_0=0.25	120
5-23	Velocity Contours with Conductivity Variation σ_c/σ_0=0.05	122
5-24	Current Streamlines with Conductivity Variation σ_c/σ_0=0.05	123
5-25	Partitioning of the Channel	126
5-26	Velocity Contours Full Channel M=100, K=0.91	131
5-27	Current Streamlines Full Channel M=100, K=0.91	132
5-28	Velocity Contours Partitioned Channel M=100, K=0.91	133
5-29	Current Streamlines Partitioned Channel M=100, K=0.91	134
5-30	Efficiency versus Load Factor for Various Aspect Ratios M=20	137

LIST OF FIGURES--Continued

Figure		Page
5-31	Efficiency versus Load Factor for Various Aspect Ratios M=50	138
5-32	Efficiency versus Aspect Ratio for Various Hartmann numbers	140
5-33	Efficiency versus Electrode Resistivity	143
5-34	Flow Rate versus Aspect Ratio	147
5-35	Flow Rate and Efficiency for Conductivity Variation	151
5-36	Maximum Velocity for Conductivity Variation	153
5-37	Efficiency for Viscosity Variation	155

KEY TO SYMBOLS

a	half-height of the channel, meters
b	half-width of the channel between electrodes, meters
B	magnetic flux density, magnetic induction nondimensional
B_0	applied magnetic flux density, Teslas
B_z	magnetic induction, Teslas
B_1	magnetic flux density at the insulating wall
B^*	intermediate value of the induction finite difference equation
E	electric field, volts per meter
E_Y^W	electric field in Y direction in the electrode wall, volts per meter
F	fluid conductivity ratio
G	fluid viscosity ratio
h	spacing between nodes of the finite difference grid
I_E	current flowing in the electrode, amps
I_0	net current output of the generator, amps
J_X	current density in the X direction, amps per meter^2
J_Y	current density in the Y direction, amps per meter^2
J_Y^E	current density in the Y direction in the electrode, amps per meter^2
J_η	nondimensional current density in the η direction
J_ξ	nondimensional current density in the ξ direction
k	increment in time relaxation step
K	load factor

K_w electrode resistance factor $W_R/(W_R + 1)$

L^V_η, L^V_ξ, L^B_η, L^B_ξ } linear operators defined by equations (4-6)

M Hartmann number

m number of nodes in the X direction

n number of nodes in the Y direction

n_1 number of partition divisions in the X direction

n_2 number of partition divisions in the Y direction

P pressure, newtons per meter^2

P_E electrical power out of the channel, watts

P_F power of fluid pressure work, watts

R relative resistance ratio

R_L load resistance, ohms

t thickness of the electrode, meters

V nondimensional velocity

V_z velocity in the downstream direction, meters per second

V* intermediate value in the finite difference momentum equation

$\overline{V}$ average velocity

W_R electrode resistance ratio

X coordinate between the electrodes

Y coordinate parallel to the applied field

Z coordinate in the downstream direction

Z_0 half the length of the channel, meters

α void fraction

α_c conductivity profile parameter

α_v viscosity profile parameter

γ aspect ratio

ε convergence parameter

η nondimensional coordinate parallel to the applied field

η_e electrical generation efficiency

η_o ratio of ohmic losses to the input pressure work

η_v ratio of viscous losses to the input pressure work

μ_e magnetic permeability

μ_o reference viscosity, newton seconds per meter^2

μ_ℓ liquid viscosity, newton seconds per meter^2

μ_g gas viscosity, newton seconds per meter^2

ξ nondimensional coordinate between the electrodes

σ_o reference conductivity, mhos per meter

σ_w conductivity of the liquid phase, mhos per meter

σ_ℓ conductivity of the liquid phase, mhos per meter

ϕ nondimensional voltage potential

Φ voltage potential, volts

χ mixture quality

ω boundary condition relaxation parameter

Abstract of Dissertation Presented to the Graduate Council of the University of Florida in Partial Fulfillment of the Requirements for the Degree of Doctor of Philosophy

MHD GENERATOR DUCT FLOW WITH CROSS STREAM DEPENDENT FLUID PROPERTIES

By

Thomas Albert Trovillion

June 1978

Chairman: Ulrich H. Kurzweg
Major Department: Engineering Sciences

The problem of steady laminar flow of an incompressible viscous conducting fluid in a rectangular duct is considered with finite aspect ratio of the cross section. An external magnetic field is applied transverse to the flow in a Faraday generator configuration. Such flows are capable of producing electrical energy from the mechanical energy of the flow at high power densities without the use of rotating parts. To model the use of a two-phase mixture of gas and liquid metal, which is employed as the working fluid in these devices, the conductivity and viscosity of a homogeneous fluid are allowed to vary in continuous fashion over the cross section of the channel. The governing equations for this problem are derived from the usual magnetohydrodynamic assumptions yielding two simultaneous equations in terms of the velocity and induced magnetic field. A finite difference approach is taken to the solution of these equations using a modification of the Peaceman Rachford alternating direction implicit relaxation scheme. The boundary conditions

appropriate to the MHD generator case with electrodes of arbitrary conductivity are applied and solutions are obtained for values of the Hartmann number between zero and 100. The solutions are then used to determine where it is sufficient to approximate the finite aspect ratio case with the closed form solution of the one-dimensional Hartmann flow problem. The finite difference solution is employed to obtain plots of the current streamlines and velocity contours, the volume flow rate through the channel, and the efficiency of the generator. These results are then examined to determine the effect on the flow characteristics produced by changes in load resistance, electrode conductivity, aspect ratio, and the assumed profile of conductivity and viscosity variation.

CHAPTER I
INTRODUCTION

The generation of electrical power directly from a moving fluid by various magnetohydrodynamic (MHD) schemes has been recognized for many years to have some advantages over conventional power generation. Chief among these is the simplicity of a device that contains no moving parts. In the basic MHD generator configuration a conducting fluid moves down a channel under the influence of a pressure gradient while a magnetic field is applied perpendicular to the flow. The electric current is tapped off perpendicular to both the flow and the magnetic field by electrodes in contact with the fluid. This configuration is referred to as a Faraday generator in recognition of Faraday (1832) who first alluded to possible MHD generator schemes.

In addition to its simplicity, an approximate theoretical analysis (Jackson 1963) indicates that these devices are capable of very high efficiencies of 85 to 95 percent. Although this efficiency is reduced somewhat in a practical device, since losses due to electrical end effects (Sutton et al. 1962), electrode contacts (Tanatugu et al. 1971), fluid drag, and required power for the magnetic field were neglected, the efficiency can still be high when these losses are compensated for in a well-designed device. The other major advantage of these MHD generators is their very high power density, on the order of 10 megawatts per cubic meter. This indicates the possibility of a

small and light device, which can be very important in some applications such as naval and space systems (Petrick and Roberts 1967).

However, these devices are not without their disadvantages. Of the two possible fluids commonly used, plasmas and liquid metals, the former suffers the disadvantage of having low conductivity at the temperature limit imposed by the current materials technology. To improve the conductivity at these temperatures generally requires the added complexity of seeding the plasma with cesium to obtain sufficient current, although the voltages obtained from the fast-moving plasmas are sufficiently high. The alternative strategy of using liquid metals as the working fluid eliminates the problem of low conductivity, but for reasonable pressure drops the liquid moves so slowly that the voltage output of the device is correspondingly low. This creates the problem of having a large power output in the form of very large currents and low voltages typical of homopolar generators. To make effective use of these devices as generators the above problems have to be overcome.

With the preceding advantages and disadvantages in mind, considerable theoretical work has gone into analyzing what goes on within the fluid of the generator. These analytical studies apply not only to the generator case but also have application to other related devices. Among these are MHD pumps for transporting radioactive and corrosive liquid metals, flowmeters for use when the fluid is conducting, and pump generator combinations for voltage transformation schemes.

The problem receiving the most attention and to be further extended here is that of fully developed laminar flow of an incompressible viscous conducting fluid down a channel of rectangular cross section with a magnetic field applied perpendicular to the flow direction. The end effects are assumed negligible and the pressure drop constant, so that all the variables depend only on the cross sectional dimensions of the channel. These assumptions make the equations manageable mathematically, as well as being an effective approximation to the real situation, while giving insight into the workings of these devices.

The first significant analysis of this problem is that of Hartmann (1937) who reduces it to an ordinary differential equation in only the one dimension parallel to the applied magnetic field by neglecting the effect of the boundary layer formed on the electrode walls. Although this assumption is strictly true only in the case of a rectangular channel with infinite cross sectional aspect ratio, the experiments performed by Hartmann and Lazarus (1937) indicate the solutions for the flow rate and pressure drop down the channel are good approximations, even when the aspect ratio is approaching one if the applied magnetic field is sufficiently strong. These experiments, done under conditions where ordinary flow would be turbulent, show that increasing the magnetic field tends to damp out the turbulence of the flow, which lends weight to the assumption of laminar flow in the stated problem. The damping of turbulence by a magnetic field is further quantified in the work by Murgatroyd (1953), Branover et al. (1976a, 1977), and Hua and Lykoudis (1974).

Hartmann (1937) finds in his solution that the significant nondimensional parameter associated with the flow is the quanity M defined as

$$M = aB_0 \sqrt{\frac{\sigma_0}{\mu_0}} \tag{1-1}$$

where B_0 is the applied magnetic flux density in Teslas, a is an appropriate length scale usually taken to be the half height of the channel in the direction of the applied field, σ_0 is the conductivity of the fluid in mhos per meter, and μ_0 is the viscosity of the fluid in Newton seconds per meter squared. This nondimensional quantity is the Hartmann number and represents the ratio of the magnetic to viscous forces. Hartmann finds that the velocity profile scales on this parameter, with the thickness of the boundary layer along the insulating walls going as a/M. As the value of M becomes large the velocity profile flattens out in the center of the channel and eventually approaches a uniform slug flow across the entire width of the channel. Also the magnitude of the average velocity for a given pressure gradient decreases rapidly as the Hartmann number increases.

Although the Hartmann solution gives good approximations in most situations, in the case of low aspect ratio channels and low Hartmann number the two-dimensional solution is required for accuracy. The first solution of the two-dimensional case is that of Shercliff (1953). Since his interest is in the application of the equations to flow meters where no appreciable current is tapped off, but only the electrical potential is measured, he solves the problem for the case

where the channel has insulating walls on all sides. Shercliff derives the two simultaneous equations describing the flow in terms of the velocity and the induced magnetic field and then converts these to two independent equations by transforming into two variables representing the sum and difference of the previous variables. The solution is then given as an infinite Fourier cosine series.

Using this solution Shercliff is able to show that it approaches the Hartmann case at large values of M. He also describes the flow as having a central core region where the profile is flat and the viscosity does not play a part, and a boundary layer region on each wall. He is able to confirm the a/M thickness of the boundary layer on the wall perpendicular to the applied field and also determines the thickness on the wall parallel to the field to be of order $a/\sqrt{M}$. Shercliff also obtains an approximate solution based on a boundary layer approach that is simpler mathematically and can be generalized to channels of arbitrary cross section. Comparing these results to the experiments of Hartmann and Lazarus (1937) he finds good agreement for the exact theory and the boundary layer approximation if the Hartmann number is greater than 18 times the aspect ratio squared. In a later paper (Shercliff 1956) he solves the problem of flow in a circular channel with conducting walls and finds the boundary layer thickness to be inversely proportional to the normal component of the magnetic field when the Hartmann number is sufficiently high.

The case of flow in a rectangular duct with walls that are perfectly conducting represents the opposite extreme to the case

solved by Shercliff. This problem is solved exactly by Chang and Lundgren (1961) and independently in Russia by Uflyand (1961). Neither paper gives an exact solution for walls of arbitrary conductivity, but Chang and Lundgren do give a solution for finite wall conductivity when the aspect ratio is infinite, which is a generalization of the one-dimensional Hartmann problem. They are able to show that for a given pressure drop the average velocity is inversely proportional to M with nonconducting walls and inversely proportional to M squared for perfectly conducting walls. Thus they show that increasing the wall conductivity will decrease the average velocity if the pressure gradient remains the same.

A paper by Hunt (1965) completes the list of exact solutions for the rectangular duct problem by solving two cases with mixed boundary conditions. The first case has perfectly conducting walls perpendicular to the field and thin walls of arbitrary conductivity parallel to the field. The second has nonconducting walls parallel to the field and thin walls of arbitrary conductivity perpendicular to the field. All of the exact solutions to these various problems are in the form of infinite Fourier series with rather complicated expressions for the coefficients that make them somewhat difficult to analyze and evaluate. Also, except for the solutions by Hunt, the rate of convergence of the series tends to decrease as the Hartmann number increases, making it necessary to develop approximations to the expansions at high values of M. Of more importance is the failure so far to come up with an exact solution to the physical

situation found in the magnetohydrodynamic generator, where the rectangular duct has conducting walls parallel to the magnetic field and insulating walls perpendicular to the field.

Chiang and Lundgren (1967) give an approximate solution to this problem at large values of the Hartmann number. Their approach is to use boundary layer methods which are valid at large M and cast the problem in the form of an integral equation. They are then able to solve for the current streamlines near the perfectly conducting electrode wall, but at the same time showing a boundary layer on the insulating wall that is infinitely thin. Another approach taken by Wissmiller (1964) solves the full equations by breaking them up into their finite differences. He then solves these on the computer using a successive overrelaxation technique. He achieves limited results, obtaining only the velocity profile and the current streamlines for values of the Hartmann number less than five because of the particular relaxation scheme chosen.

All of these solutions analyze the cases where the fluid is assumed to be homogeneous in its properties of conductivity and viscosity over the cross section of the channel. In a practical device this may not be true either by accident or by design. To effectively use a magnetohydrodynamic generator as part of a heat engine it has to be incorporated in a thermodynamic cycle (Petrick 1965). To do this usually involves adding a compressable gas to the conducting liquid to form a two-phase mixture. This mixture is then either accelerated through a nozzle imparting kinetic energy to the liquid

which is then separated before entering the MHD channel (Elliott 1962; Prem and Parkins 1964), or the mixture itself is used as the conducting fluid in the generator and the gas is separated downstream of the channel (Petrick and Lee 1964a). The gas phase goes through either a Brayton or Rankine cycle with the MHD generator performing the function of the turbine in the cycle, with the added advantages that the energy is converted directly to electrical energy and because of the high heat capacity of the liquid phase the gas expands isothermally.

It is the use of the two-phase mixture in the generator channel that causes a modification of the MHD problem stated previously, since the gas phase acts to reduce the conductivity of the mixture as a whole. Also any nonuniform distribution of the gas bubbles causes an effective conductivity gradient within the cross section of the channel as well as some variation in the effective viscosity. This problem occurs to some extent even if the phases are separated before entering the generator, since the separation process cannot be completely effective and some small quantity of gas inevitably is present in the generator channel.

The development of a two-phase liquid metal MHD generator is necessary to obtain a practical working system. Therefore, considerable experimental work is being done in several countries throughout the world. The Argonne National Laboratory has a blowdown facility operating on a mixture of sodium and potassium (NaK), with nitrogen as the gas (Hantman et al. 1975). This apparatus is giving experimental

data on the velocities and pressures as well as measurements of the distribution of the gas voids at various locations in the channel (Petrick et al. 1977). There are also plans for a system using tin and water in a Rankine cycle. In Japan an experimental apparatus is in operation with a NaK-N_2 mixture in a generator using an induction scheme rather than the Faraday approach (Tanatugu et al. 1973). In Israel, Branover and Gershon (1976a) are doing experiments with a gravity-fed system using a mixture of mercury and nitrogen.

This dissertation attempts to extend the theoretical work done on the MHD channel flow to include assumed variations in the conductivity and viscosity of the liquid. In this way the two-phase mixture is modeled in an average sense as a liquid with variable properties, such that the conductivity and viscosity at a point in the mixture is dependent on the void fraction at that point.

The addition of this aspect of the problem is such that the equations do not lend themselves to solution in the form of infinite series. For this reason the equations are solved by the finite difference method. Since the successive overrelaxation scheme of Wissmiller (1964) is limited to low Hartmann numbers, a scheme referred to as the Peaceman-Rachford alternating direction implicit method (Peaceman and Rachford 1955) is modified to solve the MHD equations. This scheme has superior stability and rate of convergence than that of Wissmiller. This allows solution of the equations quickly up to Hartmann numbers of 100. The finite difference solution

also has the advantage that all the generator parameters can be easily evaluated from it without significant loss in accuracy, whereas the series solutions are often difficult to evaluate and require a different series for each parameter. In addition, the boundary conditions appropriate to the generator case with arbitrary conductivity electrodes can be easily applied while the series solution does not exist for this case.

CHAPTER II
FORMULATION OF PROBLEM

In this section the problem of steady laminar flow of an electrically conducting fluid in a duct of rectangular cross section is formulated. A magnetic field is applied perpendicular to the flow down the channel and an electric field is generated and current removed perpendicular to these two directions. The setup and orientation is as shown in Figure 2-1. In the following derivation the approximation is made that none of the parameters or variables change in the flow direction so that the problem is reduced to essentially a two-dimensional one depending only on the cross section coordinates. This approximation is consistent with previous work done on the related problems and is found to be an effective approximation (Shercliff 1953).

Governing Equations

The magnetohydrodynamic equations for channel flow are derived by first taking Maxwell's equation for the curl of the magnetic field and writing it in two dimensions.

$$J_X = \frac{1}{\mu_e} \frac{\partial B_Z}{\partial Y}$$

$$J_Y = \frac{-1}{\mu_e} \frac{\partial B_Z}{\partial X} \qquad (2\text{-}1)$$

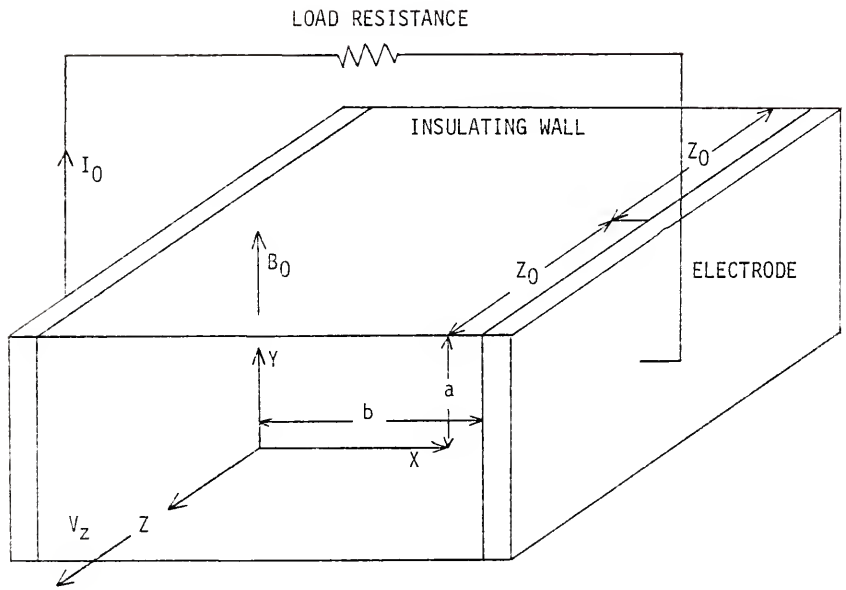

Figure 2-1. Coordinates for Magnetohydrodynamic Channel

From this it can be seen that the magnetic induction in the z direction can be used as a stream function for the current in the plane of the cross section. This is then combined with Ohm's law for current flowing in a moving liquid which is given in two dimensions by

$$J_X = \sigma \left[- \frac{\partial \Phi}{\partial X} - V_Z B_0 \right]$$

$$J_Y = \sigma \left[- \frac{\partial \Phi}{\partial Y} \right] \qquad (2\text{-}2)$$

Combining these two sets of equations gives

$$\frac{1}{\mu_e} \frac{\partial B_Z}{\partial Y} = \sigma \left[- \frac{\partial \Phi}{\partial X} - V_Z B_0 \right]$$

$$\frac{1}{\mu_e} \frac{\partial B_Z}{\partial X} = \sigma \left[- \frac{\partial \Phi}{\partial Y} \right] \qquad (2\text{-}3)$$

whose derivatives in each of the two directions are combined to give the equation for the magnetic induction.

$$\frac{\partial}{\partial X} \left(\frac{1}{\sigma \mu_e} \frac{\partial B_Z}{\partial X} \right) + \frac{\partial}{\partial Y} \left(\frac{1}{\sigma \mu_e} \frac{\partial B_Z}{\partial Y} \right) + B_0 \frac{\partial V_Z}{\partial Y} = 0 \qquad (2\text{-}4)$$

Here the assumption is not made that the conductivity is constant since it will be used to model the two-phase nature of the fluid.

The equation for the velocity is obtained from the momentum equation in the direction of the fluid motion with the force due to the current perpendicular to the magnetic field added.

$$\frac{dP}{dZ} = \frac{\partial}{\partial X} \left(\mu \frac{\partial V_Z}{\partial X} \right) + \frac{\partial}{\partial Y} \left(\mu \frac{\partial V_Z}{\partial Y} \right) + J_X B_0 \qquad (2\text{-}5)$$

Here also the viscosity is not assumed constant since it is likely variable in a two-phase system. The inertia terms of the equation are left out due to the assumption of steady laminar flow in the channel with no downstream acceleration. The equation for the current from Maxwell's equation is then substituted to give

$$\frac{\partial}{\partial X}\left(\mu \frac{\partial V_z}{\partial X}\right) + \frac{\partial}{\partial Y}\left(\mu \frac{\partial V_z}{\partial Y}\right) + B_0 \frac{1}{\mu_e} \frac{\partial B_z}{\partial Y} = \frac{dP}{dZ} \tag{2-6}$$

This equation and that for the magnetic induction represent the two magnetohydrodynamic equations that are to be solved simultanously.

The equations (2-4) and (2-6) are treated more easily if they are put into a nondimensional form. This is accomplished by introducing the following nondimensional terms commonly used in the literature

$$\xi = X/a \qquad \eta = Y/a \qquad M = aB_0\sqrt{\sigma_0/\mu_0}$$

$$V = \frac{\mu_0 V_z}{a^2(-dP/dZ)}$$

$$B = \frac{B_z}{\mu_e a^2(-dP/dZ)}\sqrt{\frac{\mu_0}{\sigma_0}}$$

$$F(\xi,\eta) = \frac{\sigma_0}{\sigma} \qquad G(\xi,\eta) = \frac{\mu}{\mu_0} \tag{2-7}$$

The magnetohydrodynamic equations then assume the form

$$F\left[\frac{\partial^2 B}{\partial \xi^2} + \frac{\partial^2 B}{\partial \eta^2}\right] + \left[\frac{\partial F}{\partial \xi}\frac{\partial B}{\partial \xi} + \frac{\partial F}{\partial \eta}\frac{\partial B}{\partial \eta}\right] + M\frac{\partial V}{\partial \eta} = 0 \quad \text{induction}$$

$$G\left[\frac{\partial^2 V}{\partial \xi^2} + \frac{\partial^2 V}{\partial \eta^2}\right] + \left[\frac{\partial G}{\partial \xi}\frac{\partial V}{\partial \xi} + \frac{\partial G}{\partial \eta}\frac{\partial V}{\partial \eta}\right] + M\frac{\partial B}{\partial \eta} = -1 \quad \text{momentum} \tag{2-8}$$

The nondimensionalization is such that the velocity is being compared to the parameters found in normal Poiseuille flow with the entire solution being scaled on the applied pressure gradient. This form of the equations also shows the importance of the Hartmann number in determining the character of the solution. With the Hartmann number set equal to zero and using a one-dimensional approximation to the channel it can be seen that the momentum equation immediately reduces to the ordinary Poiseuille flow equation.

Although the momentum and induction equations (2-8) are derived here from considerations of a continuous fluid with variable properties, they can also be justified by starting with the equations for the two phases and taking averages at points in the flow with respect to time. This is done by Elkins et al. (1978) and results in flow equation (2-8) in the limit of zero turbulence. In this case the equations have variable fluid properties specified in terms of the fluid properties of the liquid phase and the void fraction of the mixture, which is defined as the time average at a point of the ratio of the volume of gas to the total volume of the mixture.

The relationship between the conductivity and the void fraction is analyzed theoretically by Maxwell (1904), but it is necessary to make the assumption of low void fractions. Of more importance are several empirical studies of the conductivity versus void fraction done by Tanatugu et al. (1972), Petrick and Lee (1964b), and Lafferty and Hammitt (1967). Petrick and Lee fit their data with the empirical equation.

$$\sigma/\sigma_\ell = \exp(-3.8\alpha)$$

But since these data are taken in whole channels with the void fraction being the total average regardless of the profile, the accuracy for the present purposes is not great. Therefore this relation can be taken as an indication of the proper effect and the simpler straight line relation of Lafferty and Hammitt,

$$\sigma/\sigma_\ell = 1 - \alpha \tag{2-9}$$

can be used without much loss of accuracy.

The relation between void fraction and viscosity has been analyzed theoretically by Einstein (1906) and Taylor (1932), but again the assumption is made that the void fraction is low and the bubbles are spherical. The empirical work done is with respect to determining a homogeneous friction factor for flow of two-phase fluids in terms of a "virtual viscosity" (Wallis 1969). This gives relations such as the following by McAdams et al. (1942), where the viscosity is given in terms of the viscosity of the two fluids and the quality (χ) of the mixture, which is defined as the time average at a point of the ratio of the mass flow rate of the gas to the total mass flow rate of the mixture.

$$\frac{u}{\mu_\ell} = \left[\chi \frac{\mu_e}{\mu_g} + (1 - \alpha)\right]^{-1}$$

Here again, the accuracy is not considered very good for the present purposes.

The nondimensional terms F and G in Equations (2-8) represent the variations of conductivity and viscosity, respectively. Although, using the above relations, they could be specified in terms of the void fraction or quality of the mixture, for the present analysis the variations of each are to be considered separately, so that no advantage is achieved in doing this. Therefore, the functions are specified arbitrarily, as long as they are symmetric about the mid-channel lines, and the value of the functions along with their derivatives in the two directions are assumed to be known inputs to the problem. The solutions are then examined to see how they are affected by a given conductivity or viscosity variation.

Boundary Conditions

The two simultaneous governing equations (2-8) are of second order in each of the two directions and therefore require two boundary conditions for each of the two variables of velocity and magnetic flux density. Because of the basic symmetry of the problem, assuming symmetric functions for F and G, the solution does not have to be found for the entire channel but can be limited to only one quadrant of the channel cross section. This is helpful in reducing the amount of calculations that have to be performed. Thus the boundary conditions are derived for the upper right-hand quadrant with the origin of the coordinate axis at the center of the channel as shown in Figure (2-2).

The boundary conditions on the velocity are the usual ones for viscous flow, that the velocity is zero at the walls. The

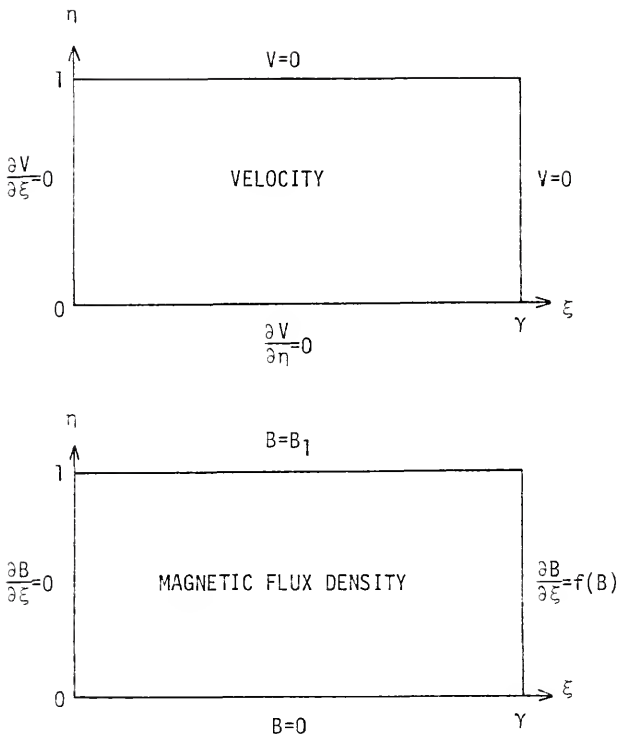

Figure 2-2. Boundary Conditions for the Quadrant

symmetry conditions are then used to obtain the conditions for the quarter channel case, that the normal derivatives at the mid-channel lines are zero.

The boundary conditions for the magnetic flux density are derived from consideration of the current flow using Maxwell's law (2-1). Since the main current flow is between the electrodes in the ξ direction, the symmetry conditions dictate that there be no current in the η direction at the mid-channel lines. Therefore, on these lines the derivative with respect to ξ of the magnetic flux density is equal to zero. On the mid-channel line, η=0, this implies that the magnetic induction is constant. Since the magnetic induction serves as a potential function only and can therefore be adjusted by an arbitrary constant without effect, its value along the η=0 line will be chosen as zero.

At the electrode wall the boundary condition should take into account the conductivity of the electrode wall. This can be done easily if the assumption is made that the electrode is thin compared to its length so that Maxwell's equations don't have to be solved, but the current in the wall can be given as

$$I_E(Y) = J_Y^E(Y)\ 2Z_0 t \tag{2-10}$$

which can then be related to the electric field by Ohm's law (2-2).

$$I_E(Y) = \sigma_w E_Y^w(Y)\ 2Z_0 t \tag{2-11}$$

But the current in the electrode also has to equal the integral of the current in the ξ direction flowing into the electrode. This can be related to the value of the magnetic induction along the boundary by

$$I_E(Y) = 2Z_0 \frac{1}{\mu_e} \int_a^Y \frac{\partial B_z}{\partial Y} dY = \frac{2Z_0}{\mu_e} (B_z(Y) - B_1) \tag{2-12}$$

Equating these two values for the current in the electrode gives the following relation between the electric field in the Y direction and the value of the magnetic induction.

$$E_Y^W(Y) = \frac{1}{\mu_e \sigma_w t} (B_z(Y) - B_1) \tag{2-13}$$

This must also be the value of the electric field in the fluid just at the electrode which can then be related to the Y component of the current through Ohm's law (2-2) since the velocity is zero at the wall. Therefore,

$$J_Y(Y) = \frac{1}{\mu_e} \frac{\partial B_z}{\partial X} = \sigma E_Y^W(Y) \tag{2-14}$$

After nondimensionalizing and defining the conductivity ratio

$$W_R = \frac{\sigma_0 a}{\sigma_w t} \tag{2-15}$$

The relation between the derivative of the magnetic induction in the ξ direction and its value at the point becomes

$$\frac{\partial B}{\partial \xi} = \frac{W_R}{F} (B_1 - B(\eta)) \tag{2-16}$$

It can be seen that in the case of perfectly conducting electrodes the value of the conductivity ratio becomes zero and the boundary condition reduces to the normal derivative being equal to zero.

On the insulated wall at $\eta=1$, the magnetic induction is constant as can be determined from the fact that no current flows in the η direction into the wall. This constant can easily be related to the net current flow out of the channel. Since the total current in the channel must be conserved, this can be found by integrating the ξ component of the current density along any vertical line between the two insulating walls to give

$$I_0 = 4Z_0 \int_0^a J_X dY \tag{2-17}$$

or using the relation between the current density and the B field

$$I_0 = 4Z_0 \frac{1}{\mu_e} B_1 \tag{2-18}$$

The net current out of the channel can be used as a parameter of the problem and by setting it positive or negative the channel can be analyzed as either a pump or generator. But, for the purposes of analyzing the generator configuration it is more useful and common in the literature to relate the net current to the load resistance in the external circuit and to use this as the fundamental parameter in terms of a load factor applied to the generator.

To accomplish this it is necessary to calculate the voltage at the point where the current is tapped off the electrode. This is

done by integrating the electric field along the insulating wall and down the electrode to where the current is tapped off at the center of the electrode. This facilitates the calculation because along the wall the velocity of the fluid is zero and therefore the electric field can be directly related to the current density by Ohm's law (2-2). The total potential drop for the whole channel is then twice the calculated value due to symmetry, and given by

$$\Delta\Phi = -2\left[\int_0^b \frac{J_X}{\sigma}\bigg|_{Y=a} dX + \int_a^0 \frac{J_Y}{\sigma}\bigg|_{X=b} dY\right] \tag{2-19}$$

Using the relation between the current density and the magnetic induction (2-1), and the equation (2-16) for the boundary condition on the electrode, the relation between the voltage potential and the magnetic induction is found to be

$$\Delta\Phi = \frac{-2}{\mu_e}\left[\frac{1}{\sigma_w t}\int_0^a (B_1 - B_z(Y))dY - \int_0^b \frac{1}{\sigma}\frac{\partial B_z}{\partial Y}\, dX\right] \tag{2-20}$$

It is then a simple matter to relate this to the total current leaving the channel once the total resistance of the external circuit is known, by

$$I_0 = \frac{\Delta\Phi}{R_L} \tag{2-21}$$

Equating this to the total current found previously gives

$$4Z_0 B_1 = \frac{-2a}{R_L \sigma_w t} B_1 + \frac{2}{R_L t \sigma_w}\int_0^a B_z(Y)dY - \frac{2}{R_L}\int_0^b \frac{1}{\sigma}\frac{\partial B_z}{\partial Y}\, dX \tag{2-22}$$

Nondimensionalizing and defining the following resistance ratio simplifies the expression to

$$R = \frac{2R_L Z_0 a \sigma_0}{b} \qquad \gamma = b/a$$

$$B_1 = \left[\frac{1}{\gamma R + W_R}\right]\left[W_R \int_0^1 B(\eta)\Big|_{\xi=\gamma} d\eta - \int_0^\gamma F \frac{\partial B}{\partial \eta}\Big|_{\eta=1} d\xi\right] \tag{2-23}$$

It is clear that this expression cannot be applied as a boundary condition since the integrals in it cannot be evaluated until the solution is known. Therefore, to use the load resistance ratio as a fundamental parameter of the solution this expression must be applied in an iterative fashion. In essence the total current, or B_1, is chosen and this expression is used to find what load conditions are solved for. Corrections to the initial guess can then be made using this expression. Fortunately some very good approximations are available on which to base the initial guess.

It can be seen that for the case of perfectly conducting electrodes the expression (2-23) reduces to the simpler calculation

$$B_1 = -\frac{1}{\gamma R}\int_0^\gamma F \frac{\partial B}{\partial \eta}\Big|_{\eta=1} d\xi \tag{2-24}$$

For the infinite aspect ratio one-dimensional approximation this reduces to the following which can be evaluated using the Hartmann solution if the conductivity does not vary.

$$B_1 = -\frac{F(\eta=1)}{R} \frac{\partial B}{\partial \eta}\Big|_{\eta=1} \tag{2-25}$$

It should be noted that for the case of infinite external resistance there is no net current flow out of the channel and the boundary condition is simply that the induced magnetic field is zero on the insulating wall.

CHAPTER III
APPROXIMATIONS TO THE FULL EQUATIONS

It has been mentioned that there is no analytic solution to the problem of magnetohydrodynamic flow for a Faraday generator configuration that takes into account the full two-dimensional nature of the problem. However, there are approximations to the full problem that can be solved analytically under the assumptions of either neglecting the viscosity, or the end effects at the electrodes, or making an approximation to the boundary layer and solving for the core flow. These approximations are extremely useful in providing analytic expressions that can be used to find approximate solutions and the location of optimum values, after which the two-dimensional numerical solution can be used to confirm the answer or refine it taking into account the full effects present. The approximate solutions can also be looked on as limiting cases for the full equations, or in some cases as the ideal values from which all other effects detract. In this respect they are useful as comparators in determining how well the generator is optimized by a given set of conditions. And lastly the analytic expression, as long as they are close approximations, are more helpful than the numerical solution in obtaining an intuitive feel for how the solutions will behave with the variation of certain parameters and in understanding the operation of the generator.

Slug Flow Approximation

The simplest approximation to the full equations in terms of the simplicity of the equations used is the slug flow. Here the viscosity of the fluid is neglected, and for our purposes the conductivity variation will also be ignored. The fluid then sustains no shear gradients and produces no boundary layers on any of the walls. This creates a uniform flow field where the velocity is constant throughout the cross section and the fluid moves down the channel as a uniform slug.

With the viscosity not present the momentum equation reduces to just the pressure drop term and the cross product of the current density and the applied magnetic induction.

$$\frac{dP}{dZ} = J_X B_0 \tag{3-1}$$

Nondimensionalizing as was done previously, the current density is determined directly and the magnetic induction is derived from this by the relation (2-1) to give

$$J_\xi = -\frac{1}{M} = \frac{\partial B}{\partial \eta}$$

$$B = -\eta/M \tag{3-2}$$

The velocity of the fluid can then be obtained simply from Ohm's law once the current density is known.

$$J_X = \sigma_0 \left[\frac{\partial \Phi}{\partial X} - V_Z B_0\right] \tag{3-3}$$

Nondimensionalizing the current density and the velocity as was done before and the voltage potential in the following manner this equation is put in the form

$$\phi = \frac{\Phi\sqrt{\mu_0\sigma_0}}{a^2(-dP/dZ)}$$

$$J_\xi = -\frac{\partial\phi}{\partial\xi} - MV \tag{3-4}$$

The voltage gradient is equal to the electric field and can be found by looking at the external electric circuit. The voltage drop between the two electrodes is given by the product of the load resistance and the net current out of the generator, where the net current is found by integrating the x component of the current density along a vertical line at any point in the channel. This gives

$$\Delta\Phi = I_0R_L = 4Z_0R_L\int_0^a J_x dY \tag{3-5}$$

From Ohm's law (3-4) the potential gradient is seen to be constant and so can also be related to the voltage drop between the electrodes. So that

$$\frac{\partial\Phi}{\partial X} = \frac{\Delta\Phi}{2b} \tag{3-6}$$

Combining these relations and nondimensionalizing give the value of the potential gradient to be

$$\frac{\partial\phi}{\partial\xi} = R\int_0^1 J_\xi d\eta = -\frac{R}{M} \tag{3-7}$$

Substituting this result into Ohm's law (3-4) with the constant value of the current density derived from the momentum equation yields the velocity relation

$$V = \frac{1 + R}{M^2} \tag{3-8}$$

It can be seen that this is a constant with respect to the cross section dimensions and so represents a slug flow. It should be noted that as R goes to infinity an insulated channel is approximated and the velocity becomes infinite. This arises because in this case no external current is allowed due to the infinite resistance, and no internal currents due to the assumptions that produce the slug flow. With no currents flowing there are no magnetic forces in the fluid and no viscous forces according to the assumptions made. Therefore there are no forces to react with the pressure force and the velocity becomes infinite.

Hartmann Flow Approximation

The slug flow equations are the simplest approximation that give insight into the workings of the generator, but at large values of the load resistance the approximation breaks down. A superior analytic solution was given by Hartmann (1937) at the expense of being slightly more complex in form. Hartmann takes into account the viscosity of the fluid but considers only the change of variables in the η direction with all terms remaining constant in the ξ direction between the electrodes. With the addition of viscosity the velocity and the

current density no longer remain constant throughout the cross section.

The Hartmann flow equations can be derived by removing the derivatives in the ξ direction and the conductivity and viscosity variation from the induction and momentum equations (2-8), yielding

$$\frac{\partial^2 B}{\partial \eta^2} + M\frac{\partial V}{\partial \eta} = 0 \qquad \text{induction equation}$$

$$\frac{\partial^2 V}{\partial \eta^2} + M\frac{\partial B}{\partial \eta} = -1 \qquad \text{momentum equation} \tag{3-9}$$

The partial derivatives are now total derivatives and the equations are one dimensional. The induction equation can be integrated to give the derivative of the magnetic induction in terms of the velocity and an arbitrary constant (E).

$$\frac{\partial B}{\partial \eta} + MV = E \tag{3-10}$$

This is then substituted into the momentum equation to give the ordinary differential equation for the velocity.

$$\frac{\partial^2 V}{\partial \eta^2} - M^2 V = -\left[1 + ME\right] \tag{3-11}$$

This is solved in terms of the hyperbolic sine and cosine functions with the two additional constants determined by the boundary conditions on the velocity at the wall and the center of the channel

$$V(\eta=1) = 0$$

$$\left.\frac{\partial V}{\partial \eta}\right|_{\eta=0} = 0 \tag{3-12}$$

yielding for the velocity

$$V = \frac{1}{M^2}\left[1 + ME\right]\left[1 - \frac{\text{Cosh } M\eta}{\text{Cosh } M}\right] \tag{3-13}$$

This relation can then be subsituted back into the integrated value of the induction equation (3-10) to give the differential equation for the magnetic induction,

$$\frac{\partial B}{\partial \eta} = E - \frac{1}{M}\left[1 + ME\right]\left[1 - \frac{\text{Cosh } M\eta}{\text{Cosh } M}\right] \tag{3-14}$$

Solving this and applying the boundary condition that the magnetic induction is zero at the center of the channel yields the equation for the induced magnetic flux density,

$$B = -\frac{\eta}{M} + \left[\frac{1 + ME}{M^2}\right]\frac{\text{Sinh } M\eta}{\text{Cosh } M} \tag{3-15}$$

The arbitrary constant involved in the equations for the velocity and magnetic induction can be found by comparing the integrated form of the induction equation (3-10) with Ohm's law (3-4). This shows that the constant is just the negative of the potential gradient and is therefore the electric field.

$$E = -\frac{\partial \Phi}{\partial \xi} \tag{3-16}$$

The assumptions made in deriving the relation for the potential gradient in the slug flow approximation are still valid in this case

since there is assumed no variation in the parameters in the ξ direction, including the potential gradient. Therefore the potential gradient is given by

$$\frac{\partial \phi}{\partial \xi} = R\int_0^1 J_\xi d\eta \tag{3-17}$$

Using the relation between the ξ component of the current density and the η derivative of the magnetic flux density (2-1), this can be integrated to give

$$E = -RB_1 \tag{3-18}$$

The value of B_1 can be evaluated in terms of the arbitrary constant from the derived equation for the magnetic induction (3-15). Substituting this into the relation for the potential gradient (3-18) gives the electric field to be

$$E = \frac{R}{M}\left[\frac{M - \text{Tanh } M}{M + R \text{ Tanh } M}\right] \tag{3-19}$$

Substituting this into the relations (3-13) and (3-15) gives the Hartmann equations, similar to the derivation of Hughes and Young (1966).

$$V = \frac{R+1}{M(M+R \text{ Tanh } M)}\left[1 - \frac{\text{Cosh } M\eta}{\text{Cosh } M}\right]$$

$$B = -\frac{\eta}{M} + \frac{R+1}{M(M+R \text{ Tanh } M)}\left[\frac{\text{Sinh } M\eta}{\text{Cosh } M}\right] \tag{3-20}$$

This relation now has a profile where the velocity drops from a core velocity to zero at the wall according to the hyperbolic cosine

function. By taking the proper limits as the Hartmann number goes to zero, it can be shown that this relation reduced to the parabolic profile of the Poiseuille flow. As the Hartmann number becomes larger, the character of the profile becomes one of a large core region of uniform velocity and a boundary layer region where the velocity decreases to zero. This can be shown more clearly if at large Hartmann number the hyperbolic function is approximated by the exponential to give

$$V = \frac{R+1}{M(M+R\ \mathrm{Tanh}\ M)}\left[1 - e^{-M(1-\eta)}\right]$$

$$B = -\frac{\eta}{M} + \left[\frac{R+1}{M(M+R\ \mathrm{Tanh}\ M)}\right] e^{-M(1-\eta)} \qquad (3\text{-}21)$$

It is in this approximation that the boundary layer thickness is seen to be inversely related to the Hartmann number.

Two relations that will be of use in further derivations are the average velocity and the value of the induced magnetic flux density at the wall, which is directly related to the external current. These are given by

$$\bar{V} = \frac{1+R}{M(M+R\ \mathrm{Tanh}\ M)}\left[1 - \frac{\mathrm{Tanh}\ M}{M}\right]$$

$$B_1 = \frac{\mathrm{Tanh}\ M - M}{M(M+R\ \mathrm{Tanh}\ M)} \qquad (3\text{-}22)$$

It is seen from the velocity relation that in this approximation the core velocity goes as the inverse of the Hartmann number square when the generator is short circuited and the resistance ratio goes to

zero. This is the same as for the slug flow approximation. But as the resistance ratio becomes very large, as in the insulated channel case, the velocity goes as the inverse of the Hartmann number rather than becoming infinite as in the slug flow approximation. The resistance to the pressure gradient in this case is due not only to the viscosity present but also to the electromagnetic forces arising from internal currents in the channel. Although there is no net current produced, this is allowed because reverse currents can flow in the boundary layer where the velocity generated potential is decreased. This can be seen in Figure 3-1 where the velocity, induced magnetic field, and current density are plotted for an insulated channel case at low Hartmann number. Note the current density is just the slope of the magnetic induction which changes sign in the boundary layer. Also the magnetic induction goes to zero indicating no net current flowing through the channel.

Generator Voltage

Of fundamental importance in the design of the generator is the voltage drop between electrodes. The relation for this can be derived in the general case by noting that the voltage drop is equal to the load resistance times the net current through the generator,

$$\Delta\phi = 2\gamma R \int_0^1 J_\xi d\eta \qquad (3\text{-}23)$$

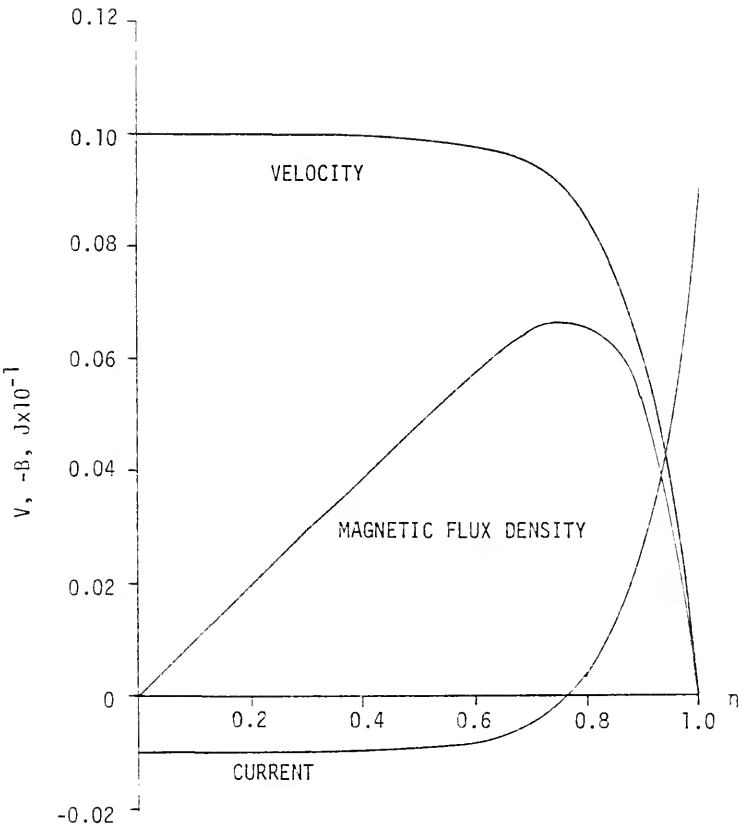

Figure 3-1. Hartmann Boundary Layer Profile

Rather than solving for the voltage in terms of the current density, the physical interpretation will be clearer by substituting Ohm's law (3-4) for the current density to give

$$\Delta\phi = -2\gamma R\left[\int_0^1 \frac{\partial\phi}{\partial\xi}\,d\eta + M\int_0^1 V d\eta\right] \tag{3-24}$$

This equation can then be integrated in the ξ direction from the center of the channel to the electrode where the potential will be assumed constant, so that

$$\int_0^\gamma \Delta\phi d\xi = -\gamma R[2\int_0^\gamma\int_0^1 \frac{\partial\phi}{\partial\xi}\,d\eta d\xi + 2M\int_0^\gamma\int_0^1 V d\eta d\xi] \tag{3-25}$$

The integrand of the left-hand side is constant and so can be easily evaluated. By changing the order of integration on the first double integral, and noting that the second is just the average velocity times the area of the cross section, the relation becomes

$$\Delta\phi = -R\int_0^1 \Delta\phi d\eta - 2\gamma RM\bar{V} \tag{3-26}$$

At this point the assumption must be made that the electrode is perfectly conducting so that the voltage does not vary as a function of η. This assumption is closely approximated even for electrodes with finite conductivity, and makes possible the evaluation of the integral to produce the simplified relation

$$\Delta\phi = -2\gamma KM\bar{V} \tag{3-27}$$

where

$$K = \frac{R}{R + 1}$$

The parameter K is the load factor and represents the fraction of the external resistance to the total resistance in the circuit. It is found more often in the literature than the resistance ratio and varies from zero for the short circuit case to 1 for the insulated channel.

The above relation for the voltage potential is shown to be true in the general case as long as the electrodes are perfectly conducting. Therefore the voltage for the Hartmann or slug flow case can be found simply by substituting in the average velocity into (3-27). The relation is also true in the two-dimensional case regardless of the boundary layers on the electrodes.

Since the value of the integral of the ξ component of the current density in Equation (3-23) can be evaluated in terms of the magnetic induction, it is of interest to note the following relation between the average velocity and the value of the magnetic flux density at the insulating wall, namely

$$B_1 = \frac{M}{1 + R} \bar{V} \qquad (3\text{-}28)$$

This relation in effect links the average velocity of the fluid in the channel to the net current produced by the generator.

Efficiency of the Generator

Of primary importance in the design of the generator is the overall efficiency with which it converts the mechanically input flow

work to the desired electrical power output. The generator efficiency is then defined as the ratio of the electrical power out to the power of the fluid going through the pressure drop of the generator section.

The work done by the fluid is given in terms of the pressure gradient down the channel and the average velocity of the fluid by

$$P_F = - \frac{dP}{dZ} 8Z_0 ab \bar{V}_z \tag{3-29}$$

The electrical power generated in the channel is given in terms of the load resistance and the square of the net current. Integrating the current density as the derivative of the magnetic flux density gives the value of the net current as a function of the value of the magnetic flux density at the insulated wall, so that the electrical power is given by

$$P_E = 8Z_0 ab \frac{R}{a^2 \sigma_0} \left(\frac{1}{\mu_e} B_z \Big|_{\eta=1} \right)^2 \tag{3-30}$$

The efficiency is then the ratio of these two powers. After nondimensionalizing the terms as was done previously, the efficiency is

$$\eta_e = \frac{P_E}{P_F} = \frac{RB_1^2}{\bar{V}} \tag{3-31}$$

If the slug flow values of the magnetic induction and average velocity are substituted into the above equation, the effiency is seen to be

$$\eta_e = \frac{R}{1 + R} = K \tag{3-32}$$

This indicates that as the load resistance becomes infinite the generator becomes perfectly efficient even though no current leaves the channel. This is only true because the viscosity of the fluid has been neglected in the slug flow approximation. If the viscosity is present, energy will be dissipated in the boundary layers when the resistance ratio is infinite so that the efficiency must be zero. This effect can be seen by substituting the value of the magnetic induction and average velocity derived from the Hartmann approximation into the equation for the efficiency, to give

$$\eta_e = \frac{R}{1 + R} \left[\frac{M - \text{Tanh } M}{M + R \text{ Tanh } M}\right] \tag{3-33}$$

Here the load factor of the slug flow approximation is modified by a term that goes to zero as the resistance ratio becomes infinite. It can also be seen that as the Hartmann number becomes very large the slug flow efficiency is more closely approximated. Because of the viscosity present, there is a maximum in the efficiency curve with respect to the resistance ratio, located at

$$R_{max} = \left[\frac{M}{\text{Tanh } M}\right]^{\frac{1}{2}} \tag{3-34}$$

This relation will be modified to a small extent in the two-dimensional case by the added viscous losses in the boundary layer on the electrodes. But, because the major factor is the reverse currents along the insulating wall, this is found to be a very good approximation.

Since the efficiency for the normal case is never equal to one, the two sources of energy dissipation should be noted. One is the ohmic dissipation of the internal currents flowing through the fluid of finite conductivity. The other is the viscous dissipation of energy in the boundary layers on the walls of the channel due to the friction of the fluid. Since both of these effects are heat generating, the ultimate result of the inefficiency of the generator is that the fluid temperature increases while passing through the channel.

The relative magnitude of these energy input, output, and losses can be approximated by analyzing the Hartmann flow equations. The energy equation is most easily derived by multiplying the momentum equation (3-9) by the local velocity of the fluid. To give

$$V\frac{\partial^2 V}{\partial \eta^2} + MV\frac{\partial B}{\partial \eta} + V = 0 \tag{3-35}$$

The velocity in the middle term is eliminated by substituting Ohm's law (3-4) yielding

$$V\frac{\partial^2 V}{\partial \eta^2} + E\frac{\partial B}{\partial \eta} - \left(\frac{\partial B}{\partial \eta}\right)^2 + V = 0 \tag{3-36}$$

The entire equation is then integrated over the volume of the generator section to give

$$\int_0^1 V\frac{\partial^2 V}{\partial \eta^2}\, d\eta + E\int_0^1 \frac{\partial B}{\partial \eta}\, d\eta - \int_0^1 \left(\frac{\partial B}{\partial \eta}\right)^2 d\eta + \int_0^1 V d\eta = 0 \tag{3-37}$$

The electric field can be substituted for in terms of the load resistance ratio and the value of the magnetic flux density at the insulating wall by the relation (3-18). The second integral can be integrated exactly and the first can be integrated by parts to yield

$$- \int_0^1 \left(\frac{\partial V}{\partial \eta}\right)^2 d\eta - RB_1^2 - \int_0^1 \left(\frac{\partial B}{\partial \eta}\right)^2 d\eta + \bar{V} = 0 \qquad (3\text{-}38)$$

Each of the terms in this equation is positive and when divided through by the average velocity can be interpreted as an efficiency or loss ratio;

$$\eta_e = RB_1^2/\bar{V} \qquad (3\text{-}29)$$

is the efficiency as derived previously as the ratio of the electrical power output to the pressure work done;

$$\eta_v = \frac{1}{\bar{V}} \int_0^1 \left(\frac{\partial V}{\partial \eta}\right)^2 d\eta \qquad (3\text{-}40)$$

is the ratio of the viscous power dissipated to the pressure work done; and

$$\eta_0 = \frac{1}{\bar{V}} \int_0^1 \left(\frac{\partial B}{\partial \eta}\right)^2 d\eta \qquad (3\text{-}41)$$

is the ratio of the ohmic power dissipated to the pressure work done. For the case of the Hartmann approximation, the efficiency was given previously (3-33), and the viscous power losses are given by

$$\eta_v = \frac{1}{2} \left(\frac{M}{M - \text{Tanh } M}\right)\left(\frac{1 + R}{M + R \text{ Tanh } M}\right)(\text{Tanh } M + M \text{ Tanh}^2 M - M) \qquad (3\text{-}42)$$

The ohmic power losses are most easily evaluated by taking the difference between one and the sum of the efficiency and the viscous power losses, according to

$$\eta_0 = 1 - \eta_e - \eta_v \tag{3-43}$$

Again these relations are only valid for the Hartmann approximation of the one-dimensional case and will be slightly modified for the two-dimensional case where there is the added viscous dissipation in the boundary layers on the electrode walls and the added ohmic dissipation of currents in the η direction near the electrodes. In real channels there are even more significant losses due to entrance and exit effects that can greatly reduce the efficiency. These relations are then just optimum values that can be approached in a well-designed channel.

Figure 3-2 shows the Hartmann efficiency and viscous and ohmic losses evaluated for a typical case at a Hartmann number of 20. Plotted against the load factor, the curves follow pretty much the the slug flow approximation until the peak efficiency is reached at $R=\sqrt{M}$. For this first part the viscous loss is fairly negligible with the efficiency and ohmic losses linearly increasing and decreasing respectively. After the peak the generator approaches the insulated channel case where the load resistance is infinite and the efficiency goes to zero because no current flows out. At this point the viscous and ohmic losses equally share the dissipation of the pressure work done by the fluid.

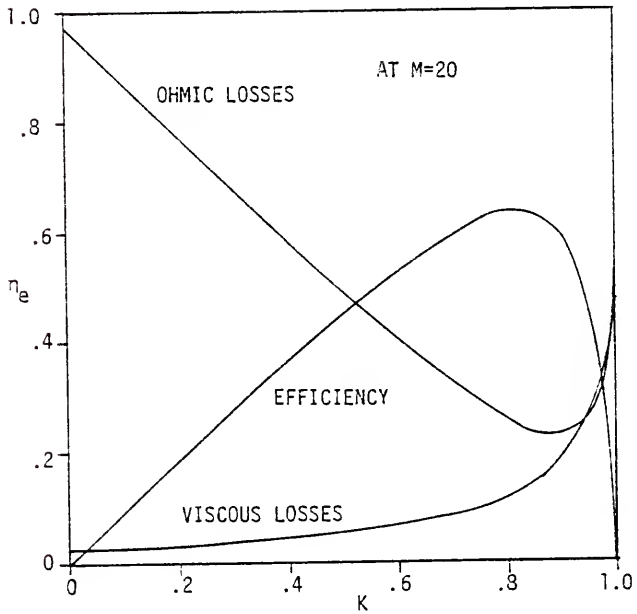

Figure 3-2. Hartmann Efficiencies versus Load Factor

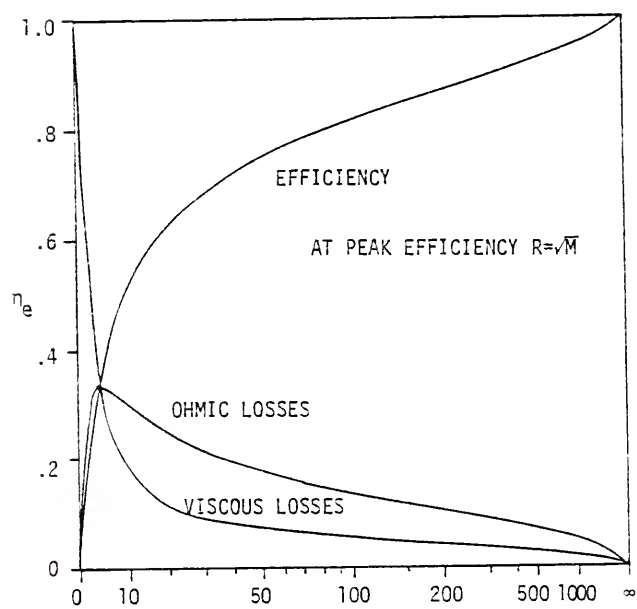

Figure 3-3. Hartmann Efficiencies versus Hartmann Number

Figure 3-3 shows the evaluation of the equations for a range of Hartmann numbers from zero to infinity, with the resistance ratio set at the maximum efficiency point. At a Hartmann number of zero the equations represent laminar Poiseuille flow of a fluid in the channel with only the viscous forces present to dissipate the pressure work. The efficiency increases from zero at this point to one as the Hartmann number approaches infinity, where the flow approaches the slug flow conditions. This demonstrates the advantage of going to higher Hartmann numbers which in most cases means going to more intense applied magnetic fields.

Inviscid Core Approximation

As was mentioned in the introduction, when the Hartmann number becomes large, the flow can be described as having separate characteristics in two regions of the channel. Near the walls the flow takes on a boundary layer approximation derivable from the Hartmann flow equations. But in the core region the velocity profile becomes flat and the flow takes on an inviscid slug flow approximation. In this core region the inviscid approximation can be generalized to include the effects of changes in the conductivity of the fluid at different points in the channel.

With the viscosity absent, the current density is given directly as in the slug flow approximation by the simplified momentum equation

$$J = -\frac{1}{M} \tag{3-2}$$

But Ohm's law can be generalized to include the conductivity of the fluid. This yields

$$J = \frac{1}{F}(E - MV) \tag{3-44}$$

Solving for the velocity and making the substitution for the current density gives the velocity in terms of the electric field and the conductivity ratio, as

$$V = \frac{1}{M}\left[E + \frac{F}{M}\right] \tag{3-45}$$

As long as the conductivity varies only in the core region and not in the Hartmann boundary layers, the electric field will remain constant throughout the channel until the boundary layer on the electrodes is reached. Therefore the electric field obtained in the derivation of the Hartmann flow equations (3-19) can be substituted to obtain the equation

$$V = \frac{1}{M^2}\left[\frac{R(M - \text{Tanh } M)}{M + R \text{ Tanh } M} + F\right] \tag{3-46}$$

From this equation it is seen that as the conductivity decreases the velocity increases to maintain a constant current density in the core. This equation remains an effective approximation until the conductivity starts to change significantly over distances of the order of the Hartmann boundary layer. This case would produce significant gradients in the velocity that would again make the viscosity a comparable force and negate the assumptions made in the approximation.

To analyze this case the full two-dimensional equations are required to account for the effects produced.

CHAPTER IV
FINITE DIFFERENCE SOLUTION

The two simultaneous equations (2-8) that have been derived for this problem cannot be solved analytically in any convenient fashion. Therefore it is necessary to find numerical solutions to the equations by breaking them up into finite differences and programming the computer to obtain the desired results. This is the major effort behind the work done in this dissertation and is the basis of the results achieved.

PRADI Solution

The choice of the proper numerical technique to best solve the equations in terms of speed and accuracy is essential in making any extensive analysis of the physical aspects of the problem. Since no standard technique will fit the problem exactly, the choice of a technique with good qualities of stability and speed of convergence is necessary so that the modifications which must be made will not destroy its ability to obtain a solution.

The two simultaneous equations are elliptic in nature, and with the two second derivatives being the primary terms, they appear to most closely resemble the Laplace equation. For this reason a technique that has proven most effective on the Laplace equation was chosen. This method is the Peaceman Rachford Alternating Direction

Implicit (PRADI) method (Mitchell 1969; Mitchell and Fairweather 1964). This technique is a relaxation scheme that sets the Laplacian term equal to the time derivative of the dependent variable, thus converting the equation into a parabolic form of the diffusion type.

$$\frac{\partial^2 B}{\partial \eta^2} + \frac{\partial^2 B}{\partial \xi^2} = \frac{\partial B}{\partial t} \tag{4-1}$$

An initial guess is taken for the solution and the equation is solved stepwise in time. This solution will, after a number of iterations, reach a steady state since the boundary conditions are constant with respect to the time variable. In the steady state the added time derivative term disappears and the solution satisfies the original equation.

To derive the PRADI finite difference form for the two simultaneous equations, first look at the Taylor series expansion some time step k ahead for the variable B, given by

$$B(t+k) = B(t) + \left.\frac{\partial B}{\partial t}\right|_t k + \frac{1}{2}\left.\frac{\partial^2 B}{\partial t^2}\right|_t k^2 + \frac{1}{3!}\left.\frac{\partial^3 B}{\partial t^3}\right|_t k^3 + \ldots \tag{4-2}$$

Viewing the variable at t and t+k as the n^{th} and the $n+1^{th}$ iterations respectively and the expansion as an operator on the variable gives

$$B^{n+1} = \mathrm{EXP}\left(k\frac{\partial}{\partial t}\right) B^n \tag{4-3}$$

Using this equation would give an explicit scheme since all the operation is performed on the variable at the n^{th} iteration. Peaceman and Rachford followed the lead of Crank-Nicolson, who derived a method for

the diffusion equation in one space dimension and created an implicit scheme by splitting the operation to apply equally to the value of the variable known and the value to be derived for the next time step.

$$\mathrm{EXP}\left(-\frac{1}{2}k\frac{\partial}{\partial t}\right)B^{n+1} = \mathrm{EXP}\left(\frac{1}{2}k\frac{\partial}{\partial t}\right)B^{n} \tag{4-4}$$

This use of an implicit scheme rather than an explicit one gives a great advantage in the stability of the scheme and insensitivity to the choice of the time step constant k, although it adds somewhat in the complexity of the calculation for each iteration.

The two simultaneous equations (2-8) derived previously with the artificially added time derivatives are given by

$$F\left[\frac{\partial^2 B}{\partial\eta^2}+\frac{\partial^2 B}{\partial\xi^2}\right] + \left[\frac{\partial F}{\partial\eta}\frac{\partial B}{\partial\eta}+\frac{\partial F}{\partial\xi}\frac{\partial B}{\partial\xi}\right] + M\frac{\partial V}{\partial\eta} = \frac{\partial B}{\partial t}$$

$$G\left[\frac{\partial^2 V}{\partial\eta^2}+\frac{\partial^2 V}{\partial\xi^2}\right] + \left[\frac{\partial G}{\partial\eta}\frac{\partial V}{\partial\eta}+\frac{\partial G}{\partial\xi}\frac{\partial V}{\partial\xi}\right] + M\frac{\partial B}{\partial\eta} + 1 = \frac{\partial V}{\partial t} \tag{4-5}$$

Defining the following four linear operators,

$$L_\eta^B = F\frac{\partial^2}{\partial\eta^2} + \frac{\partial F}{\partial\eta}\frac{\partial}{\partial\eta} \qquad L_\xi^B = F\frac{\partial^2}{\partial\xi^2} + \frac{\partial F}{\partial\xi}\frac{\partial}{\partial\xi}$$

$$L_\eta^V = G\frac{\partial^2}{\partial\eta^2} + \frac{\partial G}{\partial\eta}\frac{\partial}{\partial\eta} \qquad L_\xi^V = G\frac{\partial^2}{\partial\xi^2} + \frac{\partial G}{\partial\xi}\frac{\partial}{\partial\xi} \tag{4-6}$$

gives the relation for the time derivative operator on the variable B, as

$$\frac{\partial}{\partial t} = L_\eta^B + L_\xi^B + M\frac{\partial V}{\partial\eta} \tag{4-7}$$

Substituting this into the iteration equation (4-4) puts it in the form of space derivatives which can be calculated

$$\mathrm{EXP}\left(-\frac{1}{2}kL\frac{B}{\xi} - \frac{1}{2}kL\frac{B}{\eta} - \frac{1}{2}kM\frac{\partial V}{\partial \eta}\right)B^{n+1} = \mathrm{EXP}\left(\frac{1}{2}kL\frac{B}{\xi} + \frac{1}{2}kL\frac{B}{\eta} + \frac{1}{2}kM\frac{\partial V}{\partial \eta}\right)B^{n} \tag{4-8}$$

Breaking up the exponential of the sum into the product of exponentials and then expanding them for just the first two terms gives the following approximation to the complete equation, namely

$$\left(1 - \frac{1}{2}kL\frac{B}{\xi}\right)\left(1 - \frac{1}{2}kL\frac{B}{\eta}\right)\left(1 - \frac{1}{2}kM\frac{\partial V}{\partial \eta}\right)B^{n+1} = \left(1 + \frac{1}{2}kL\frac{B}{\xi}\right)\left(1 + \frac{1}{2}kL\frac{B}{\eta}\right)\left(1 + \frac{1}{2}kM\frac{\partial V}{\partial \eta}\right)B^{n} \tag{4-9}$$

The term $(\frac{1}{2}kM\frac{\partial V}{\partial \eta})$ is viewed as a constant operator that operates on B to produce itself. Since V is also a variable that will be relaxing in time and governed by the other of the two simultaneous equations, it is necessary to specify an iteration number for it also. It is found in working with the numerical solution that the two variables V and B have to be solved simultaneously in order to achieve a stable solution. Therefore in keeping with the implicit nature of the numerical scheme the term on the left is taken at the $n+1^{th}$ time step and that on the right at the n^{th}. Therefore letting the last term operate on B gives the following equation which represents the finite difference expansion in time of the fundamental equation.

$$\left(1-\frac{1}{2}kL_{\xi}^{B}\right)\left[\left(1-\frac{1}{2}kL_{\eta}^{B}\right)B^{n+1}-\frac{1}{2}kM\frac{\partial V^{n+1}}{\partial \eta}\right]=\left(1+\frac{1}{2}kL_{\xi}^{B}\right)\left[\left(1+\frac{1}{2}kL_{\eta}^{B}\right)B^{n}+\frac{1}{2}kM\frac{\partial V^{n}}{\partial \eta}\right] \tag{4-10}$$

In similar fashion the other of the two simultaneous equations is approximated from the expansion of the time derivative of the variable V, giving

$$\left(1-\frac{1}{2}kL_{\xi}^{V}\right)\left[\left(1-\frac{1}{2}kL_{\eta}^{V}\right)V^{n+1}-\frac{1}{2}k\left(1+M\frac{\partial B^{n+1}}{\partial \eta}\right)\right]=\left(1+\frac{1}{2}kL_{\xi}^{V}\right)\left[\left(1+\frac{1}{2}kL_{\eta}^{V}\right)V^{n}+\frac{1}{2}k\left(1+M\frac{\partial B^{n}}{\partial \eta}\right)\right] \tag{4-11}$$

To use these two equations in the present form would be very difficult due to the nature of the implicit terms on the left side. The differential operators must be evaluated by considering the adjacent nodes to any point to be evaluated, which produces sets of coupled equations that must be solved simultaneously. With the operators in both the ξ and η directions on the left side of the equation, all the nodes in the entire channel must be solved simultaneously for each iteration. To alleviate this problem, which makes the scheme unworkable, Peaceman and Rachford made the following innovation which allows the problem to be solved one row at a time in alternating directions. They did this by introducing an intermediate value to be calculated and breaking up each of the two finite difference equations into two parts.

$$\left(1-\frac{1}{2}kL_{\xi}^{B}\right)B^{*}=\left(1+\frac{1}{2}kL_{\eta}^{B}\right)B^{n}+\frac{1}{2}kM\frac{\partial V^{n}}{\partial \eta}$$

$$\left(1 - \frac{1}{2}kL_\eta^B\right)B^{n+1} - \frac{1}{2}kM\frac{\partial V^{n+1}}{\partial \eta} = \left(1 + \frac{1}{2}kL_\xi^B\right)B^*$$

$$\left(1 - \frac{1}{2}kL_\xi^V\right)V^* = \left(1 + \frac{1}{2}kL_\eta^V\right)V^n + \frac{1}{2}k\left(1 + M\frac{\partial B^n}{\partial \eta}\right)$$

$$\left(1 - \frac{1}{2}kL_\eta^V\right)V^{n+1} - \frac{1}{2}kM\frac{\partial B^{n+1}}{\partial \eta} = \frac{1}{2}k + \left(1 + \frac{1}{2}kL_\xi^V\right)V^* \qquad (4\text{-}12)$$

It can be shown by multiplying each by the appropriate operator and combining, that these represent the same equations, but in this form the implicit operations are separated along the directions ξ and η. Thus each equation couples implicitly only with the nodes along a given row or column. This greatly simplifies the task of solving for the values of the variables at the next time step or intermediate value, since it is only necessary to solve a number of simultaneous algebraic equations equal to the number of nodes in the row, and, as will be shown, these form a tridiagonal system.

The two equations for the calculation of the starred quantities, V* and B*, can each be solved independently but the two equations for finding the values at the next time step must be solved simultaneously since both involve the two variables V and B. This adds only a small complexity to each iteration and the method is still remarkably efficient. It should be noted that the starred quantities are mathematical fictions and do not necessarily bear any physical relation to the quantities V and B. Therefore it is necessary to derive boundary conditions to be applied to the two equations in terms

of the known boundary conditions for V and B. This is very easily done by subtracting the two equations containing the V* and similarly the B* to get

$$2V^* = (V^n + V^{n+1}) + \frac{1}{2}kM\frac{\partial}{\partial\eta}(B^n - B^{n+1})$$

$$2B^* = (B^n + B^{n+1}) + \frac{1}{2}kM\frac{\partial}{\partial\eta}(V^n - V^{n+1}) \qquad (4\text{-}13)$$

When the steady state is reached, the n^{th} term will equal the $n+1^{th}$ so that the boundary conditions for the starred quantities are easily seen to be the same as for the V and B variables in this case. Since the starred quantities are only solved for in the ξ direction, only the boundary conditions at ξ=0 and at the electrode are required. These are

$$\frac{\partial V^*}{\partial\xi} = \frac{\partial B^*}{\partial\xi} = 0$$

and

$$V^* = \frac{\partial B^*}{\partial\xi} = 0 \qquad (4\text{-}14)$$

respectively.

Generalized Nodal Spacing

To effectively use the equations derived so far requires the proper evaluation of the linear operators for the space derivatives. When the nodes to be evaluated are evenly spaced the normal procedure

is to use the central difference method where the first and second derivatives are determined at the central node by proper weighting of the value at that node and at the two immediately adjacent to it. For the purposes of this work it is felt that more flexibility would be an advantage so the central difference has been generalized so that an arbitrary spacing may be used between nodes. Using the operator acting on B in the ξ direction as an example, the following spacings are defined about the m^{th} node in the row.

$$\chi_m = \xi_{m-1} - \xi_m \qquad \chi_p = \xi_m - \xi_{m+1}$$

$$\chi_{mp} = \xi_{m-1} - \xi_{m+1} \tag{4-15}$$

The first and second derivatives are then approximated by the finite differences.

$$\frac{\partial B}{\partial \xi} = \left[\frac{-\chi_m}{\chi_p \chi_{mp}}\right] B_{m+1} + \left[\frac{\chi_m - \chi_p}{\chi_m \chi_p}\right] B_m + \left[\frac{\chi_p}{\chi_m \chi_{mp}}\right] B_{m-1}$$

$$\frac{\partial^2 B}{\partial \xi^2} = \left[\frac{2}{\chi_p \chi_{mp}}\right] B_{m+1} + \left[\frac{-2}{\chi_m \chi_p}\right] B_m + \left[\frac{2}{\chi_m \chi_{mp}}\right] B_{m-1} \tag{4-16}$$

Inserting these into the definition of the linear operator (4-6) gives the finite difference operator to be

$$L_\xi^B B = \frac{1}{\chi_p \chi_{mp}} \left[2F - \frac{\partial F}{\partial \xi}\chi_m\right] B_{m+1} + \frac{1}{\chi_m \chi_p} \left[-2F + \frac{\partial F}{\partial \xi}(\chi_m - \chi_p)\right] B_m$$

$$+ \frac{1}{\chi_m \chi_{mp}} \left[2F + \frac{\partial F}{\partial \xi}\chi_p\right] B_{m-1} \tag{4-17}$$

The other operators are derived in a similar fashion with the substitution of G for F in the velocity operator and η for ξ when the η direction is used.

The derivatives of the functions F and G in these equations are not broken up in the finite differences, although they could be approximated using the value of the function at m-1 and m+1. This is done for the sake of accuracy, since the functions F and G are inputs to the problem and their derivatives are presumably known exactly.

Using the equation for V* as an example, it can be seen that these finite difference equations become a series of simultaneous algebraic equations that can easily be written in the following matrix form.

$$\begin{bmatrix} a_1 & b_1 & & & & \\ c_2 & a_2 & b_2 & & & \\ & c_3 & a_3 & b_3 & & \\ & & \ddots & \ddots & \ddots & \\ & & & a_{m-1} & b_{m-1} & \\ & & & c_m & a_m & \end{bmatrix} \begin{Bmatrix} V_1^* \\ V_2^* \\ \vdots \\ V_m^* \end{Bmatrix} = \begin{Bmatrix} R_1 \\ R_2 \\ \vdots \\ R_m \end{Bmatrix} \qquad (4\text{-}18)$$

Here the elements of the matrices are defined in the following manner.

$$a_i = 1 - \frac{1}{2}k\frac{1}{\chi_m \chi_p}\left[-2G + \frac{\partial G}{\partial \xi}(\chi_m - \chi_p)\right]$$

$$b_i = \frac{1}{2}k\frac{1}{\chi_p \chi_{mp}}\left[2G - \frac{\partial G}{\partial \xi}\chi_m\right]$$

$$c_i = \frac{1}{2}k\frac{1}{\chi_m \chi_{mp}}\left[2G + \frac{\partial G}{\partial \xi}\chi_p\right]$$

$$R_i = \left(1 + \frac{1}{2}kL\frac{V}{\eta}\right)V^n + \frac{1}{2}k\left(1 + M\frac{\partial B^n}{\partial \eta}\right) \qquad (4\text{-}19)$$

To establish the equations for the first and last rows the boundary conditions must be invoked. For the first, the derivative of V* equals zero. Therefore the V_0^* term is set equal to the V_2^*, so that the b_1 term is then the sum of the b_1 and c_1 terms and the c_1 term is dropped. In the m^{th} row the V* is explicitly given the value of zero, so a_m=1 and c_m and R_m equal zero.

This choice of approximating the operators by just the adjacent nodes gives the very desirable result that the matrix is in a tridiagonal form with just the terms on the three center diagonals having values. This simplifies much of the calculations since the tridiagonal system is easily solved by Gaussian elimination rather than having to go to very sophisticated means of matrix inversion. The calculations involved in the solution are to simply find sequentially the values

$$a_i^* = a_i - c_i b_i / a_{i-1}^* \qquad R_i^* = R_i - c_i R_{i-1}^* / a_{i-1}^* \qquad (4\text{-}20)$$

where $a_1^*=a_1$ and $R_1^*=R_1$.

Then the required solution is given in the reverse sequence by the calculations

$$V_i^* = (R_i^* - b_i V_{i+1}^*)/a_i^* \qquad (4\text{-}21)$$

where $V_m^*=R_m^*/a_m^*$. It is the simplicity of this calculation that gives this method its speed and provides the reason for the alternating direction approach to the finite difference equations.

The equation for B* is solved in a similar manner, but when the next time step is solved, a modification to the basic method is required. The two equations must be solved for simultaneously since they contain both V and B. The matrix equation takes the form

$$\begin{bmatrix} a_1^V & b_1^V & & & & d_1^V & e_1^V & & & \\ c_2^V & a_2^V & b_2^V & & & f_2^V & d_2^V & e_2^V & & \\ & \ddots & \ddots & \ddots & & & \ddots & \ddots & \ddots & \\ & & c_n^V & a_n^V & & & & f_n^N & d_n^V & \\ a_1^B & b_1^B & & & & d_1^B & e_1^B & & & \\ c_2^B & a_2^B & b_2^B & & & f_2^B & d_2^B & e_2^B & & \\ & \ddots & \ddots & \ddots & & & \ddots & \ddots & \ddots & \\ & & c_n^B & a_n^B & & & & f_n^B & d_n^B & \end{bmatrix} \begin{Bmatrix} V_1^{n+1} \\ V_2^{n+1} \\ \vdots \\ V_n^{n+1} \\ B_1^{n+1} \\ B_2^{n+2} \\ \vdots \\ B_n^{n+1} \end{Bmatrix} = \begin{Bmatrix} R_1^V \\ R_2^V \\ \vdots \\ R_n^V \\ R_1^B \\ R_2^B \\ \vdots \\ R_n^B \end{Bmatrix} \tag{4-22}$$

where the elements are defined as the coefficients of two equations from (4-12) by

$$\left(1 - \frac{1}{2}kL_\eta^B\right)B^{n+1} - \frac{1}{2}kM\frac{\partial V^{n+1}}{\partial\eta} = \left(1 + \frac{1}{2}kL_\xi^B\right)B^*$$

$$\left(1 - \frac{1}{2}kL_\eta^V\right)V^{n+1} - \frac{1}{2}kM\frac{\partial B^{n+1}}{\partial\eta} = \frac{1}{2}k + \left(1 + \frac{1}{2}kL_\xi^V\right)V^* \tag{4-23}$$

With the appropriate boundary conditions applied the matrix is seen to be a combination of four tridiagonal systems. Although this is more complex than the tridiagonal system, it can be solved in an analogous

fashion taking into account the simultaneous nature of the equations. The following intermediate calculations are made in sequence.

$$a_{i+1}^{V*} = a_{i+1}^{V} + [c_{i+1}^{V}(d_i^{V*}b_i^{B} - d_i^{B*}b_i^{V}) + f_{i+1}^{V}(a_i^{B*}b_i^{V} - a_i^{V*}b_i^{B})]/(a_i^{V*}d_i^{B*} - a_i^{B*}d_i^{V*})$$

$$a_{i+1}^{B*} = a_{i+1}^{B} + [c_{i+1}^{B}(d_i^{V*}b_i^{B} - d_i^{B*}b_i^{V}) + f_{i+1}^{B}(a_i^{B*}b_i^{V} - a_i^{V*}b_i^{B})]/(a_i^{V*}d_i^{B*} - a_i^{B*}d_i^{V*})$$

$$d_{i+1}^{V*} = d_{i+1}^{V} + [c_{i+1}^{V}(d_i^{V*}e_i^{B} - d_i^{B*}e_i^{V}) + f_{i+1}^{V}(a_i^{B*}e_i^{V} - a_i^{V*}e_i^{B})]/(a_i^{V*}d_i^{B*} - a_i^{B*}d_i^{V*})$$

$$d_{i+1}^{B*} = d_{i+1}^{B} + [c_{i+1}^{B}(d_i^{V*}e_i^{B} - d_i^{B*}e_i^{V}) + f_{i+1}^{B}(a_i^{B*}e_i^{V} - a_i^{V*}e_i^{B})]/(a_i^{V*}d_i^{B*} - a_i^{B*}d_i^{V*})$$

$$R_{i+1}^{B*} = R_{i+1}^{B} + [c_{i+1}^{B}(d_i^{V*}R_i^{B*} - d_i^{B*}R_i^{V*}) + f_{i+1}^{B}(a_i^{B*}R_i^{V} - a_i^{V*}R_i^{B*})]/(a_i^{V*}d_i^{B*} - a_i^{B*}d_i^{V*})$$

$$R_{i+1}^{V*} = R_{i+1}^{V} + [c_{i+1}^{V}(d_i^{V*}R_i^{B*} - d_i^{B*}R_i^{V*}) + f_{i+1}^{V}(a_i^{B*}R_i^{V*} - a_i^{V*}R_i^{B*})]/(a_i^{V*}d_i^{B*} - a_i^{B*}d_i^{V*}) \qquad (4\text{-}24)$$

The solution is then found from the following calculations made in the reverse sequence.

$$V_i^{n+1} = [d_i^{B*}(R_i^{V*} - b_i^V V_{i+1}^{n+1} - e^V B_{i+1}^{n+1})$$
$$- d_i^{V*}(R_i^{B*} - b_i^B V_{i+1}^{n+1} - e_i^B B_{i+1}^{n+1})]/(d_i^{B*} a_i^{V*} - d_i^{V*} a_i^{B*})$$

$$B_i^{n+1} = [a_i^{B*}(R_i^{V*} - b_i^V V_{i+1}^{n+1} - e_i^V B_{i+1}^{n+1})$$
$$- a_i^{V*}(R_i^{B*} - b_i^B V_{i+1}^{n+1} - e_i^B B_{i+1}^{n+1})]/(a_i^{B*} d_i^{V*} - a_i^{V*} d_i^{B*}) \qquad (4\text{-}25)$$

with the n^{th} term given by the following.

$$V_n^{n+1} = [d_n^{B*} R_n^{V*} - d_n^{V*} R_n^{B*}]/[d_n^{B*} a_n^{V*} - d_n^{V*} a_n^{B*}]$$

$$B_n^{n+1} = [a_n^{B*} R_n^{V*} - a_n^{V*} R_n^{B*}]/[a_n^{B*} d_n^{V*} - a_n^{V*} d_n^{B*}] \qquad (4\text{-}26)$$

Both of these matrix solutions have the advantage of being straightforward simple sequences of calculations that allow each iteration to be solved quickly and efficiently. The tridiagonal system (4-18) must be solved once for each variable on each row in the ξ direction. The other matrix (4-22) is then solved once for both variables on each vertical column in the η direction in the grid.

Reasons for the PRADI Method

The PRADI method is chosen because of the similarity of the governing equations to the Laplace equation for which the method was developed. There are other methods though that could have been used such as the Gauss-Seidel or the Successive Overrelaxation method used

by Wissmiller (1964). But because of the modifications that are required for any method to work for these equations, such as the addition of terms to the equations and the simultaneous nature of the problem, it was necessary to choose the method that was most advantageous in terms of the stability of the iterations, the speed of convergence to the solution, and insensitivity to choice of spacing between the nodes and the time step between iterations.

In the book by Mitchell (1969) a significant analysis is done of the stability and convergence of the various methods. The conclusions reached indicate that the implicit schemes are inherently more stable than the explicit ones, and the PRADI method is stable for the Laplace equation at any choice of the iteration parameter (k). It is also found that for the Laplace equation on a square grid of equal spacing the method will converge to the steady state answer for any constant value of the iteration parameter. Although it was found to be of little use in solving the present problem, the book also indicates the work of Varga (1962), Wachspress (1966), and Douglas (1962) that shows the rate of convergence can be increased by increasing geometrically the value of the iteration parameter at each iteration for the Laplace problem.

The assumptions made in determining these properties of the PRADI method are not satisfied by the magnetohydrodynamic equations to be solved here. This is because of the added terms in the equations, the simultaneous nature of the two equations, the non-square nature of the grid, and the use of variable spacing between

nodes to reduce the total number required. In spite of the many modifications that had to be made, it will be assumed, and found to be generally true, that the required properties of stability and convergence will be carried over due to the powerful nature of the method. A separate analysis of these properties was precluded for this dissertation due to the complex nature of the present modified method.

Selection of Nodal Spacing

The selection of where the nodes are to be placed and the arrangement of the grid become very important considerations when looking at the storage requirements for a computer program to solve the finite difference equations. The use of the symmetry conditions available in the problem reduces the required number of nodes to one-fourth that needed to solve for the whole channel, but the need to carry two variables at each node has in essence doubled the storage. Therefore by proper selection of the placing of the nodes significant reductions in the storage requirements can be made.

The grid of nodes must be arranged in a rectangular array of rows and columns to satisfy the method of calculating the derivatives, but other than this the spacing between individual rows can be set at any constant value or variably adjusted across the channel independently in either direction. It would seem desirable to be able to vary the spacing so that the nodes would be close together in regions where the value of the variables are changing rapidly or in a

nonlinear fashion, and keep the spacing broad where little change is taking place. In the ordinary case, these regions would be unknown until after the problem is solved and therefore little would be gained in variable spacing, but in the present study it is possible to draw on the analytical work of Shercliff (1956) and others to adjust the grid spacing in a more efficient manner.

As was stated in the introduction, it is found from the analytical solutions that the magnetohydrodynamic flow in the duct can be viewed as being divided into two regions. One is the boundary layer region that is found along the insulating walls and the electrodes, and the other is the broad center of the flow that is nearly constant in terms of the velocity profile and linear as far as the induced magnetic field is concerned. It is realized that the core flow region does not retain its slug flow form when the conductivity and viscosity are allowed to vary within it, but the primary region of variability is still the boundary layers. Therefore it is advantageous to initially put half the rows along each direction in the boundary layer evenly spaced, and then broaden the spacing for the rest to extend across the channel.

Fortunately, good approximations are available for the thickness of the boundary layers. Hartmann's (1937) solution to the one-dimensional infinite aspect ratio problem shows the boundary layer on the insulating walls to form an exponential profile in the velocity with an exponential folding distance equal to a/M, where a is the half-height of the channel and M is the Hartmann number.

Shercliff's (1956) work shows that the thickness of the layers on the electrodes is of the order of $a/\sqrt{M}$. Using these estimates, which are very good, it is found that good results are obtained by placing the first ten rows evenly spaced from the wall to a point five times the exponential folding distance into the channel. Then an equal number of rows are placed at a greater spacing to cover the remaining distance to the center of the channel, as is shown in Figure 4-1. Of course, at very low Hartmann number the spacing in the boundary layer is greater than the spacing in the core and so the scheme defaults to an evenly spaced array.

This scheme of grid spacing creates a twenty-by-twenty grid with a total of four-hundred nodes and two equations at each node. Thus the method is in effect solving a matrix of some eight-hundred simultaneous algebraic equations. This arrangement is found through the course of the calculations to work quite well as long as the Hartmann number is less than thirty. Above this, the solution arrived at is stable but the answer contains a significant oscillation between nodes, as shown in Figure 4-2, that are known not to be part of the desired results. This is not a problem of the solution of the finite difference equations but is a result of the errors involved in how close those equations approximated the original differential equations. This problem and its solution can be analyzed by the following error analysis.

For the purposes of this analysis it is sufficient to consider only one dimension of the MHD equations, since at the higher

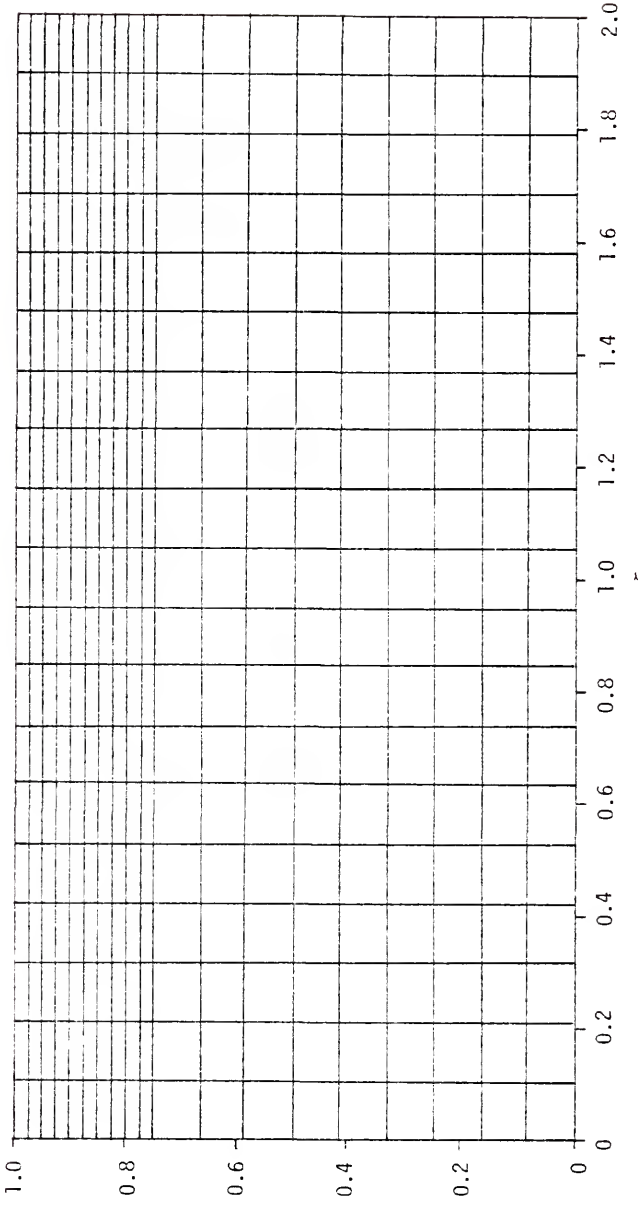

Figure 4-1. Quadrant Nodal Spacing

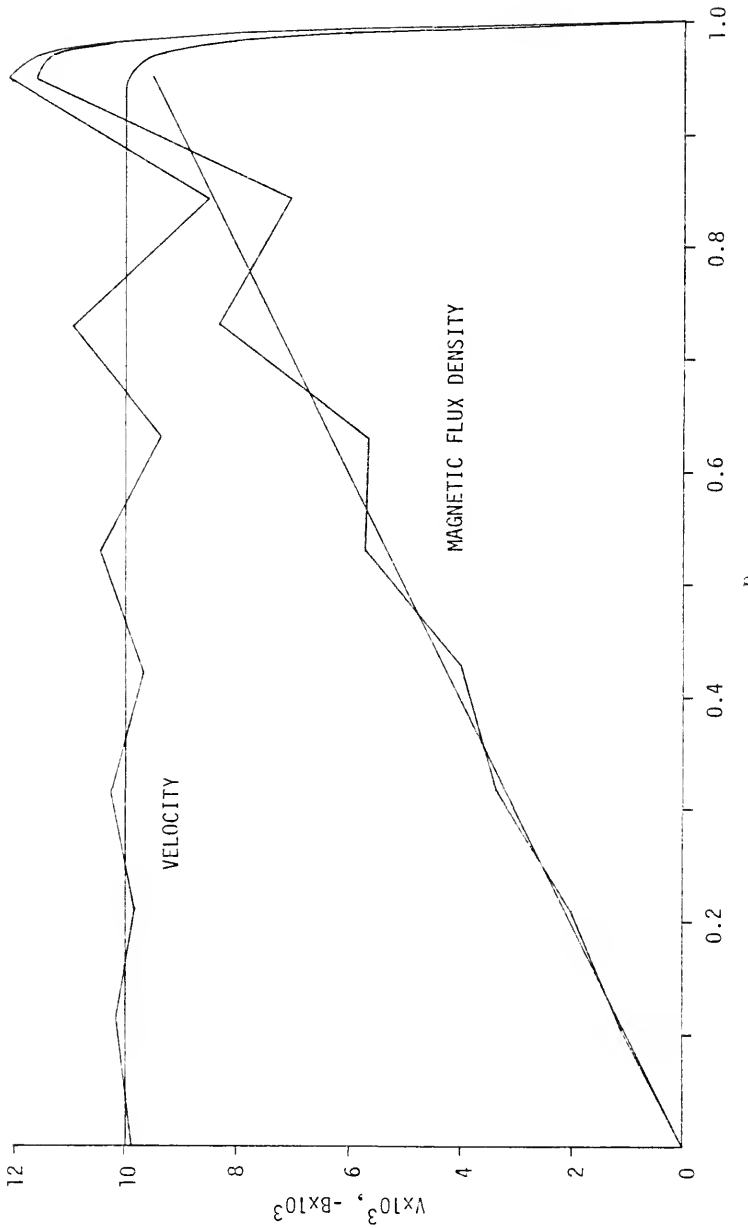

Figure 4-2. Finite Difference Profile Error
M=100 K=1 20x20 Grid

Hartmann numbers the flow at the center of the channel is determined by the derivatives in the η direction alone. Also neglecting the variations in conductivity and viscosity the equations become

$$\frac{\partial^2 B}{\partial \eta^2} + M\frac{\partial V}{\partial \eta} = 0 \qquad \text{induction equation}$$

$$\frac{\partial^2 V}{\partial \eta^2} + M\frac{\partial B}{\partial \eta} + 1 = 0 \qquad \text{momentum equation} \qquad (4\text{-}27)$$

The finite difference approximation to these equations assuming a constant spacing between nodes is given by

$$\frac{1}{h^2}(B_{j+1} + B_{j-1} - 2B_j) + \frac{M}{2h}(V_{j+1} - V_{j-1}) = 0$$

$$\frac{1}{h^2}(V_{j+1} + V_{j-1} - 2V_j) + \frac{M}{2h}(B_{j+1} - B_{j-1}) + 1 = 0 \qquad (4\text{-}28$$

This is not the form of the finite difference equations in which they are solved, but under the assumptions made, the PRADI solution must satisfy these equations.

The values of the variables at the adjacent nodes of the finite difference equation can be evaluated in terms of the value of the variable and its derivatives at the central position by the series expansions,

$$B_{j+1} = B + h\frac{\partial B}{\partial \eta} + \frac{h^2}{2}\frac{\partial^2 B}{\partial \eta^2} + \frac{h^3}{6}\frac{\partial^3 B}{\partial \eta^3} + \ldots$$

$$B_{j-1} = B - h\frac{\partial B}{\partial \eta} + \frac{h^2}{2}\frac{\partial^2 B}{\partial \eta^2} - \frac{h^3}{6}\frac{\partial^3 B}{\partial \eta^3} + \ldots$$

$$V_{j+1} = V + h\frac{\partial V}{\partial \eta} + \frac{h^2}{2}\frac{\partial^2 V}{\partial \eta^2} + \frac{h^3}{6}\frac{\partial^3 V}{\partial \eta^3} + \ldots$$

$$V_{j-1} = V - h\frac{\partial V}{\partial \eta} + \frac{h^2}{2}\frac{\partial^2 V}{\partial \eta^2} - \frac{h^3}{6}\frac{\partial^2 V}{\partial \eta^3} + \ldots \qquad (4\text{-}28)$$

Substituting these into the finite difference equations (4-28) gives the following differential equations which are in effect being solved for by the PRADI solution scheme.

$$\frac{\partial^2 B}{\partial \eta^2} + \frac{h^2}{12}\frac{\partial^4 B}{\partial \eta^4} + M\frac{\partial V}{\partial \eta} + \frac{1}{6}h^2 M\frac{\partial^3 V}{\partial \eta^3} + \ldots = 0$$

$$\frac{\partial^2 V}{\partial \eta^2} + \frac{h^2}{12}\frac{\partial^4 V}{\partial \eta^4} + M\frac{\partial B}{\partial \eta} + \frac{1}{6}h^2 M\frac{\partial^3 B}{\partial \eta^3} + 1 + \ldots = 0 \qquad (4\text{-}30)$$

The difference between these equations and the original MHD equations is the error term involved in the finite difference approximation being made. Taking only the first term in each of the series as the primary source of error (Z), it is desirable to adjust the spacing to keep these terms as small as possible without making the number of nodes prohibitively large. The error terms are

$$Z_1 = \frac{h^2}{6}\left[\frac{1}{2}\frac{\partial^4 B}{\partial \eta^4} + M\frac{\partial^3 V}{\partial \eta^3}\right]$$

$$Z_2 = \frac{h^2}{6}\left[\frac{1}{2}\frac{\partial^4 V}{\partial \eta^4} + M\frac{\partial^3 B}{\partial \eta^3}\right] \qquad (4\text{-}31)$$

The complete solution to the expanded finite difference series is not known, but since it is desired to have it approximate the original one-dimensional solution, it is possible to substitute into the equations

the Hartmann solution which is known analytically. The known solution is given by the equations

$$V = C\left[1 - \frac{\cosh M\eta}{\cosh M}\right]$$

$$B = -\frac{\eta}{M} + C\frac{\sinh M}{\cosh M} \tag{4-32}$$

Substituting the derivatives of these quantities into the error terms gives the desired result of the primary error in terms of the Hartmann number and the spacing, namely

$$Z_1 = -\frac{1}{12} CM^4 h^2 \frac{\sinh M\eta}{\cosh M}$$

$$Z_2 = -\frac{1}{12} CM^4 h^2 \frac{\cosh M\eta}{\cosh M} \tag{4-33}$$

Comparing the error term for the momentum equation (Z_2) with the major term in the equation (4-27), which is the constant term equal to one, shows that the error relative to the equation is very small except in the boundary layer. In this region, where η=1, the relative error is comparable to CM^4h^2. For the Hartmann solution C goes as as $1/M^2$ so that the error can be kept at its same relative magnitude for all values of M by keeping (Mh) constant. This is exactly what is done with the above scheme of adjusting the nodal spacing to the boundary layer thickness a/M.

The problem with this scheme arises from the consideration of the error term for the induction equation. In this equation there are

only two terms, each of which is not constant but varies with position and Hartmann number. Comparing the relative magnitude of the error term with the second derivative of the B field gives the relative error

$$Z_1 \Big/ \frac{\partial^2 B}{\partial \eta^2} = -\frac{1}{12} M^2 h^2 \tag{4-34}$$

It can be seen that in this equation the relative error is not confined to the boundary layer but is constant for a given spacing and Hartmann number throughout the core region also. Therefore, keeping the (Mh) spacing constant in the boundary layer is not enough to maintain the finite difference as a close approximation to the differential equation, since using the large spacing in the core region to reduce the number of nodes is equally detrimental to the solution. Because the two equations are coupled together, the error is induced into both variables, V and B, and so it is not possible to correct the one equation alone, but the entire grid in the core must be adjusted to correct the problem.

The straight forward approach to the problem would be to simply extend the boundary layer spacing completely across the core region. But, at the large Hartmann numbers where this problem occurs, the number of nodes required would become prohibitively large, due to the storage requirements involved with the computer program and the time requirements to iterate to a solution for that many nodes. Looking at Figure 4-2, it can be seen that the largest error occurs at the

edge of the boundary layer and the solution nearly recovers the desired approximation by the time it reaches the center of the channel. This observation suggests an intermediate method of spacing the grid that is found significantly to reduce the error involved, while at the same time minimizing the number of nodes to be added.

The approach taken is to continuously vary the spacing linearly with each step from the boundary layer to the center of the channel, with the first step at the edge of the layer being taken as the same size as the spacing in the boundary. By simply doubling the number of nodes in the core region, the final spacing size at the center of the channel is approximately what it was in the previous scheme. This method then keeps the spacing at a small value at the edge of the boundary layer where it is needed to reduce the error term in the finite difference scheme, and then increases it to cover the most space with the fewest number of nodes toward the center, where empirically the error term plays less of a role, thereby reducing the amount of storage required.

This scheme places ten rows in the boundary layer and then for Hartmann numbers up to 100 adds 20 variably spaced rows in the direction of the core region. It was found that the spacing in the ξ direction did not require the addition of any columns for the Hartmann numbers solved for, so that the previous scheme was used in that direction. The final scheme used is sketched in Figure 4-3.

A comparison between the analytically derived Hartmann solution and the results of the finite difference calculations provides

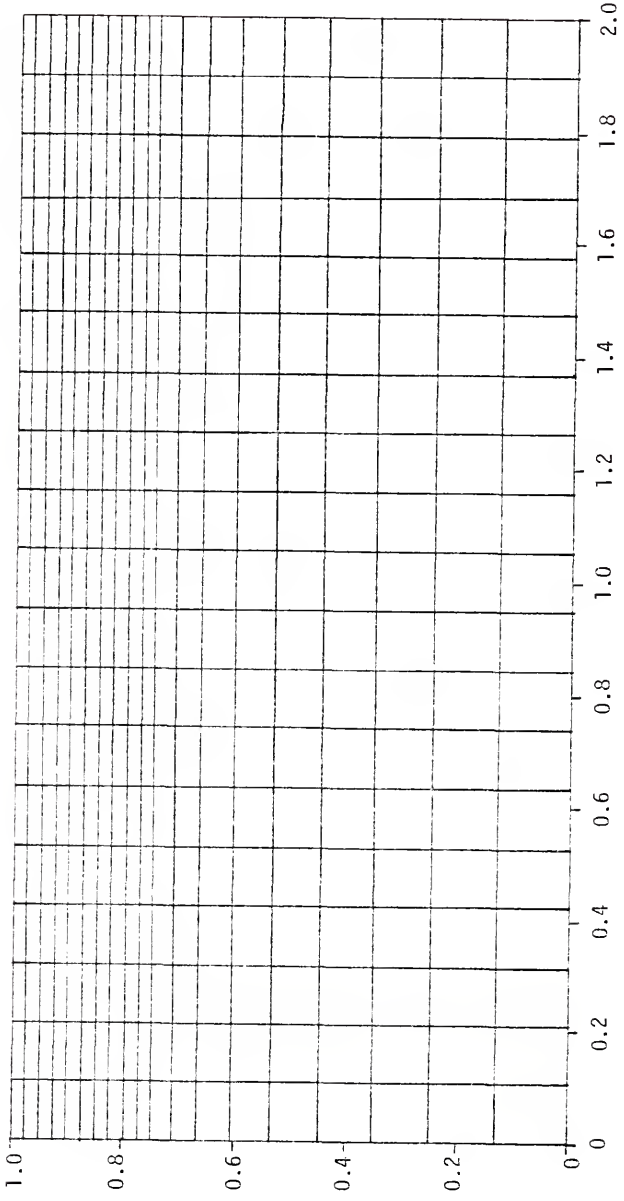

Figure 4-3. Variable Nodal Spacing within Quadrant

the easiest means of gauging the magnitude of the errors involved in the entire method. For this comparison a finite difference case is solved for large aspect ratio and Hartmann number to minimize the effects of the electrode end plates and make the solution as one dimensional as possible. The comparison is then taken with the vertical row of nodes down the center of the channel where the derivatives in the ξ direction are negligible. It would be possible to compare the solution with certain of the specialized two-dimensional cases that do happen to have analytical results, but these cases are given in terms of long series solutions that are somewhat difficult to evaluate.

The results of the comparison with the Hartmann case are given in the following table along with the relative error at each nodal location. The value of the magnetic flux density is specified at the center of the channel and at the wall, along with the value of the velocity at the wall, so that the relative error goes to zero at these points. It is interesting to note that the error in the velocity goes to zero at the center of the channel even though the first derivative and not the value is specified there. Presumedly this is due to some integral condition that the finite difference equations satisfy as well as the differential equation does.

Other than these points the error is still kept within a reasonable amount for the size of the spacing chosen in the boundary layer (Mh=0.5). It can be assumed that the error in the core region will increase from these very low values when the conductivity is

TABLE

COMPARISON OF FINITE DIFFERENCE ERRORS
M=20, R=4, Y=10

	FINITE DIFFERENCE		HARTMANN APPROXIMATION		PERCENT ERROR	
η	$Vx10^5$	$Bx10^5$	$Vx10^5$	$Bx10^5$	V%	B%
0.000	1042	0	1042	0	0.0	0.0
0.201	1042	-1007	1042	-1007	0.0	0.0
0.380	1042	-1897	1042	-1897	0.0	0.0
0.603	1041	-3016	1041	-3015	0.0	0.0
0.775	1031	-3865	1030	-3863	0.1	0.1
0.800	1024	-3983	1023	-3981	0.1	0.1
0.825	1013	-4096	1010	-4094	0.3	0.1
0.850	993	-4201	990	-4198	0.3	0.1
0.875	961	-4294	956	-4289	0.5	0.1
0.900	907	-4365	901	-4359	0.7	0.1
0.925	817	-4400	809	-4393	0.9	0.2
0.950	667	-4375	659	-4367	1.2	0.2
0.975	417	-4250	410	-4243	1.6	0.2
1.000	0	-3958	0	-3958	0.0	0.0

allowed to vary and the other terms in the finite difference equation come into play.

Iteration of the B_1 Boundary Condition

It has been mentioned previously that the value of the magnetic flux density at the insulating wall is a boundary condition that is directly related to the net amount of current flowing through the external circuit, but that this is not the quantity that is desired for a fundamental parameter of the problem. The value of the resistance in the external circuit is what is wanted, and this can be related to the magnetic field boundary condition by the relation (2-23),

$$B_1 = \frac{1}{\gamma R + W_R}\left[W_R\int_0^1 B(\eta)\Big|_{\xi=\gamma} d\eta - \int_0^\gamma F\frac{\partial B}{\partial \eta}\Big|_{\eta=1} d\xi\right]$$

The quantities on the right-hand side are known quantities except for the two integrals that must be evaluated from the finite difference solution. The first integral is evaluated in the simplest and most straightforward manner, by using the average value of the two nodes on each interval in the desired line of integration and multiplying by the distance between the nodes. The sum of these quantites is then a simple and effective approximation to the integral.

The second integral is evaluated in a similar manner except the value of the derivative along the wall must first be determined. This is calculated from the value at the wall and at the nodes immediately adjacent to it, with several degrees of approximation being

possible, depending on the number of nodes used. In general, the greater the number of nodes used, the greater will be the accuracy of the approximate derivative. For the purposes of this problem a four-point fit is found to give satisfactory values (Hamming 1973). This approximation is given by

$$\frac{\partial B}{\partial \eta} = aB_{n-3} + bB_{n-2} + cB_{n-1} + dB_n$$

where n is the number of the node at the wall, and the coefficients are determined to give the best possible fit for the lowest order polynomials. These are given by

$$a = [(\eta_{n-2}-\eta_n)(\eta_{n-1}-\eta_n)]/[(\eta_{n-3}-\eta_{n-2})(\eta_{n-3}-\eta_{n-1})(\eta_{n-3}-\eta_n)]$$

$$b = -[(\eta_{n-3}-\eta_n)(\eta_{n-1}-\eta_n)]/[\eta_{n-3}-\eta_{n-2})(\eta_{n-2}-\eta_{n-1})(\eta_{n-2}-\eta_n)]$$

$$c = [1 - a(\eta_{n-3}-\eta_n) - b(\eta_{n-2}-\eta_n)]/(\eta_{n-1}-\eta_n)$$

$$d = -a - b - c$$

These are defined for a generalized nodal spacing which may be used in some future calculation. For the present set up the spacing in the boundary layer is constant so that in essence the approximation is given by

$$\frac{\partial B}{\partial \eta} = \frac{1}{6h}\left[-2B_{n-3} + 9B_{n-2} - 18B_{n-1} + 11B_n\right] \qquad (4\text{-}36)$$

The value of the magnetic induction boundary condition can then be found once the finite difference solution is known. Since

this is impossible to know until the boundary condition is set, an iteration scheme is required to relax to a solution. Although a better calculation of the boundary condition would be obtained by iterating several steps at a given value until the solution had reached an approximate steady state, it is felt that this method wastes too much calculation time converging on the wrong boundary value. Therefore, the method used calculates a new boundary value on each iteration of the PRADI solution.

Changing the boundary condition on each iteration has one serious disadvantage in that it invalidates the assumption made in the derivation of the PRADI method, that the boundary conditions were constant in time so that the solution will relax to the steady state. By removing this condition an instability is added to the calculation where a change in the boundary value is immediately fed back into the determination of the next change through its alteration of the values adjacent to it in the boundary layer. It is found by experimenting with various methods that the instability does not arise if the boundary condition is varied smoothly in small increments. This suggests the inclusion of the following under-relaxation scheme into the calculation of the boundary condition to be applied on the next iteration, namely,

$$B_1^{n+1} = B_1^n + \omega(B_1^{n+1} - B_1^n) \qquad (4\text{-}37)$$

Here the under-relaxation parameter (ω) has a value less than one and is used to insure that the change in the boundary condition lags behind the rate of convergence of the solution. Not only

the absolute stability but also the rate of convergence on the final answer is dependent on the proper choice of the value of this relaxation parameter. Noting the constants multiplying the integrals in the calculation of B_1^{n+1} (2-23) it can be seen that the sensitivity of the boundary value calculation to changes in the integral terms is dependent on the value of the resistance and conductivity ratios, and the aspect ratio. Using the relation of these constants as an indication of the "gain" in the feedback for each iteration, and applying arbitrary constants in place of the integrals, an empirical relation for the value of the relaxation parameter is given as

$$\omega = (\gamma R + W_R)/(175.\gamma + 7.W_R) \qquad (4\text{-}38)$$

Here the arbitrary constants are determined by performing several calculations for various values of the resistance ratio, conductivity ratio, and aspect ratio and then finding the value of the relaxation parameter that produces the fastest rate of convergence. The constants in the relation are then fit in the least squares sense to these optimum parameters. This empirical relation is found to give satisfactory results throughout the range of the parameters involved in this study. It should be noted that for large values of the resistance ratio the relaxation parameter becomes greater than one since the value of the boundary condition approaches zero in all cases no matter what the value of the integrals are. For these calculations this is not allowed to happen and the relaxation parameter is fixed at a maximum value of one.

With the added relaxation that must be made, there is a noticeable increase in the number of iterations that are required. At the lower values of the Hartmann number (M=20) the increased amount of calculation is modest, since the total number of iterations is small. But the total number of iterations for the PRADI relaxation seems to increase linearly with the Hartmann number, and the addition due to the boundary value relaxation becomes increasingly severe at the higher values (M=100).

To keep the number of iterations and the computer time required to a reasonable value for a given set of conditions, it is found that for Hartmann numbers greater than 50 it is better to use the boundary conditions given by the one-dimensional Hartmann approximation. The resistance ratio that is solved for can then be calculated using the same relation that is used to calculate the B_1 boundary value. This in effect sets the total net current through the generator and then calculates the load conditions that are solved for. This significantly reduces the number of iterations that must be made, while at the same time it is not too detrimental to the usefulness of the calculations, since the Hartmann solution gives an excellent approximation to the boundary value if the Hartmann number is large and the aspect ratio is greater than one. The need to calculate the final resistance ratio that has been solved for is only cumbersome if one is attempting a correlation based on a specific value of the load resistance.

Boundary Condition on the Finite Conductivity Electrode

In order to consider the effect of having an electrode of finite conductivity rather than being perfectly conducting it is necessary to implement the boundary condition (2-16) at the nodes on the electrodes given by

$$\frac{\partial B}{\partial \xi} = \frac{W_R}{F} (B_1 - B(n))$$

This must be used in two places: first in the finite difference equation (4-12) for the calculation of the B* values, and second in the solution of the next time step for B in the column of nodes at the electrode surface.

In both cases it is necessary to know the value of the variable at the $m+1^{th}$ node location, which is a node that is not in the grid. To find this value, the differential in the above equation is broken up into its finite difference approximation with the assumed spacing to the next node the same as from the last. The value at the $m+1^{th}$ node is then given in terms of the value at the $m-1^{th}$ node and the value of the differential by

$$B_{m+1} = B_{m-1} + 2(\xi_m - \xi_{m-1}) \frac{W_R}{F} (B_1 - B_m) \qquad (4\text{-}39)$$

The relation for the B* term is identical. This is what is substituted into the finite difference equation (4-12) for B* with the value of B_m in (4-39) given by the value at the n^{th} time step.

On the surface of the electrode the boundary condition on the velocity is zero. Therefore the velocity is known and the two equations (4-12) for the prediction of the next time step (n+1) decouple leaving a simpler set of finite difference equations for the value of B^{n+1} on this column of nodes. This now becomes a simple tridiagonal system as was the finite difference equations for the V* and B* terms.

Again the value of B* at the $m+1^{th}$ node is required and the above relation (4-39) is substituted as before. But in this case the value of B_m required in the evaluation of the differential is available implicitly in each equation of the system. Therefore this term in the differential is shifted to the left-hand side of the difference equation, where it is evaluated implicitly using the value of B_m at the $n+1^{th}$ time step.

There are two extremes of the conductivity that should be noted. If the electrode is to be considered perfectly conducting, the conductivity ratio is equal to zero, as is the derivative of B for the boundary condition (4-39). In this case the above complication is eliminated and the iteration on the value of B_m for the boundary condition (4-39) is removed from the finite difference equations.

The other extreme is when the electrode is nonconducting and the channel is insulating at each of the four walls. In this case the conductivity ratio is infinite. Since the derivative of the B field must be finite at the boundary, this implies from the equation (4-39) for the derivative that the value of B on the insulated

electrode is equal to the B_1 boundary condition. This simplifies the calculations on the column of nodes at the surface of the electrode since both B and B*, as well as the values for the velocity, are then known. The value of B at these nodes, and the value of B*, which is needed for the interior calculations, are set equal to the current estimate of the boundary condition B_1 for each iteration.

If the conductivity of the electrode is set to zero while at the same time the external load resistance remains infinite, the situation is one where a net current flows out of the generator through an electrode that does not conduct electricity. This produces a conflict in the set boundary conditions on the node at the center of the electrode. It must be set equal to the value of B_1, which is finite due to a net current flowing out, but at the same time it is equal to zero, as was assumed previously, since it is on the center line of the channel. This conflict is resolved by setting the value of B at the center node equal to zero with the difference between this and the other nodes of the electrode indicating that all the net current out of the channel flows out through the spacing between the first two nodes. The interpretation of this solution is that the current is not allowed to flow down the electrode since it is non-conducting, but can still flow across the electrode, where the current is tapped out of the channel in the center.

Initial Guess

In any relaxation scheme it is necessary to supply some arbitrary initial values from which to start the relaxation process.

Although the PRADI method can relax to the correct solution from almost any starting function, the modifications made to the method, where the one boundary condition must also be relaxed, means that the absolute convergence of the method for any given initial guess cannot automatically be assumed. It is desirable for the initial calculation of the B_1 boundary condition to be fairly close to the actual final value. The one-dimensional Hartmann solution provides a very effective approximation for most cases, and has the advantage that it can be solved in closed form for a given value of the load resistance and Hartmann number. Since extreme accuracy is not necessary, the hyperbolic functions in the solution have been approximated with the simpler exponential to give the functions for the initial guess, namely

$$V = \frac{1+R}{M(M+R)} [1 - \exp M(1-\eta)]$$

$$B = -\frac{\eta}{M} + \frac{1+R}{M(M+R)} \exp M(1-\eta) \qquad (4\text{-}40)$$

These values are applied along each column of nodes for the entire width of the channel. Since the Hartmann solution is strictly applicable only for the case of infinite aspect ratio, this initial guess is not a close approximation in the boundary layer on the electrodes. This means that the majority of the relaxation is being done in the electrode boundary layer with just minor adjustments being necessary to the initial guess in the center of the channel.

In the case where the aspect ratio of the channel is small, the electrode boundary layers will extend to the center of the channel. At this point it is no longer helpful to use the Hartmann approximation, since most of the nodes will not be close to its values. For these cases it is found empirically that the solution will converge faster if the initial values are simply chosen to be zero. This is then the initial guess applied when the aspect ratio is less than one.

Convergence Criterion

The relaxation procedure, once started, continues iterating forever unless a criterion can be derived that indicates when further iterations do not produce any significant increase in accuracy. The accuracy obtained and the number of iterations necessary depend on the nature of what one considers to be a converged solution.

The testing for the convergence of the solution is done by comparing the value of the variables, V and B, at each node with the value at the previous iteration. Since this absolute difference does not tell the significance of the error left in the solution, it is divided by the maximum value of the variable to give the relative difference in convergence. The maximum value for the velocity variable is found at the node in the center of the channel, while the magnetic flux density is maximum at the edge of the boundary layer on the insulating walls and centered between electrodes.

The magnitude of this relative convergence is dependent on the size of the iteration parameter (k) specified for a given iteration. It is desirable to let the iteration parameter be a variable

quantity that can be changed for a given case or within a given run so that an optimum rate of convergence per iteration can be achieved. Therefore the relative convergence is not used as the test, but the slope of this with respect to time is. This gives the following criterion for testing the convergence at each node, where ε is the convergence parameter.

$$\frac{\Delta V}{kV_{max}} \leq \varepsilon \tag{4-41}$$

A similar relation is written for the B variable. The nodes at different locations in the grid converge at different times with each variable not necessarily converging simultaneously at each node. Therefore, the nodes are tested individually for convergence, but the final solution is not considered converged until all the nodes are simultaneously converged with respect to the criterion for each of the variables.

The value of the convergence parameter (ε) is determined by experimentation with several solutions for different cases. It is desired to obtain numerical accuracy to four significant places for all cases. A choice of the convergence parameter of 0.05 is found to achieve this degree of accuracy for a large range of conditions. But the parameter is found not to be universally constant, since it is seen to be dependent to some extent on the Hartmann number. For Hartmann numbers less than 20 the parameter has to be decreased to 0.01 to obtain the four-place accuracy, while at Hartmann numbers

approaching 100 and above the parameter can be increased to shorten the number of iterations and still maintain accuracy.

The choice of the value of the iteration parameter (k) can also be a significant factor in determining the number of iterations required for convergence. If it is chosen too small, the procedure wastes a number of iterations where the time derivatives of the variables are linear and the values are converging at a uniform rate for each iteration. If it is chosen too large, there is too much variation in the time derivatives within a given iteration, thereby giving an erroneous prediction for the next iteration. This causes the scheme to overpredict the corrections to the values required, and converge in a back-and-forth manner about the steady-state value.

Mitchell's book (1969) analyzes the ability of the PRADI method to converge to a given solution and shows that eventually the steady state will be reached no matter what the value of the iteration parameter is. It is clear, though, that the efficiency of the scheme in terms of the number of iterations required will vary with the choice of its value. Mitchell refers to the work of Wachpress (1957) and Douglas (1962) who derive, under a series of limiting assumptions, some optimum series of values that increase the value of the iteration parameter at each step, and are meant to accelerate the rate of convergence to its maximum value. It is found through experimentation that these series do not significantly aid in reaching the steady state, presumably due to the several cases where the underlying assumptions are not met.

This analysis was helpful, though, in indicating that the iteration parameter should be sized according to the spacing between nodes, and in presenting a way to moderate the initial large rates of change from the initial guess. To size the iteration parameter in this manner, it is necessary to select the nodal spacing for comparison, since there are numerous spacings in the variable set up described. It is found that the smallest spacing, which was the spacing in the η direction in the boundary layer, provides the most significant value on which to base the parameter size. Starting for the initial iteration at a value of half this spacing squared, and using the idea of Wachpress and Douglas to accelerate the size smoothly, the value of the iteration parameter is increased geometrically in the space of four iterations to its maximum value. It is found through trial and error that a maximum value of fifteen times the minimum spacing squared proves to be approximately optimum for most cases. This scheme provides small values of the iteration parameter to step closely through the initial fluctuations and then steps smoothly to the high values to speed up the rate of convergence, when only the smaller error displacements were left.

CHAPTER V
NUMERICAL RESULTS

The problem of steady laminar flow of a conducting fluid in the presence of a transverse magnetic field can now be solved numerically for the boundary conditions appropriate to a generator channel with the added possibility of including the effects of variations in the conductivity and viscosity within the cross section. Although this solution may not compare well quantitatively with real generator channels, because of the longitudinal variations that have been neglected, such as the entrance and exit effects, it can still be a very effective qualitative tool for analyzing the relative improvement or deterioration to be expected from a given variation in the channel parameters. It also is able to give the magnitude of the two-dimensional and variable conductivity effects, so that it can be determined when the approximate analytical solutions are sufficiently accurate for engineering purposes and it is unnecessary to continue with the full channel solutions.

The properties of the numerical technique selected, that make it such an effective tool for this analysis, are its balance between the storage requirements and the speed of finding the solution. This allows each set of conditions to be solved for with a minimum of expense in computer operations, thereby making it possible to do the large number of runs needed to obtain enough data points to plot

curves of the desired parameters with respect to the many variables of the generator geometry.

The results discussed in this chapter are presented for the purpose of illustrating the effects to be encountered in working with the magnetohydrodynamic generators. For this purpose the effects are demonstrated for Hartmann numbers less than 100, where they are greater in magnitude and are more easily seen. These results will be effective in giving insight into the generator problem, with the analysis of a specific generator condition being left to the longer runs required for Hartmann numbers greater than 100, or for analysis by the approximate analytical methods that become very accurate at these larger values. Because the approximate analytical expressions (mainly the Hartmann flow equations) are effective in describing the flow and giving insight to the problems of the generator, they are often used as comparisons for the numerical results and given as examples of the best that can be achieved in many cases.

Velocity Contours and Current Streamlines

Once the values of the velocity and induced magnetic field have been calculated at each of the nodes of the grid, the most effective way of displaying the major aspects of the solution is to calculate and plot the contours of constant velocity and constant magnetic flux density. For the case of the magnetic flux density the contours will represent streamlines of the current density. An example of this is given in Figures 5-1 and 5-2 where the calculations are made for a Hartmann number of 20 and a load factor of 0.95.

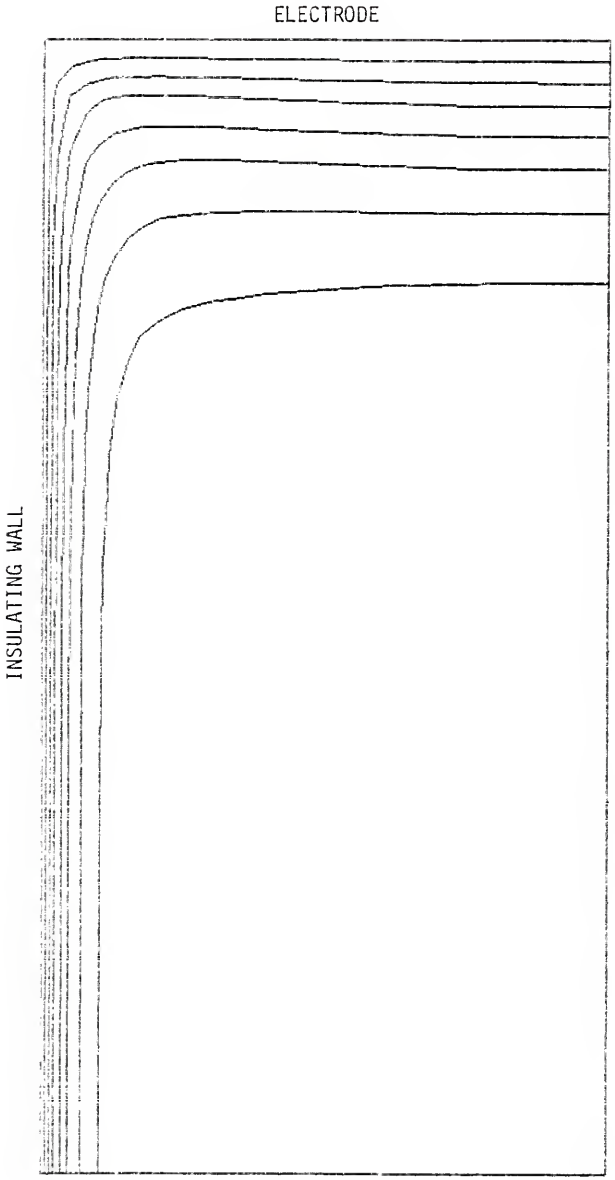

Figure 5-1. Velocity Contours M=20, K=0.95

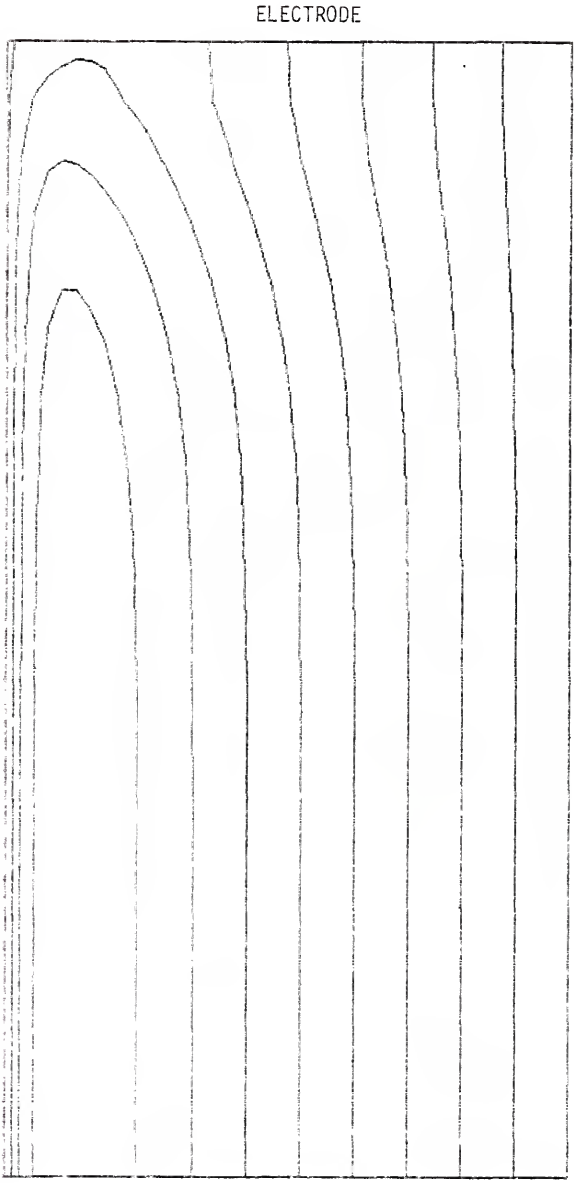

Figure 5-2. Current Streamlines M=20, K=0,95

For the qualitative purposes of describing the flow field the contours may occur at any constant value, but for the purpose of maintaining a reasonable number of contours in the plot the value of the step between each contour is based on the maximum value of the variable to be found in the cross section. In the case of the velocity field the maximum value will always occur at the node in the center of the channel. For this plot, and all the subsequent ones, the contour lines are plotted in eight equal steps from zero at the wall to the maximum value. In the case of the magnetic flux density the maximum value occurs at the edge of the boundary layer, at a node that is not the same in every case. For this reason an approximate maximum that is more consistent is used. This is the value of the magnetic flux density at the insulating wall given by the one-dimensional Hartmann solution when the generator is short circuited and the load factor is zero. In the following plots one-tenth of this value is used as the spacing between current streamlines.

The location of the contours is found by simple linear interpolation between the values of the variable at adjacent nodes until the constant value of the contour is found. This gives a series of points on the vertical and horizontal lines of the grid which are then connected by straight lines in a logical sequence. The smoothness of the contours then depends on the closeness of the spacing between nodes and the degree of linearity of the function. Since for these plots most of the curvature in the contours of the velocity and current streamlines occurs in the boundary layers where the spacing is

compressed, this scheme of contour plotting is adequate for display purposes. In later plots, when the conductivity is allowed to vary in the core region where the spacing is greater, the contours appear less smooth but are still qualitatively demonstrating the effects to be discussed.

In these plots the contours are given for only one-fourth of the channel in the upper right-hand quadrant, with the other quadrants being reflections of these plots about the center lines (ξ=0 and η=0). This follows from the symmetry conditions imposed in the derivation of the governing equations and boundary conditions and the symmetery imposed on the conductivity and viscosity variation. For the most part it is not even necessary to know in which direction the current flows down the streamlines, since the current flows into the electrode in the same way that it leaves it in the other quadrants. The plots shown are calculated for an aspect ratio of two in most cases, with the dimensions of the channel being geometrically similar to the dimensions of the quadrant plotted.

The contours of constant velocity plotted in Figure 5-1 demonstrate the main features of the flow that have been discussed previously. The most obvious feature is that all the gradation in the velocity occurs in the boundary layer adjacent to the walls, with the central core region being one of uniform velocity. It is also apparent that the boundary layer on the insulating wall is considerably thinner than the boundary layer on the electrode. This is confirmation of the fact stated and used previously that the Hartmann layer on the

insulating wall scales on the inverse of the Hartmann number, while the boundary layer on the electrode scales on the inverse of the square root of the Hartmann number.

An interesting feature of the boundary layer on the electrode is that it becomes thicker in the center of the electrode when compared to profiles closer to the corner. This can be seen by noting that the inner contours move out away from the electrode as they approach the center. It should also be mentioned that in all the calculations done in this study there is no consideration of any secondary flows in the ξ and η direction that might arise due to the corner of the rectangular channel. These secondary flows are known to arise in the ordinary hydrodynamic case and to play a significant part in the description of the flow versus the pressure drop. But in the magnetohydrodynamic case flow of the conducting fluid in the ξ direction is suppressed since it must cross the line of the applied magnetic field. The assumption is then made, but not proven, that all recirculating secondary flows are suppressed by the applied magnetic field and the fluid flows only in the direction down the channel.

The main features of the current streamlines are demonstrated in Figure 5-2 for the same channel conditions as the velocity field just described. For the core region outlined by the velocity contours, the current streamline plot shows a broad band of equally spaced streamlines. This indicates the uniform nature of the current field, where all the current is in the ξ direction and of equal density.

The current does not deviate from this uniform nature until it encounters the boundary layers. In the electrode boundary layer the streamlines spread out, indicating a loss of current density, with only the streamline at the center of the channel remaining straight. The outer lines deviate farther from straight, with the lines near the insulating wall reversing direction and returning by way of the conduction path provided by the low velocities in the Hartmann boundary layers. It is seen that it is not necessary for the current streamlines to ever arrive at an electrode. But those that do must straighten out and arrive perpendicularly to the electrode. This is necessary in this case because the electrode is assumed perfectly conducting and is therefore of equal voltage potential. It should be noted that while current is flowing into the center of the electrode, it is also flowing out of the edges and into the Hartmann layers to return to the electrode at the other side of the channel.

The closed contour of the streamline at the edge of the boundary layer indicates that the maximum of the magnetic flux density occurs in its center. The zero line occurs for the streamline proceeding along the centerline of the channel.

It is important to note in both the plot of the contours of constant velocity and the plot of the current streamlines that as long as the contours are outside of the electrode boundary layer, they are strongly one-dimensional in character, with essentially no variation in the ξ direction. This demonstrates the reason for the

success of the one-dimensional Hartmann approximation in describing the flow of the two-dimensional channel.

Variation with Load Factor

The effect of changing the load factor for a given set of channel conditions can be seen in Figures 5-3 through 5-8. One primary effect is the lack of major change in the velocity profiles. For the entire range of load factors, from short circuited to insulated, the profile is essentially unaffected in the contours as to their shape and the thickness of the boundary layers. This is not to say that the magnitude of the velocity itself is unaffected, because it does change in a very similar fashion to the one-dimensional Hartmann solution. But since the contours are chosen on the basis of the maximum velocity in the cross section there is no apparent change in the plots.

The plots of the current streamlines show a much more pronounced change in their characteristics as the load factor is varied. Figure 5-6 shows that as the load resistance is lowered the current streamlines become straighter with only a slight deflection of the outer line in the boundary layer. The load resistance chosen here is that at which the efficiency would be maximum for the one-dimensional case and is approximately so for these conditions. Rather than three streamlines returning by way of the Hartmann layer as in Figure 5-2, now only two fail to reach the electrode. This is due to the lower voltage potential on the electrodes forcing the current into the

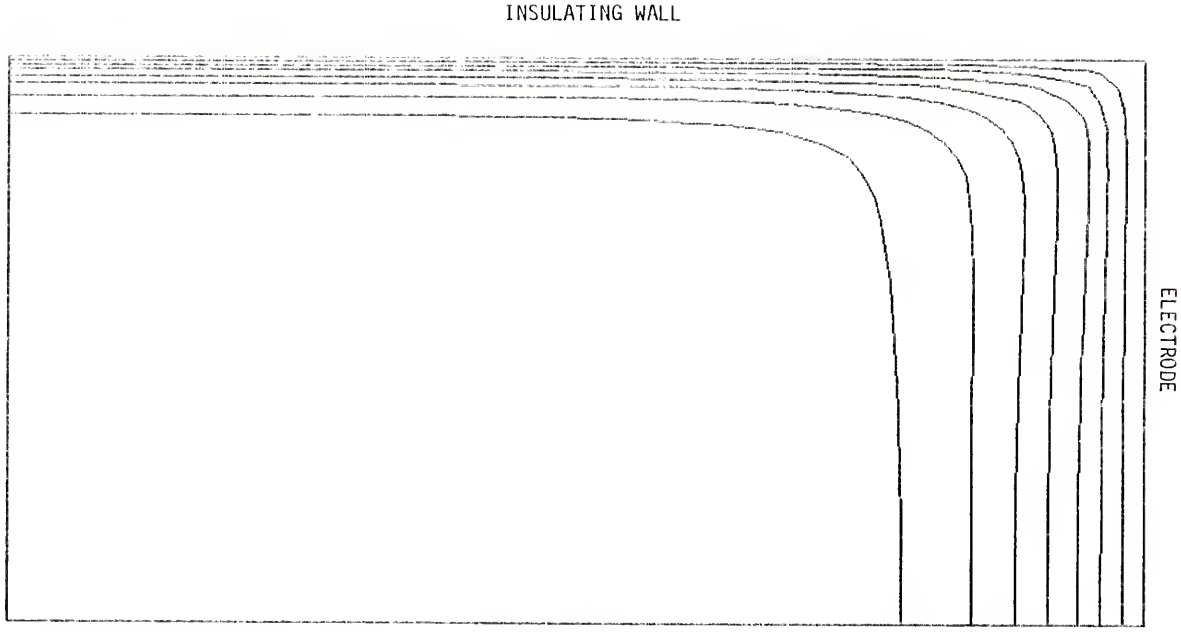

Figure 5-3. Velocity Contours M=20, K=0

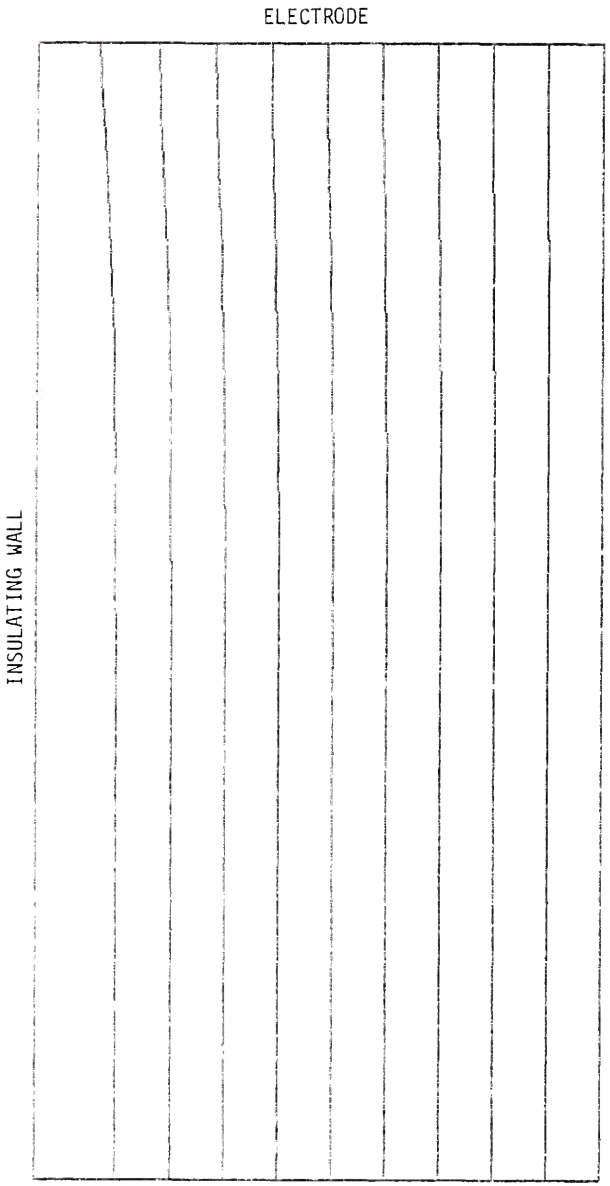

Figure 5-4. Current Streamlines M=20, K=0

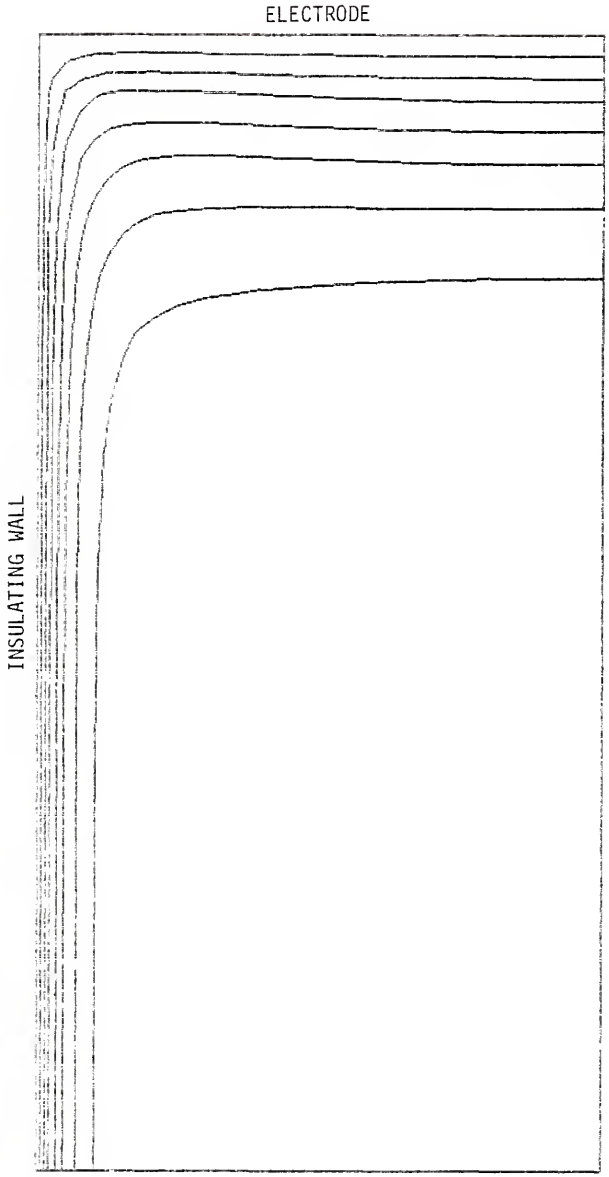

Figure 5-5. Velocity Contours M=20, K= 0.82

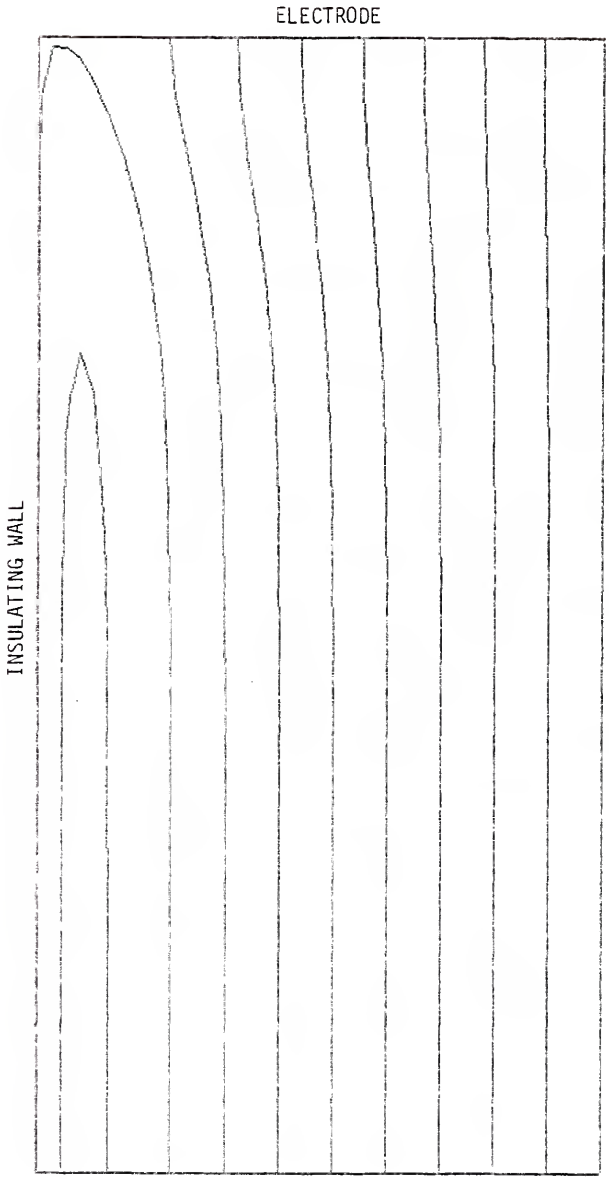

Figure 5-6. Current Streamlines M=20, K= 0.82

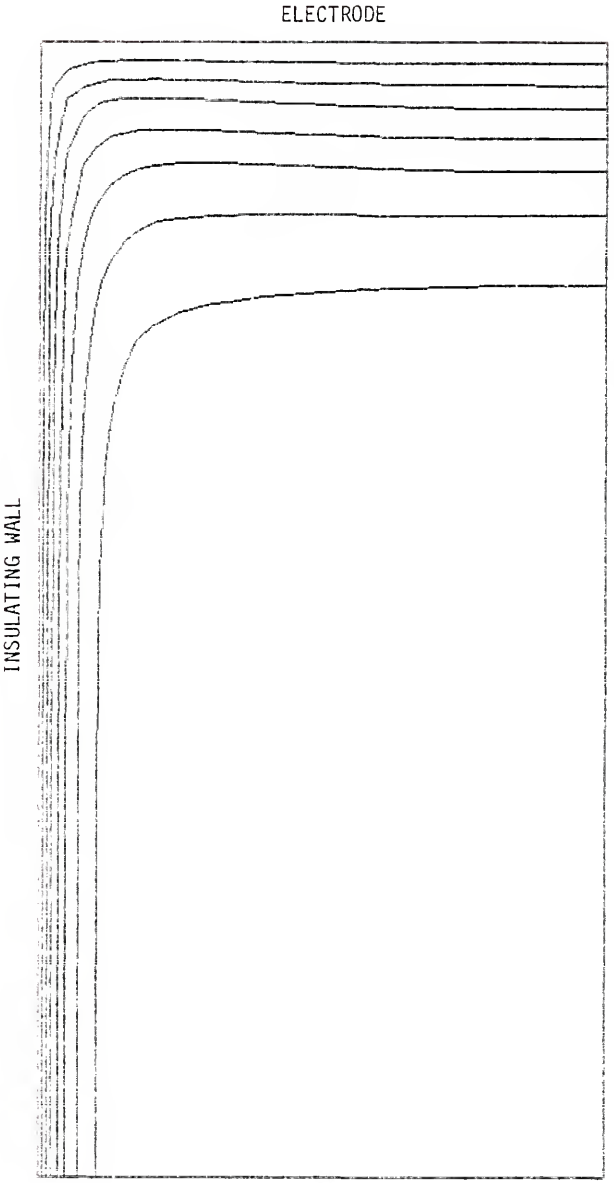

Figure 5-7. Velocity Contours M=20, K= 1.0

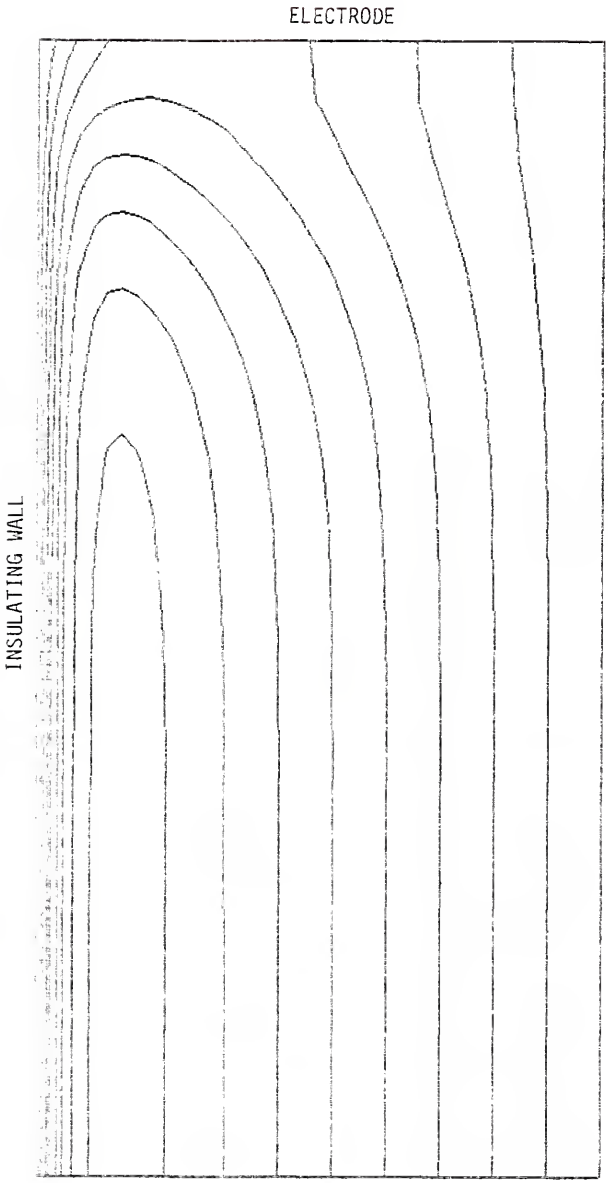

Figure 5-8. Current Streamlines M=20, K=1.0

Hartmann layers. As the load resistance is lowered, there is less return current, until the case shown in Figure 5-4 is reached, where the electrodes are short circuited and no return current flows in the boundary layer.

Figure 5-8 shows the contours when the load resistance is increased to infinity so that the electrodes are insulated from each other. Here the boundary condition on the magnetic induction is that it equals zero at both the center of the channel and on the insulating wall. Therefore the same number of streamlines leave the electrode as enter it, indicating that there is no net current through the channel. The current merely runs down the perfectly conducting electrode to exit into the Hartmann boundary layers.

It should be noted that in the core region of the flow all the current streamline plots are the same. This is reasonable since the current density has been shown to depend only on the Hartmann number in this region and the reference for choosing the values of the contours is also independent of the load resistance. The only effect of the external resistance on these plots is to determine how much of the current will be turned back into the Hartmann layer.

Variation with Electrode Conductivity

In real generators the electrodes can never be perfectly conducting as in the cases described above. The effect of using electrodes with a finite conductivity is shown in Figures 5-9 through 5-14. The current streamlines are now seen to no longer proceed perpendicularly into the electrode, since now the electrical potential

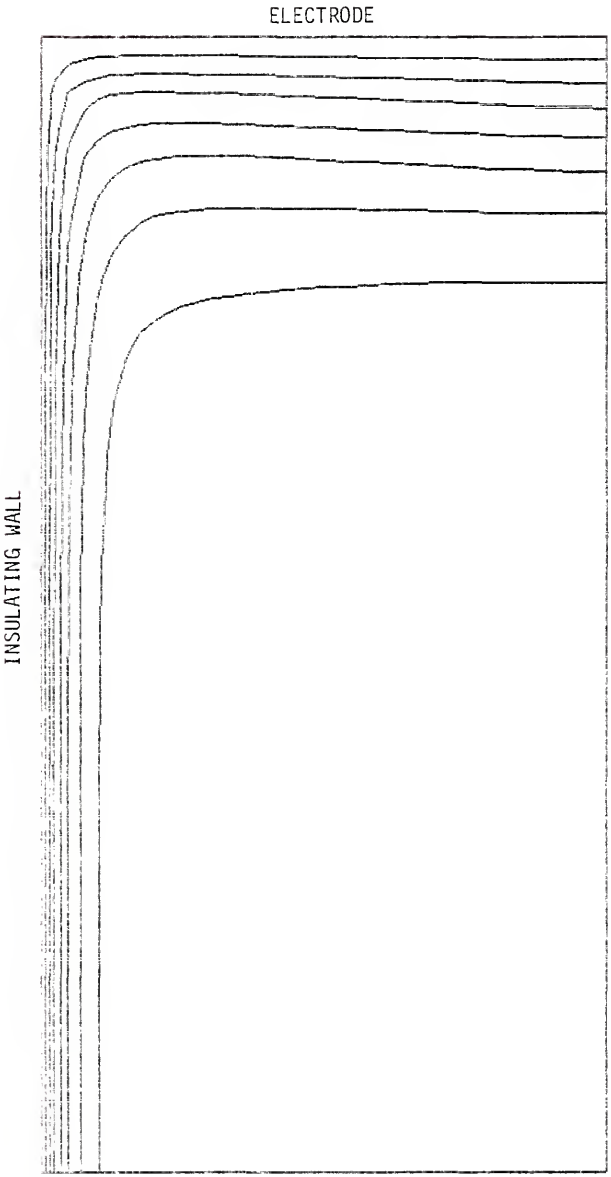

Figure 5-9. Velocity Contours M=20, K=0.95, K_w=0.5

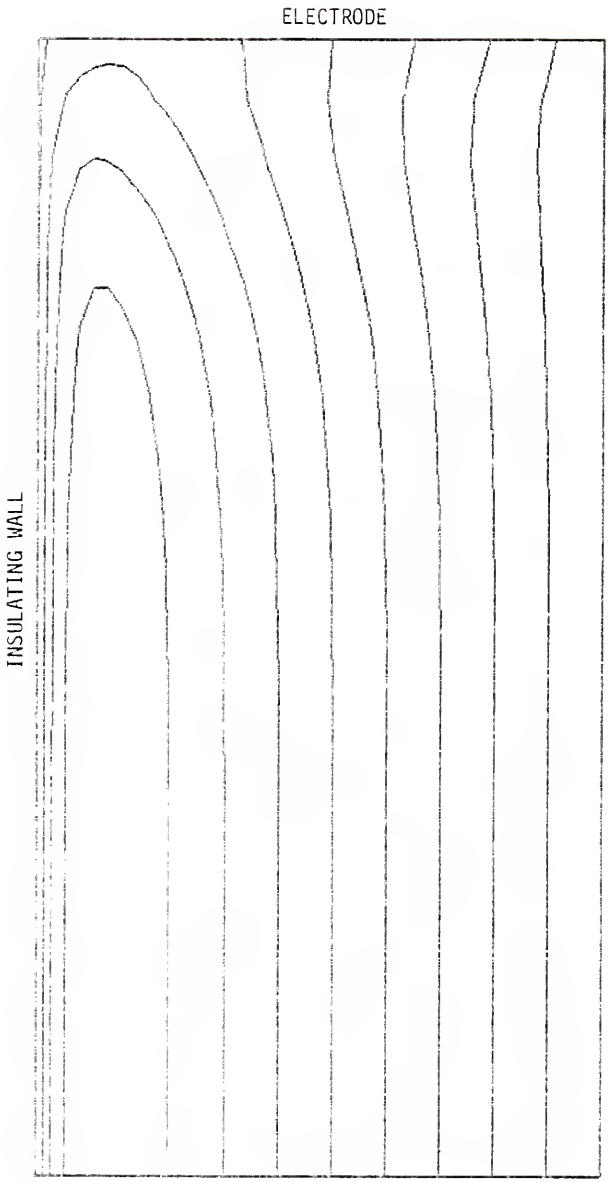

Figure 5-10. Current Streamlines M=20, K=0.95, K_w=0.5

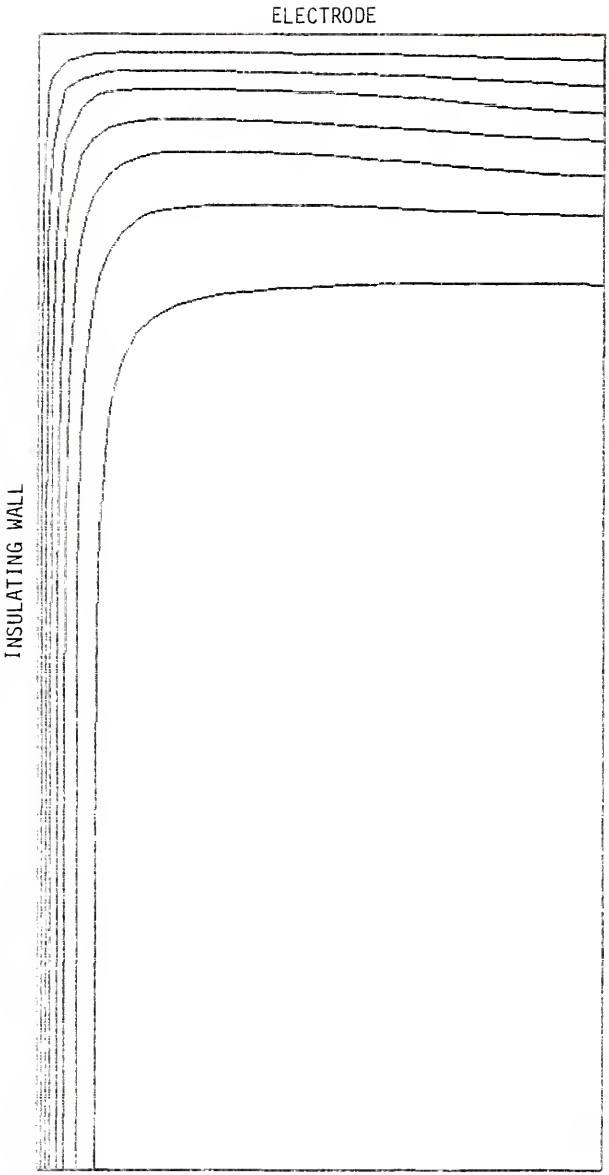

Figure 5-11. Velocity Contours M=20, K=0.95, K_w=0.75

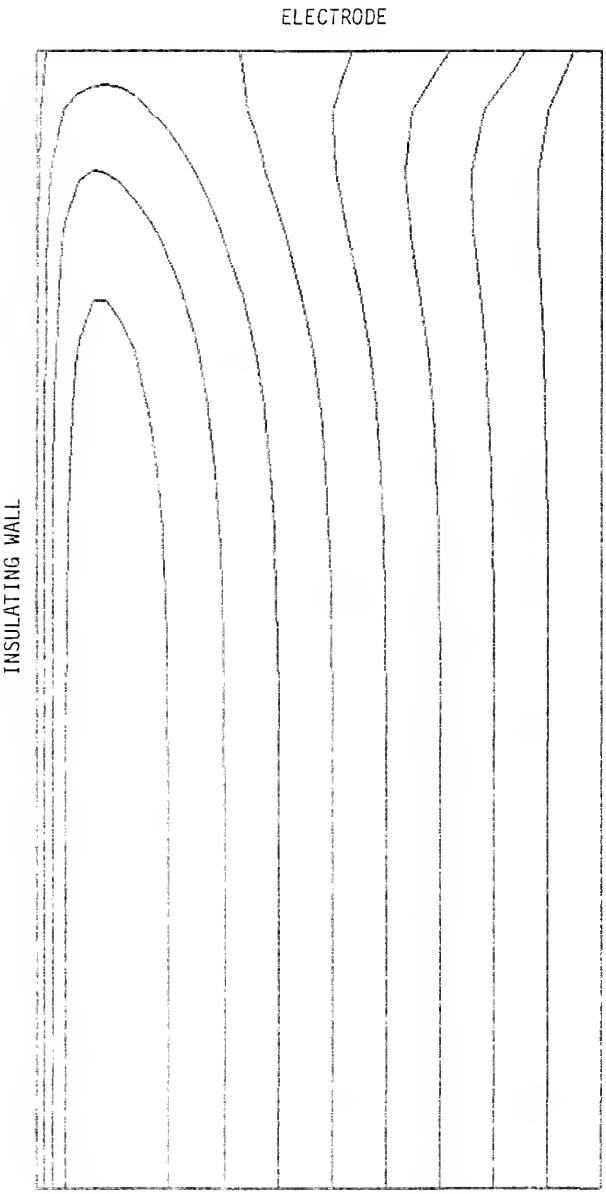

Figure 5-12. Current Streamlines M=20, K=0.95, K_w=0.75

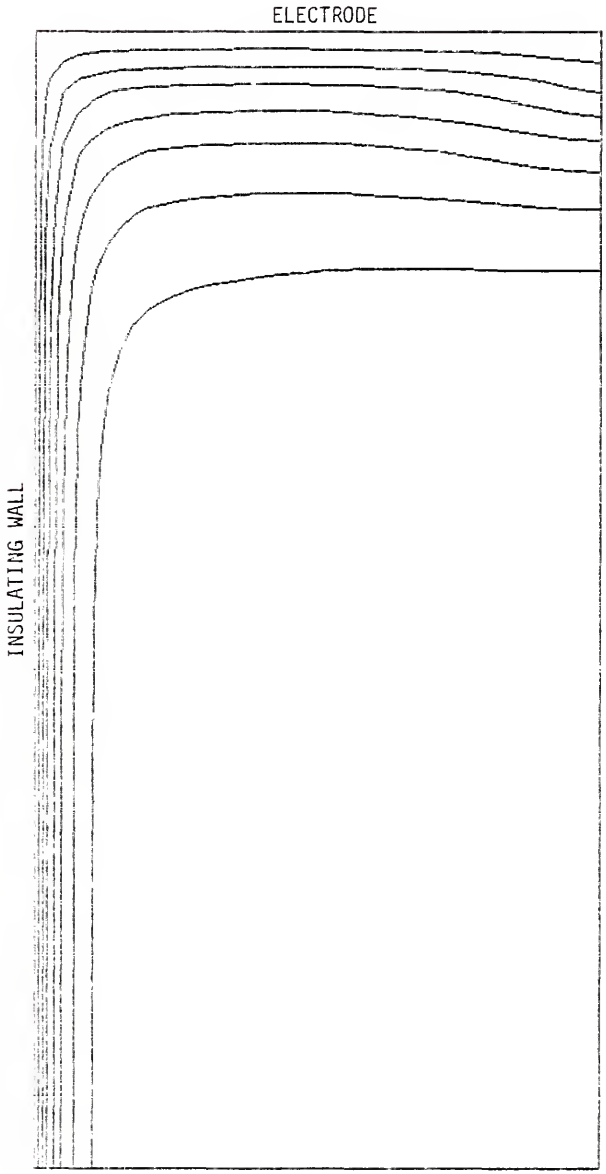

Figure 5-13. Velocity Contours M=20, K=0.95, K_w=1.0

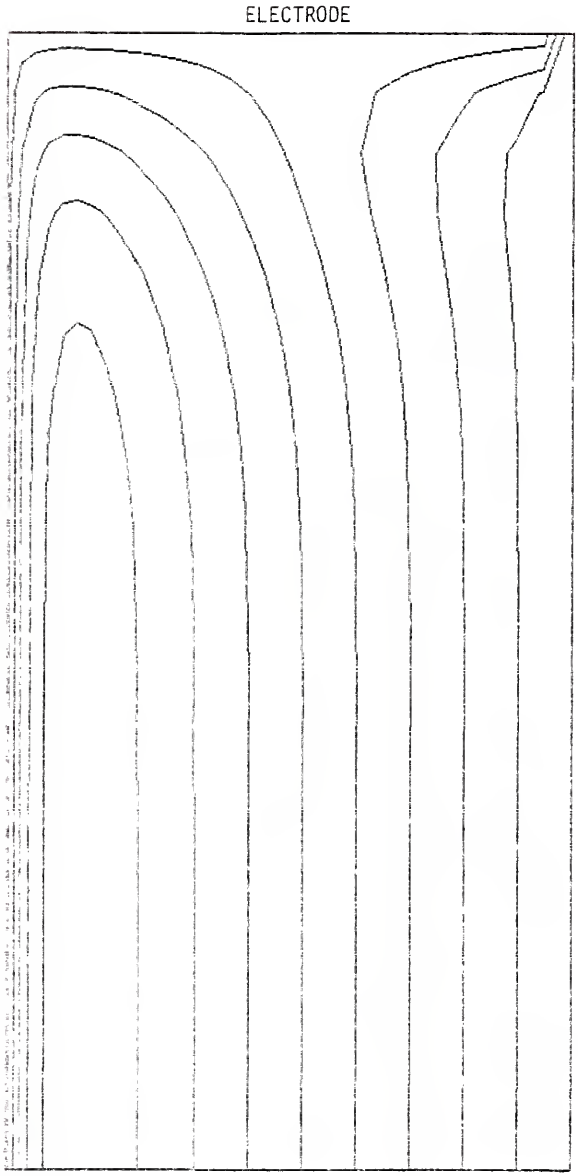

Figure 5-14. Current Streamlines M=20, K=0.95, K_w=1.0

is no longer constant along the surface, but can vary toward the center of the channel. The resistance of the electrode adds an impediment to the current flowing out of the channel, but the current finds a convenient conducting path in the boundary layer of the electrode where the velocity is low. This means that the current can flow easily to the center of the electrode where it is tapped off into the external circuit with only a minimal increase in the effective external resistance, which can be easily seen by the negligible increase in the streamlines of the return current.

Although the velocity contours are identical to the previous cases for all practical purposes, there is a noticeable change. The boundary layer at the center of the electrode is thicker with the velocity contours moved further out from the wall. The explanation for this effect is seen in the bunching together of the current streamlines at the center of the electrode before they are tapped out of the channel. This means that the current density will be higher in this region than the other areas of the electrode. The higher current densities consequently produce a larger electromotive force on the fluid retarding its flow and producing the thicker boundary layer.

Insulating Channel Case

The extreme case of increasing the resistance of both the external load and the electrode itself produces a magnetohydrodynamic channel where the walls are perfectly insulating all around. The

program derived previously to calculate the generator case is capable of handling this problem and so it is included in Figures 5-15 and 5-16 for the Hartmann number of 20 considered before.

The effect on the velocity profile is negligible as in the previous cases, without the increase in thickness of the boundary layer at the center of the electrode since no current is tapped out of the channel. The current streamlines are significantly different, though. None of the streamlines now touch the electrode, due to the fact that no current will flow out of the channel or even down the electrode. Technically the boundary of the channel taken along with the centerline of the channel (η=0) constitutes a streamline since the magnetic flux density is equal to zero at each point on it.

Variation with Hartmann Number

As in most cases with the calculations to follow, the most significant change is produced by changes in the Hartmann number. This is seen by the plots of Figures 5-17 and 5-18, where the Hartmann number has been increased to 100. In this case the velocity contours are now dramatically changed. Since the Hartmann boundary layers on the insulating wall have a thickness inversely proportional to the Hartmann number, it is seen that the contours have become a solid mass of lines. The boundary layer on the electrode is reduced also, but to a lesser extent due to its proportionality to the inverse of the square root of the Hartmann number. Again, the magnitude of the velocity at the center of the channel is decreased due to the increase

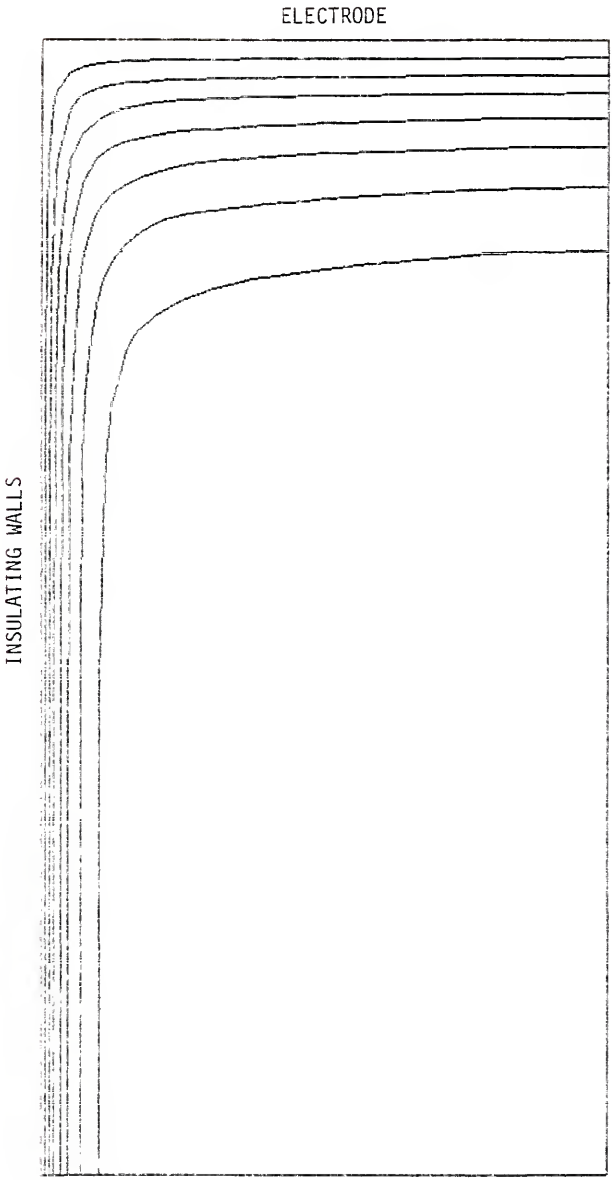

Figure 5-15. Velocity Contours in Insulated Channel M=20

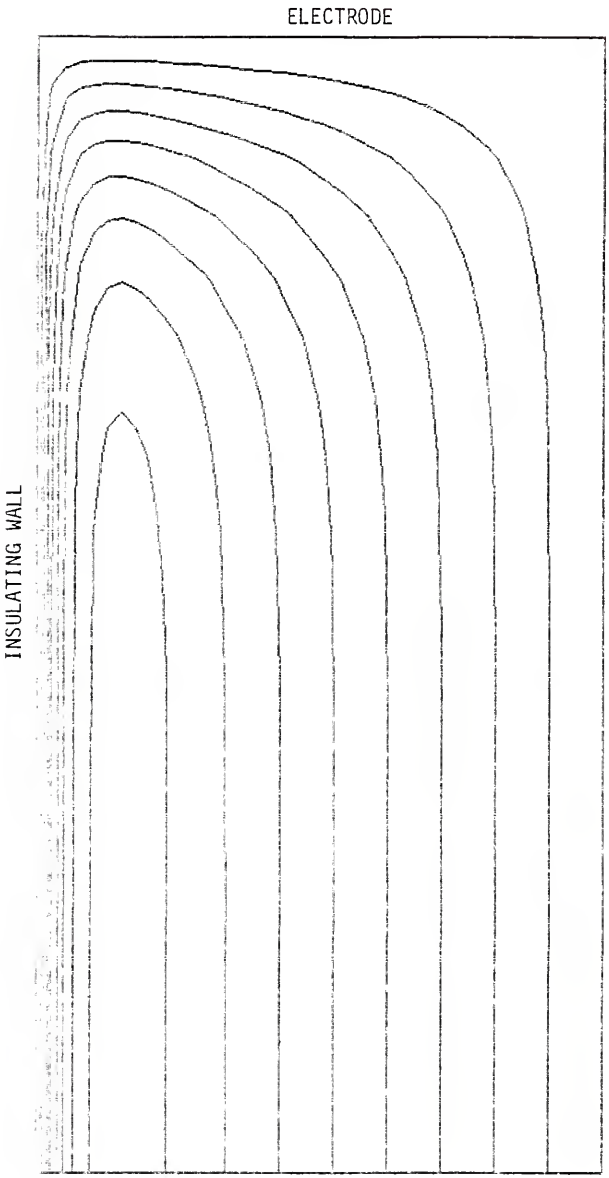

Figure 5-16. Current Streamlines in Insulated Channel M=20

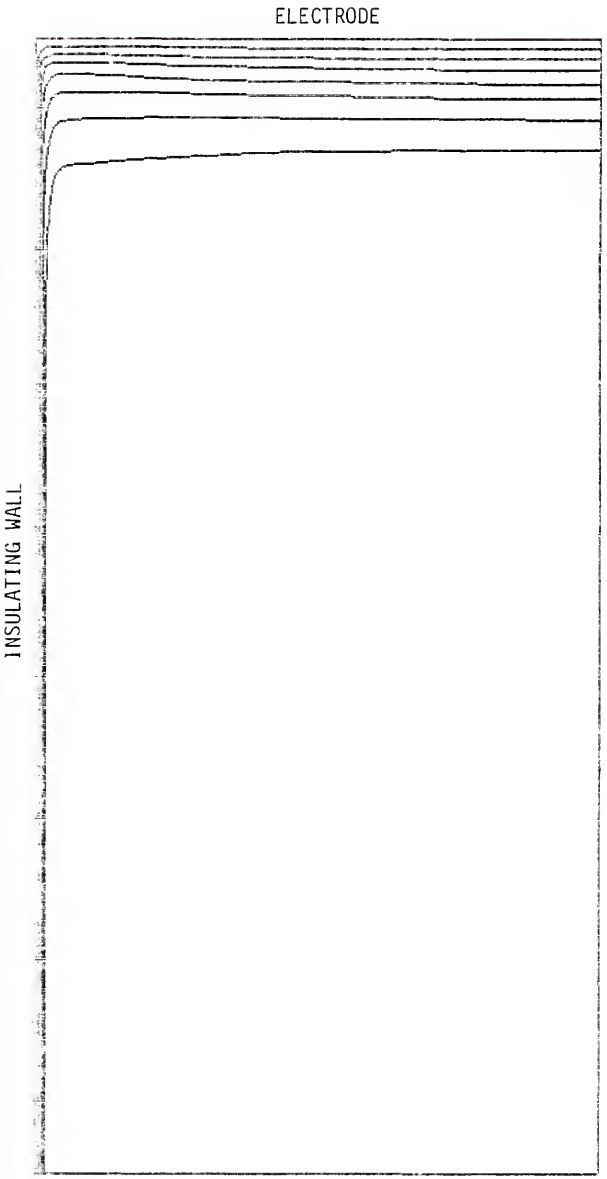

Figure 5-17. Velocity Contours M=100, K=0.95

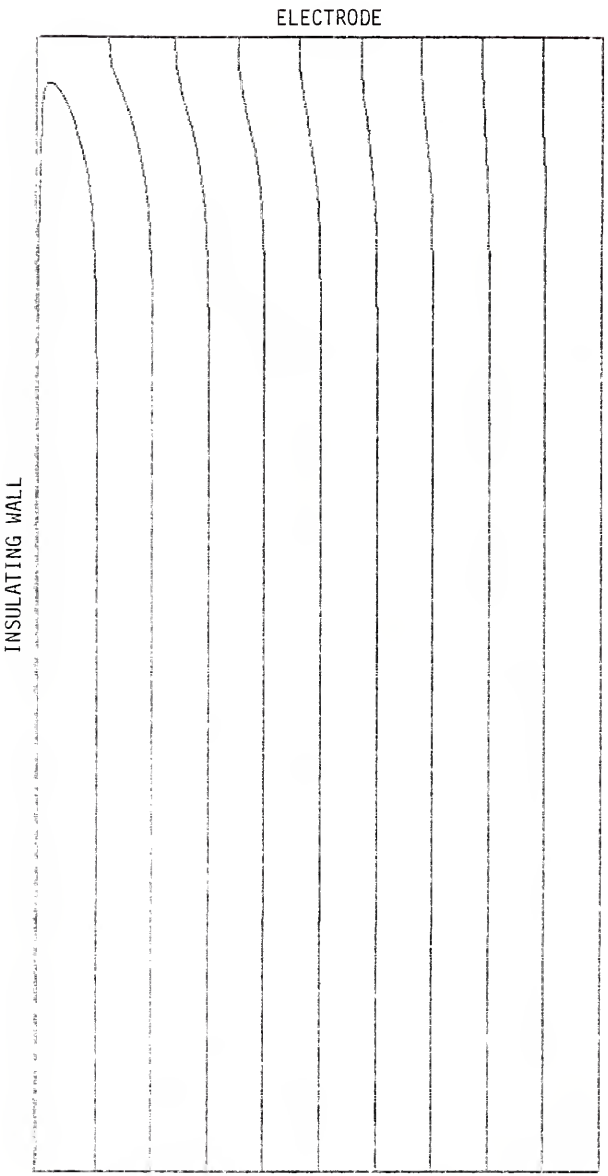

Figure 5-18. Current Streamlines M=100, K=0.95

of the Hartmann number in similar fashion to the one-dimensional approximation.

The current streamlines for this higher Hartmann number are now seen to be straight and uniformly spaced over a much broader region of the channel, indicating the increased size of the invicid core. Although the load resistance in Figure 5-18 is the same as previously, only the outer streamline returns in the Hartmann layer. This is due to the much greater resistance of the narrow boundary layer in this case as opposed to the thicker ones at lower Hartmann numbers.

The major feature to be derived from these plots is how the one-dimensional region of the channel is increased by going to the higher Hartmann numbers. The boundary layer on the electrode, which is now greatly reduced, is the only feature not predicted by the one-dimensional Hartmann solution. This gives a good intuitive feel for the reason why the Hartmann approximation is effective and becomes more so as higher Hartmann numbers are reached.

A comparison can also be made for the insulated channel case that is shown in Figures 5-19 and 5-20 where for this case the entire channel has been plotted. Here all the current streamlines are turned back and compressed into the Hartmann boundary layer. This also shows the boundary layer on the electrode more clearly.

Conductivity Variation in the Cross Section

One of the main features incorporated in the finite difference calculations of the channel is the ability to vary the

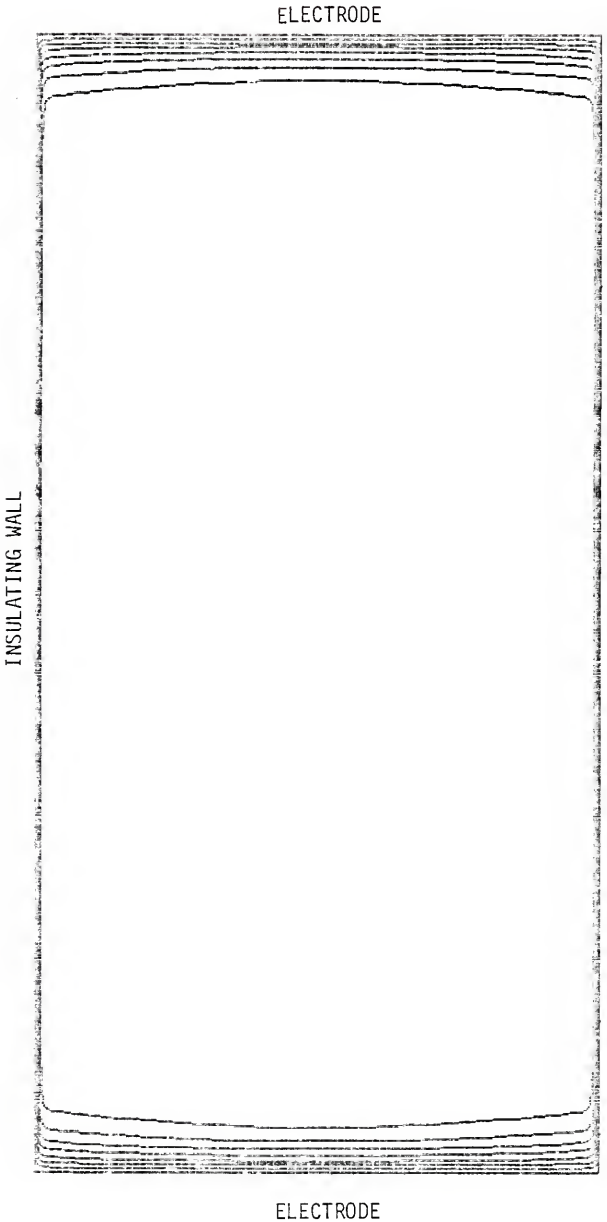

Figure 5-19. Velocity Contours in Full Insulated Channel M=100

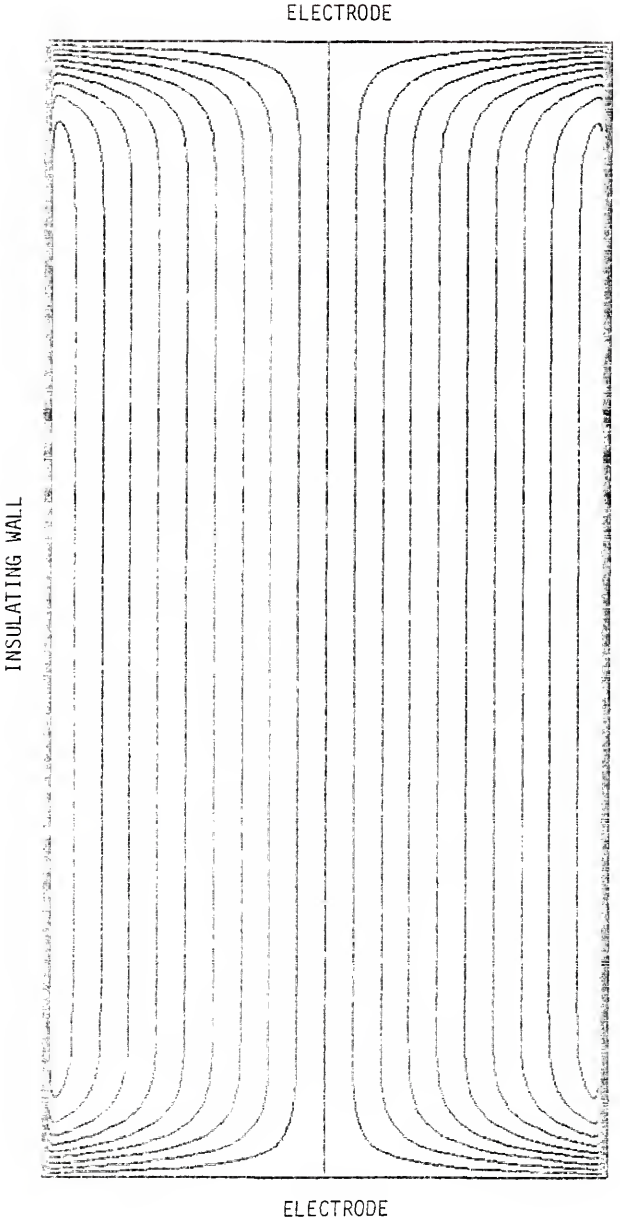

Figure 5-20. Current Streamlines in Full Insulated Channel M=100

conductivity of the fluid from point to point in the cross section. This feature is meant to simulate the two-phase nature of the flow, where the bubbles in the fluid can move about due to forces in the generator. This movement of bubbles will produce local concentrations of gas that reduce the effective conductivity of the fluid viewed as a homogeneous whole. For the purpose of demonstrating the effect of conductivity variation alone, the viscosity is held constant here.

In the calculation of the velocity and magnetic induction the conductivity and its variation from point to point is assumed to be a known input. Any functional relation can be used for the conductivity ratio (F) as long as it is symmetric about the centerlines (ξ=0, and η=0). For the purposes of demonstrating the effects an added condition will be imposed that the ratio goes to one at the insulating wall and the electrode. This is done because a change in the conductivity of the boundary layer would be equivalent to a change in the Hartmann number specified, due to the Hartmann number's dependence on the conductivity. Since the Hartmann number is already shown to produce large changes in the flow fields it is best to eliminate this change so that it does not obscure the effects to be demonstrated.

A simple functional relation is used to show the effects to be encountered in more complicated conductivity variations. The following relation using the Hyperbolic tangent simulates a smoothed step that starts at one at the wall and increases rapidly when halfway to the center of the channel to produce a plateau region at the center, where F is large and consequently the conductivity is low.

$$F(\xi,\eta) = 1 - \frac{(1-\alpha_c)}{4}\,[1 + \text{Tanh } 8(1-\xi)][1 + \text{Tanh } 8(.5-\eta)] \qquad (5\text{-}1)$$

The constant α_c is the value of F at the center of the channel. The constants in the hyperbolic tangent terms determine the degree of smoothness of the transition from one at the wall to the center value, and make the function specific to the case to be described with an aspect ratio of 2.

The effects of this conductivity variation for a moderate degree of change in the value of F can be seen in Figures 5-21 and 5-22. Here the center value of F goes to 4 and the conductivity is therefore reduced to one-fourth of its value at the wall. The effect on the velocity contours is immediate even for this small variation. The velocity in the core region is no longer constant as is indicated by the contours moving out into the core flow. Since the velocity in the center of the channel has increased and the spacing between the contours is based on one-eighth of this value, the spacing between the contours is greater, giving the false impression that the boundary layers have increased in thickness. In fact, the boundary layers are nearly identical to what they were because the variation in conductivity is confined to the region outside the boundary layers. Note that the contours in the core region occur about the point halfway to the center of the channel. This is the location of the smoothed step in the conductivity relation, which shows how closely the velocity is tied to the conductivity as is indicated by the inviscid core approximation of the previous chapter.

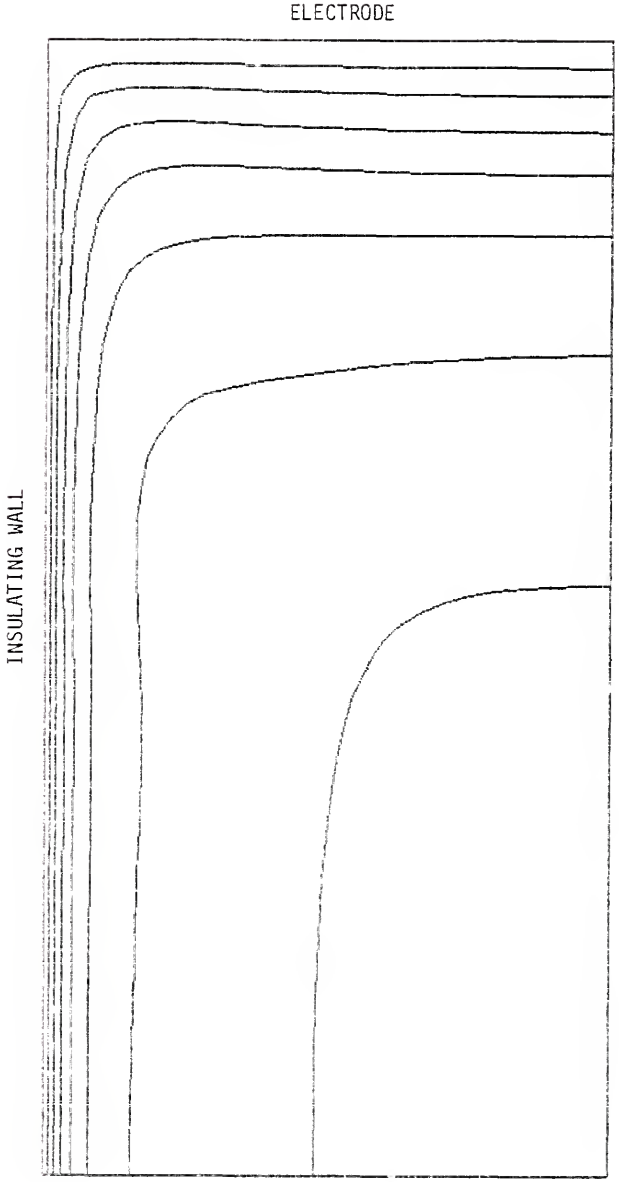

Figure 5-21. Velocity Contours with Conductivity Variation $\sigma_c/\sigma_0=0.25$

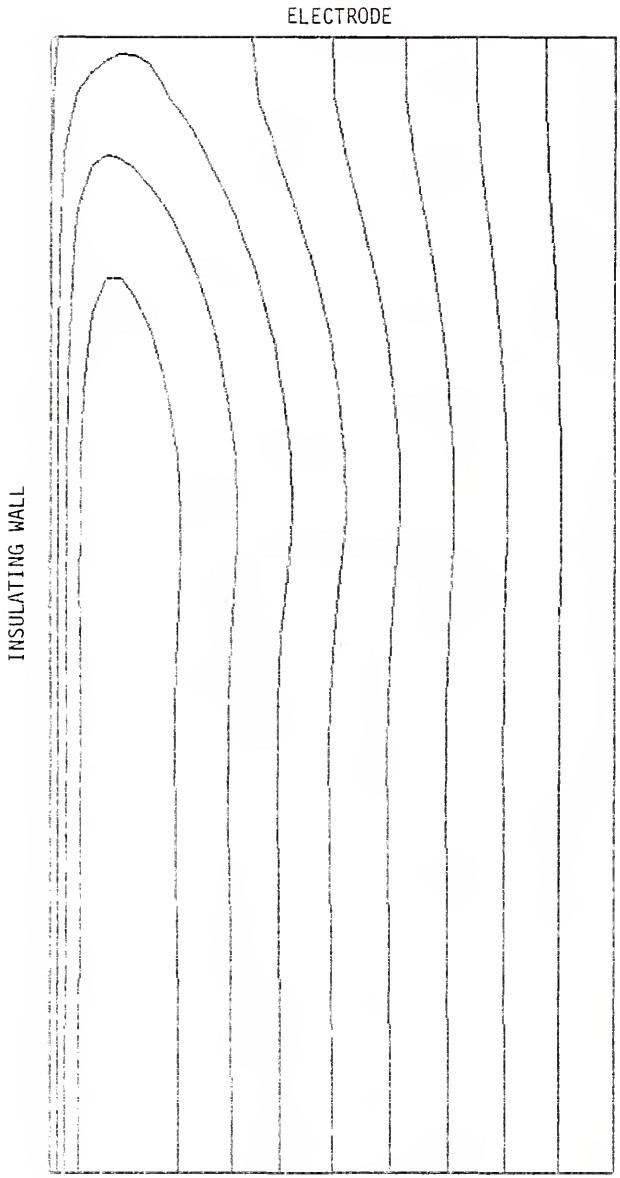

Figure 5-22. Current Streamlines with Conductivity Variation $\sigma_c/\sigma_0=0.25$

The effect of the conductivity variation on the current streamlines is much less pronounced in this case. The contours are almost identical to those in the constant conductivity case, which is a situation that is also indicated by the inviscid core approximation. Although the conductivity is lowered in the core region and tending to lower the current density, this is compensated for by the increased velocity which gives an increase to the induced potential gradient, thereby maintaining a constant current density. The streamlines are therefore unaffected by small variations in the conductivity.

As the conductivity is decreased to a greater extent in the center of the channel, the center becomes more and more approximate of a nonconducting central core and significant changes become readily apparent in the current streamlines. Figures 5-23 and 5-24 show the results when the conductivity is allowed to drop to 5 percent of its original value at the wall. The velocity in the core has now greatly increased with large gradients in the core region due to the rapid changes in conductivity. It is these gradients in the velocity that produce the shear forces in the fluid and make invalid the inviscid core approximation.

With the viscosity in the center of the channel becoming significant, the current streamlines begin to act more as one would expect them to upon encountering a region of low conductivity. The streamline spacing in the center has become greater indicating a lowering of the current density, while at the same time becoming

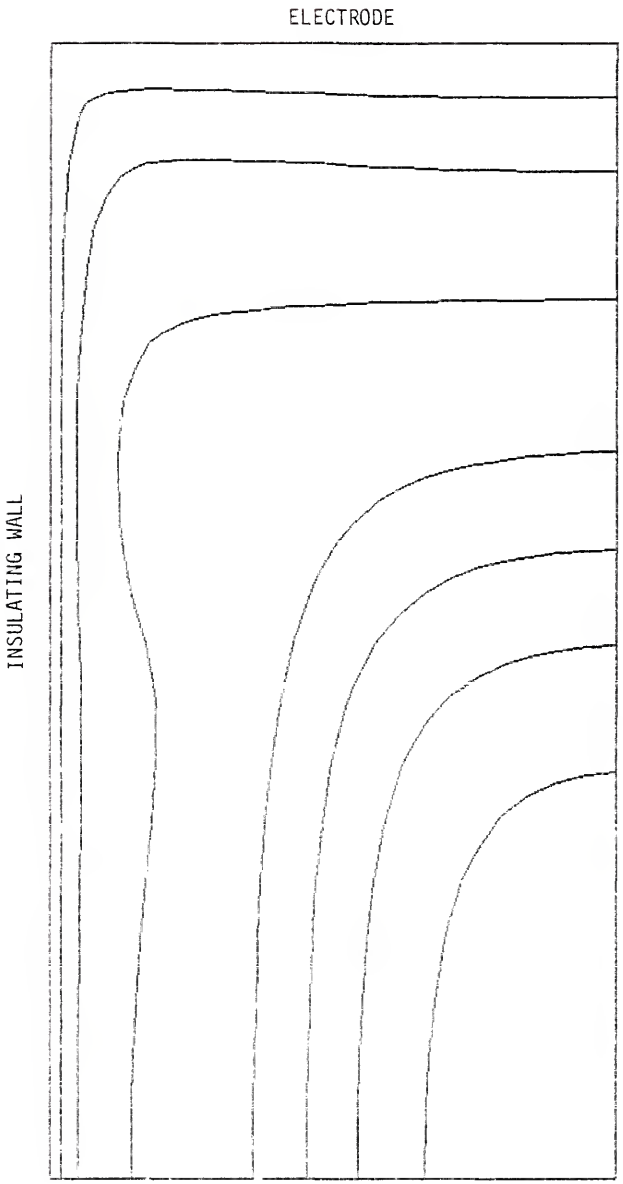

Figure 5-23. Velocity Contours with Conductivity Variation $\sigma_c/\sigma_0=0.05$

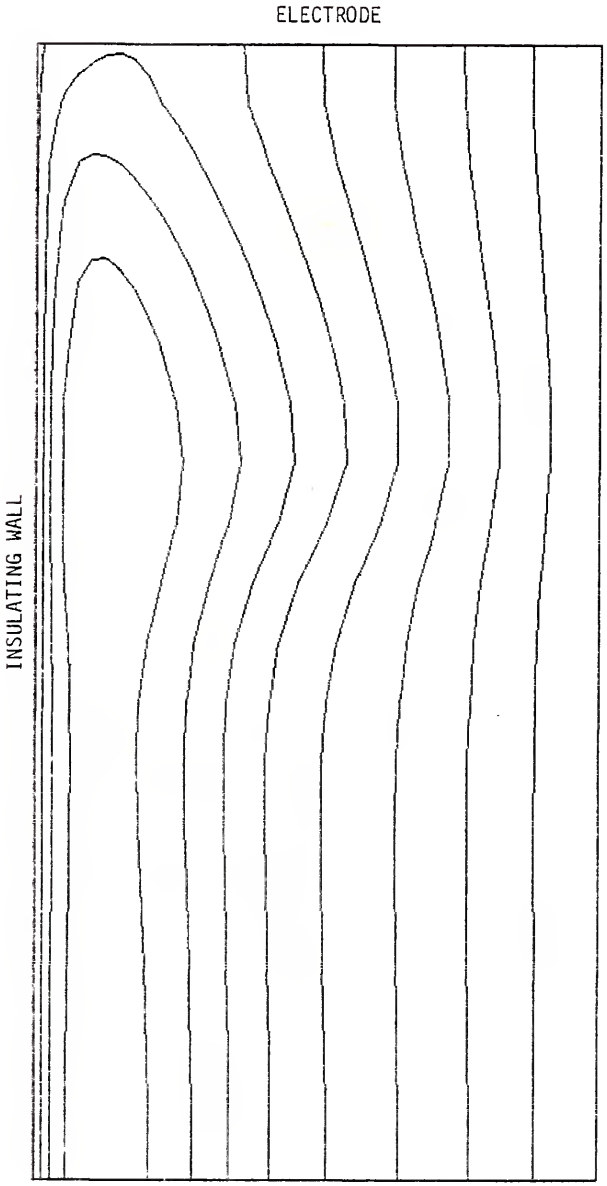

Figure 5-24. Current Streamlines with Conductivity Variation $\sigma_c/\sigma_0=0.05$

closer together just outside the Hartmann boundary layer. Thus the current tends to flow around the region of low conductivity. Once around the region the streamlines resume the approximate spacing of the previous cases and in the boundary layer the streamlines are about what they were.

The velocity contours also show an effect of the increased current density in the outer edges of the boundary layer. Because the current must flow around the core of the flow, the fluid at the edge of the boundary layer experiences a greater electromagnetic retarding force and therefore has a slower velocity. This is apparent in a thickening of the Hartmann boundary layer as the current lines are forced into the boundary layer.

This conductivity variation has a rational meaning in real two-phase flows. The large loss in conductivity is indicative of what happens when the phases become completely separated and the flow becomes one with a gas core known as an annular flow. The gas core is retarded only by the viscosity present, since there is no electromagnetic forces when there is no current flow. Since a large amount of energy is being expended in the viscous losses of this core flow without generating electrical current, this is a type of flow to be avoided in Faraday MHD generation.

Partitioned Channel

In the study of the use of two-phase flow in the generator channel the lateral movement of the gas phase bubbles from the straight

rectilinear flow down the channel can pose a severe problem to the efficiency as is indicated in the above paragraph. This could be a problem inherent in the generator itself, since there are several mechanisms producing a cross stream pressure gradient and therefore a lateral drift of the bubbles. These include the pressure gradient associated with the change in the velocity profile at the entrance and exit to the channel, and the "pinch" pressure caused by the current density crossing the induced magnetic field lines.

To prevent this separation of phases, a partitioning of the channel is proposed to prevent bubble drift (Trovillion et al. 1978). Branover (1976b) advocates a similar method for controlling the turbulence level in the channel. The scheme is illustrated in Figure 5-25 and described here to indicate the method of handling these types of calculations and the ability of the numerical scheme to analyze unusual proposals to determine their worth.

As shown in the illustration, the channel is divided into n_1 sections between the electrodes with the partitions being plates that will be assumed to be perfectly conducting and infinitely thin. The conductivity assumption is necessary since the current must pass through them. Since the current will obviously only pass across them and not down them, the setting of the conductivity at infinity will closely approximate any conductivity. In the vertical direction between the two insulating walls the channel is divided into n_2 sections. In the cases of these horizontal plates they are considered perfectly insulating as it is necessary to keep them from shorting out the generator electrodes.

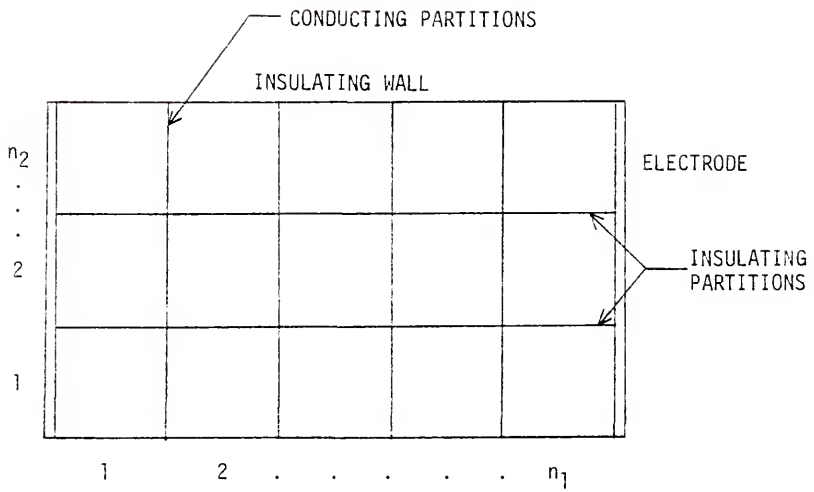

Figure 5-25. Partitioning of the Channel

By comparing each one of the individual partitions to the channel as a whole, it can be seen that they each represent a smaller individual generator that can now be analyzed in the same way as the single generator was before. The difference now is that the parameters that define the operating conditions of each segment are not the same as for the total channel which it is apart of, and the variables of velocity, magnetic induction and current density are now non-dimensionalized with respect to the different dimensions of the segments.

Denoting the quantities to be used when calculating the individual segments by the (†) superscript and the values for the total channel in the normal way, most of the relations between the variables and their corresponding segment values are derived simply by changing the nondimensionalization. These are given by

$$\gamma^{\dagger} = \frac{n_1}{n_2}\,\gamma$$

$$M^{\dagger} = \frac{1}{n_2}\,M$$

$$V^{\dagger} = n_2^2\,V$$

$$B^{\dagger} = n_2^2\,B$$

$$J^{\dagger} = n_2\,J \qquad (5\text{-}2)$$

The relation between the resistance ratio and its corresponding term is arrived at using the fact that the load resistance is the total

voltage drop divided by the net current out of the channel. Then noting that the total voltage drop is the sum of the identical voltage drops for the n_1 horizontal segments, and the total current out of the channel is the sum of the current from the n_2 vertical segments, the effective load resistance for the individual segments, all of which are identical, can be determined. Nondimensionalizing each load resistance by its appropriate dimensions, the resistance ratio of the segments is found to be the same as for the channel as a whole.

$$R^{\dagger} = R \tag{5-3}$$

The decision about the usefulness of this scheme can only be made by comparisons of the average velocity and the efficiency of the two cases. Because of the added surface area exposed to the flow in the segmented channel, there are added viscous forces retarding the velocity and dissipating energy. The only question is whether the decrease in efficiency and velocity is minor enough to sacrifice it for the advantages of reducing the lateral bubble movement and thereby the conductivity variation.

A useful approximate analysis of this situation is easily derived from the relations previously given for the Hartmann flow solution. In order to compare the average velocities of the two cases, the equation (3-22) for the average velocity of the entire channel is used with the assumption that the Hartmann number is sufficiently large to approximate the hyperbolic tangent by one.

$$\overline{V} = \frac{(1 + R)(M - 1)}{M^2(M + R)} \tag{5-4}$$

The equation for the individual segments, and therefore the entire partitioned channel, is the same except that the partition quantities are used. Converting these quantities so that they are based on the entire channel gives the following equation for the average velocity of the partitioned channel.

$$\overline{V}^{\dagger} = \frac{(1 + R)(M - n_2)n_2^2}{M^2(M + Rn_2)} \tag{5-5}$$

Taking the ratio of these two averages gives a relation that indicated the approximate effect of inserting the partitions into the flow, namely,

$$\overline{V}^{\dagger}/\overline{V} = \left(\frac{M - n_2}{M - 1}\right)\left(\frac{M + R}{M + n_2R}\right) \tag{5-6}$$

Remembering the direct relation between the average velocity and the total potential drop between the electrodes, it is seen that an identical relation also holds for the voltage output of the generator. In a similar fashion, a relation can also be derived for the ratio of the efficiency of the two channels under the assumption of Hartmann flow. This is given by

$$\eta_e^{\dagger}/\eta_e = \left(\frac{M - n_2}{M - 1}\right)\left(\frac{M + R}{M + n_2R}\right) \tag{5-7}$$

These relations indicate that as long as the Hartmann number for the entire channel is sufficiently large (M>100) the effect on the

average velocity and efficiency is small for a reasonable number of partitions. It should be noted that only the break up of the channel in the vertical direction is significant in the Hartmann approximation since it does not recognize any boundary layer on the vertical walls. This will mean that a deviation from this prediction can be expected when the aspect ratio of the individual partitions becomes small. Otherwise, the prediction should remain good since the main viscous dissipation occurs in the Hartmann boundary layers.

A comparison of the velocity contours and current streamlines is shown in Figures 5-26 through 5-29, where the Hartmann number of the total channel is 100 and the load factor is kept constant at 0.91. Here the 2:1 channel is broken up into eight partitions of an aspect ratio of one. For purposes of comparing the two cases the entire channel is plotted by reflecting the quarter channel solution about the axis of symmetry of each channel. The contours of the full channel are evaluated for the constant values that were described previously, but those for the partitioned channel are determined at the same values as for the full channel rather than in relation to their own maximum values. In this way a direct comparison can be made between the two cases.

The plot of the velocity contours for the full channel, when the Hartmann number is 100, shows how thin the Hartmann boundary layers become and how the main velocity defect is associated with the boundary layers on the electrodes. Comparing this with the velocity contours for the partitioned channel the boundary layers are seen to

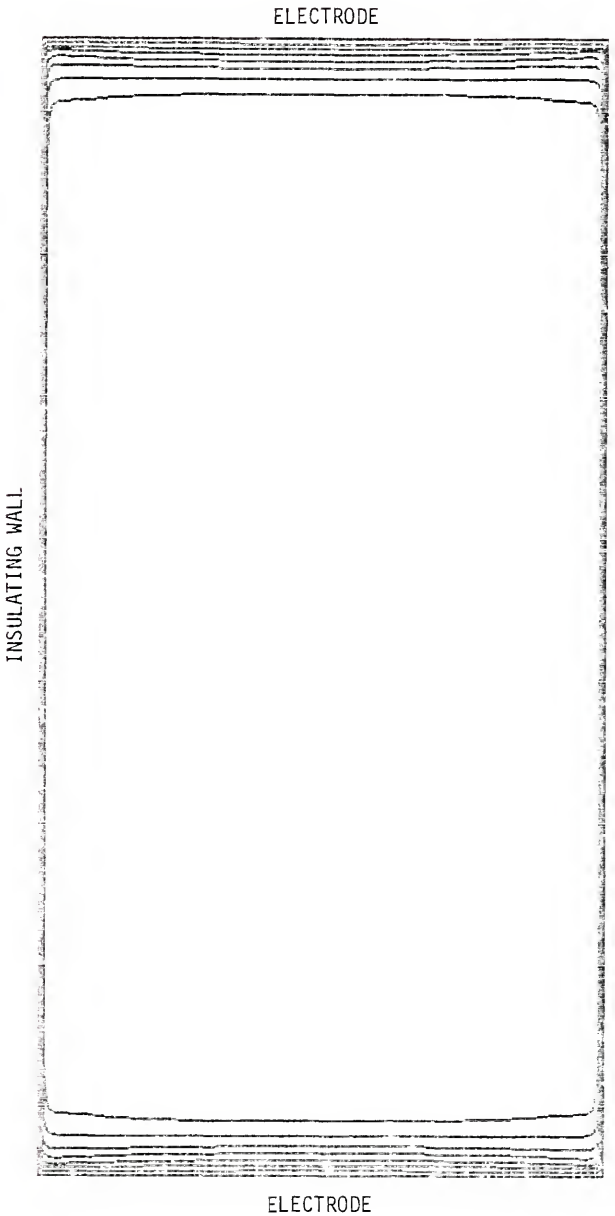

Figure 5-26. Velocity Contours Full Channel M=100, K=0.91

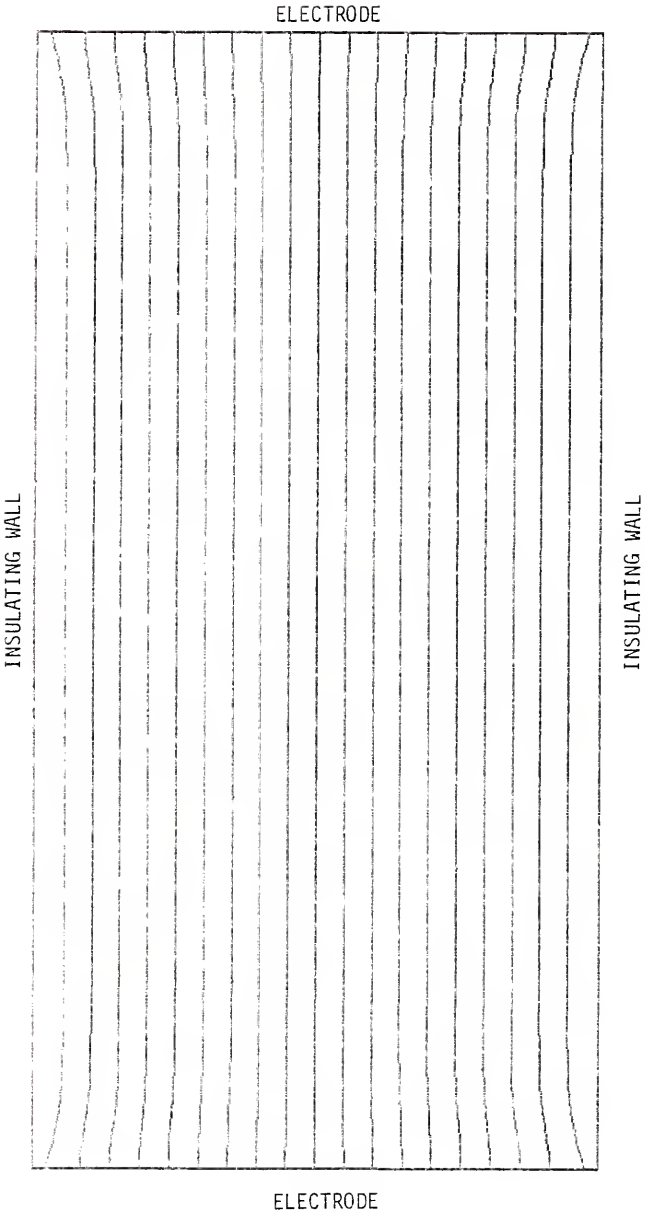

Figure 5-27. Current Streamlines Full Channel M=100, K=0.91

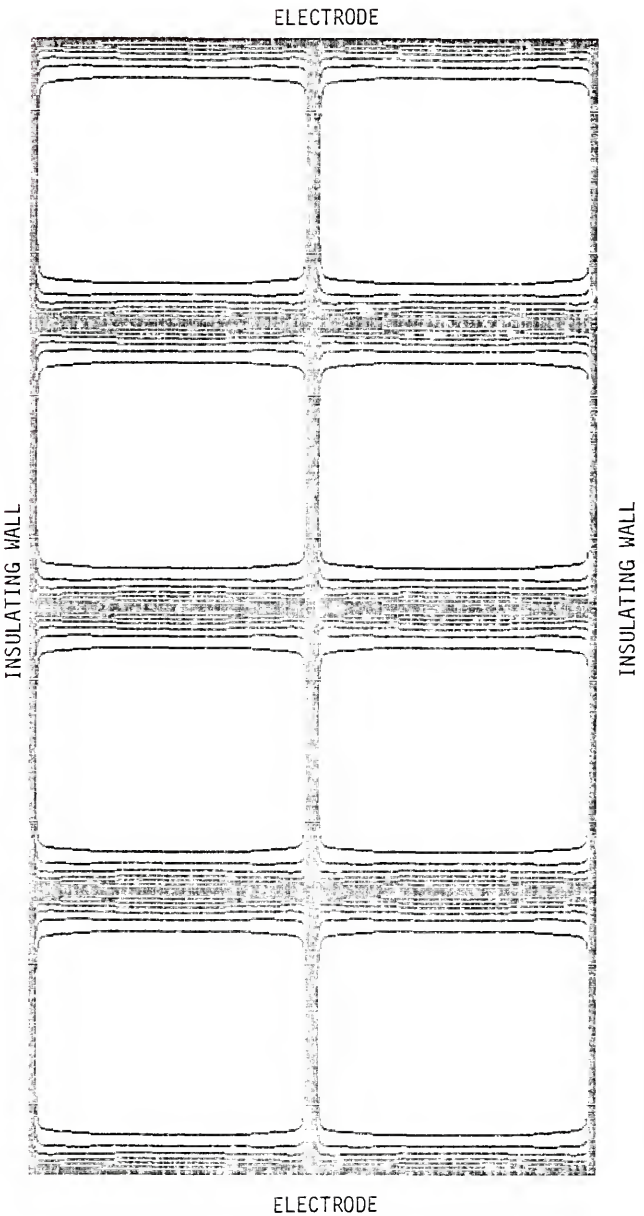

Figure 5-28. Velocity Contours Partitioned Channel M=100, K=0.91

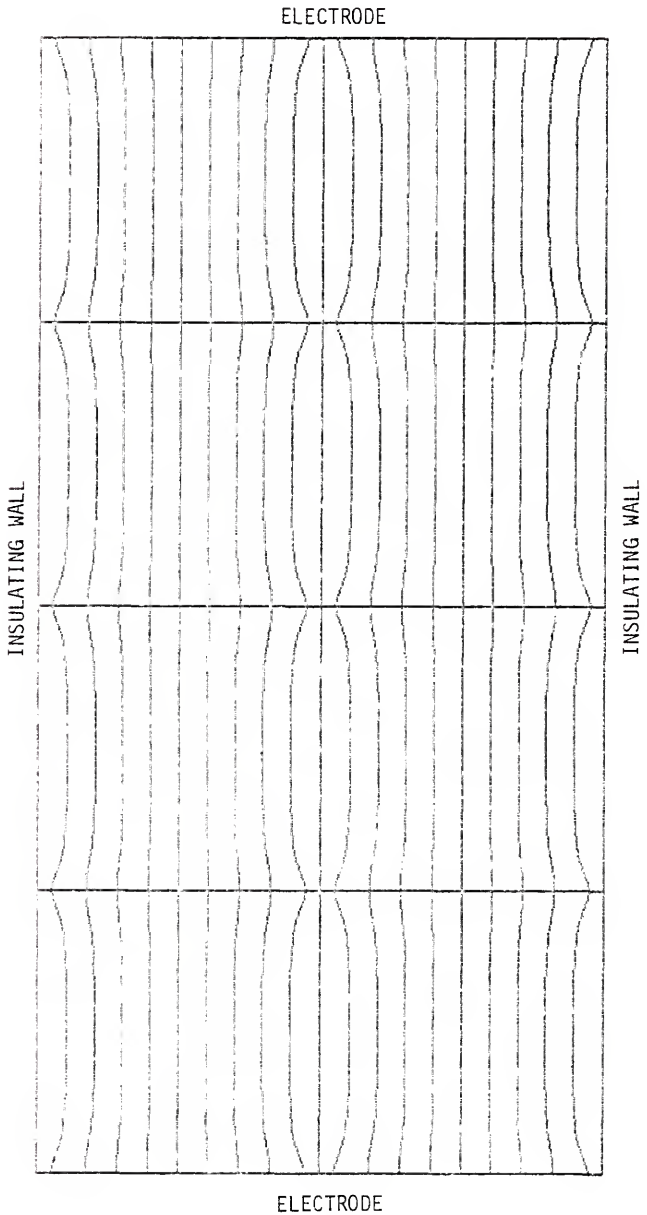

Figure 5-29. Current Streamlines Partitioned Channel M=100, K=0.91

be roughly similar in profile and thickness but now there is more surface area exposed to the flow and therefore a greater length of the boundary layers. From the numerical results this is seen to produce a one percent reduction in the maximum velocity and an 11 percent reduction in the average velocity. This compares well with a 9 percent loss predicted by the Hartmann approximation (5-6).

The current streamlines, likewise, show the uniform nature of the broad core region of the flow, deviating from straight lines only in the boundary layers on the electrodes. Because the contours are widely spaced and the load resistance is set for the approximate maximum efficiency, the contours near the insulating walls do not indicate the reverse current in the Hartmann boundary layers. They do exist, though, because the load resistance is not zero. The effect then of introducing the insulating segment wall between the electrodes is to add two more Hartmann layers in which the current can return. The return current that is lost is then approximately double that of the full channel case. This is born out by the numerical results that give a decrease of eleven percent in the net current out of the channel for the same load resistance. Performing the calculations for the efficiency, it also is found to decrease by this same amount from its original value, although this can be improved a little if the load factor is taken at the optimum for the individual segments, that are at a lower effective Hartmann number than the full channel. In all cases the loss in velocity, current, and efficiency are less as the Hartmann number of the full channel becomes larger, and greater

as the number of partitions is increased, especially the breaking up of the channel in the direction parallel to the applied magnetic field.

Efficiency of the Generator

Up to this point the discussion of the results of the calculations has centered mainly on the qualitative aspects of the channel flow that can be seen in the plots of the contours of flow velocity and current streamlines. The program, as derived, can also produce quantitative data points so that curves of the significant generator quantities, such as average flow velocity and efficiency, can be plotted against the design parameters of the channel.

The efficiency represents the most significant quantitative result. The worth of the whole two-phase system rests on being able to achieve the high efficiencies predicted by the Hartmann approximation. In turn the main parameter affecting the efficiency is the load factor imposed on the generator. This is noted in the discussion of Figure 3-2, where the Hartmann approximation for the efficiency is plotted against the load factor. The main assumption, and the chief source of error, for the Hartmann approximation is the requirement that the aspect ratio be infinite so that the problem is one-dimensional. With the two-dimensional finite difference solution available, it is possible to make this same plot for finite aspect ratios.

This plot of efficiency versus load factor for several aspect ratios is shown in Figures 5-30 and 5-31 for the Hartmann

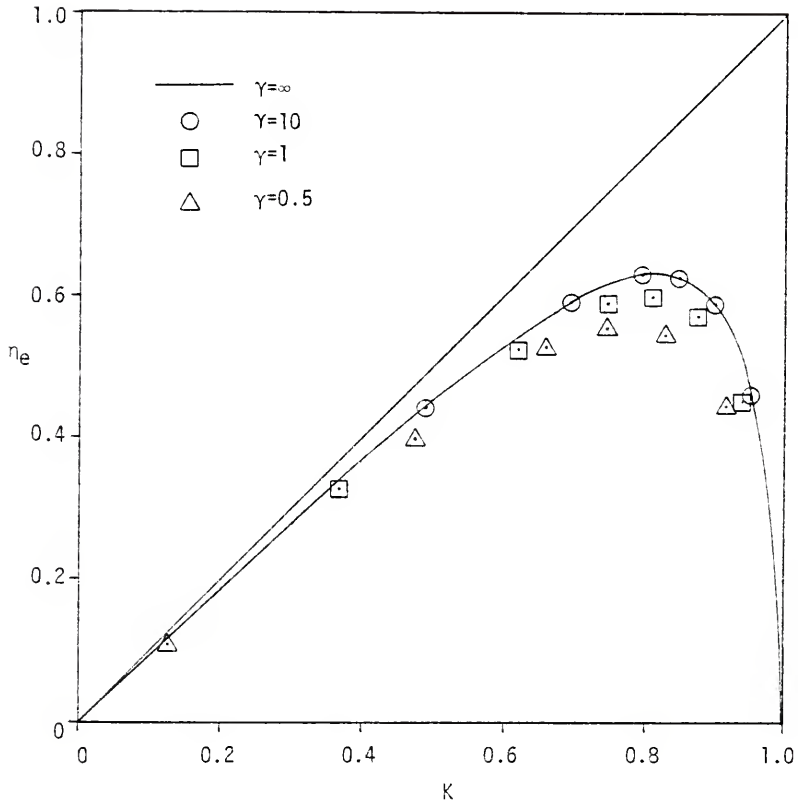

Figure 5-30. Efficiency versus Load Factor for Various Aspect Ratios
M=20

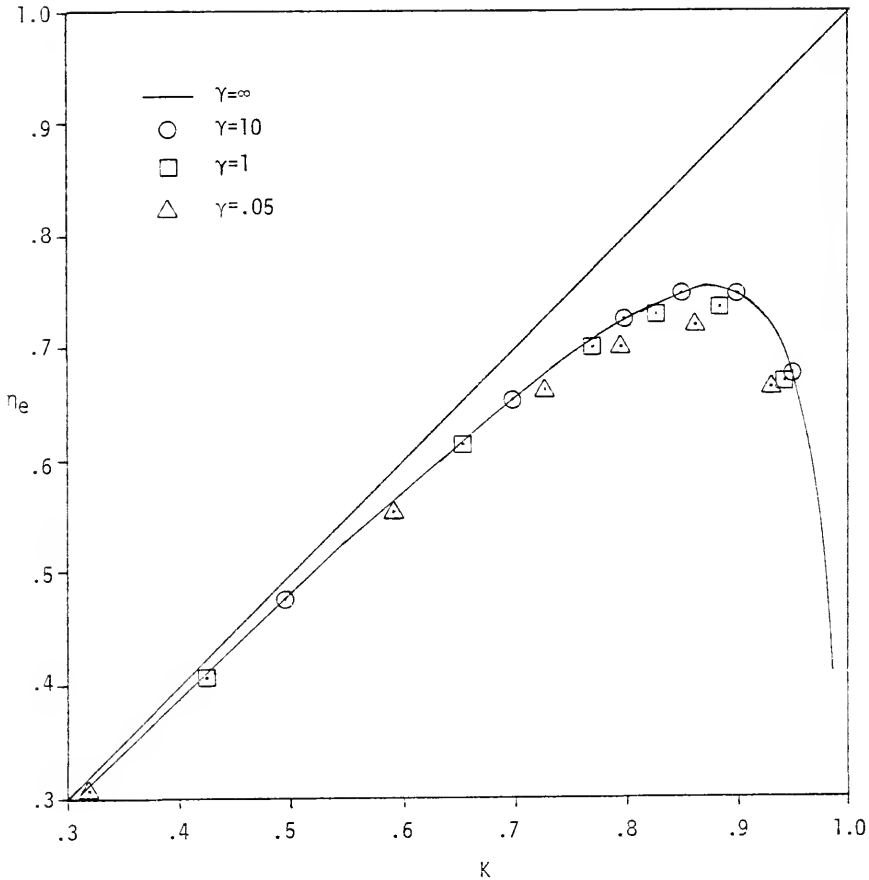

Figure 5-31. Efficiency versus Load Factor for Various Aspect Ratios
M=50

numbers of 20 and 50. Here the comparison can also be made with the approximate calculations for the slug flow and Hartmann flow cases. The slug flow is the straight line from zero to one and the Hartmann approximation is the solid curve. It is seen at both these Hartmann numbers, which are fairly low, that the data points for the calculation done at an aspect ratio of 10 fall right on the Hartmann curve for an infinite aspect ratio, thus demonstrating the correctness of the finite difference calculation and the suitability of using the Hartmann approximation at any reasonable value of the aspect ratio.

In the case of the partitioned channels the aspect ratio may become small enough to be of the order of one or less. These curves then show a significant loss in efficiency if the Hartmann number is low enough. While the curves retain their same shape they are shifted down due to the now significant viscous losses in the boundary layer on the electrode. Also the peak efficiency point of the curve has been shifted to a slightly lower load factor.

A comparison of the two figures each at a different Hartmann number shows that both the decrease in efficiency and the shift of the optimum load factor is reduced at the higher Hartmann number. This is clearly due to the decrease in thickness of the electrode boundary layer, which is the main source of the decrease in efficiency. Therefore, the Hartmann approximation can be used with good accuracy to a much lower aspect ratio if the Hartmann number is large.

This can be seen more clearly in Figure 5-32 where the efficiency is plotted against the aspect ratio for several Hartmann

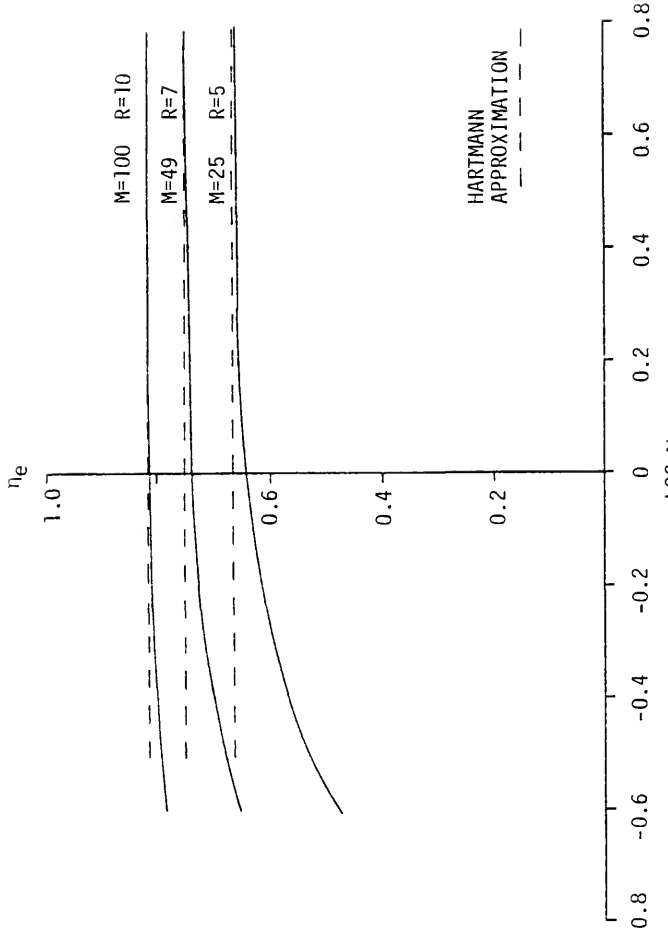

Figure 5-32. Efficiency versus Aspect Ratio for Various Hartmann Number

numbers where the load factor is set to a value very near the optimum of $R=\sqrt{M}$. The horizontal lines in this plot indicate the Hartmann prediction and therefore the maximum value these curves can achieve. It should be noted that all the curves approach this value assymtotically as the aspect ratio becomes large. It is clear from these curves that the higher Hartmann number cases will hold their efficiency to a much lower aspect ratio. In the case of low Hartmann numbers the small aspect ratios impose a severe loss in efficiency on the operation of the generator.

The thickness of the electrode boundary layer is proportional to the inverse of the square root of the Hartmann number. Since the electrode boundary layer is the significant additional loss from that calculated by the Hartmann approximation, it is a matter of determining when the boundary layer thickness is a significant fraction of the generator width to find where the Hartmann approximation breaks down. Therefore it is found that $\Upsilon\sqrt{M}$ is a reasonable criterion for determining when the Hartmann approximation is sufficiently accurate. From these calculations it is found that if $\Upsilon\sqrt{M}$ was greater than about 10, the Hartmann approximation gives an accurate indication of the efficiency as long as the fluid properties do not vary in the cross section.

Another source of loss for the efficiency is the conductivity of the electrode itself. The changing of the electrode from one that is perfectly conducting to one that has a finite resistance, lowers the voltage output of the generator where the current is tapped

off at the center of the electrode, and therefore the efficiency. Figure 5-33 shows how the efficiency drops off as the electrode resistivity factor is increased from zero, where it is perfectly conducting, to one, where it is insulating. The η_e for K_w=1 is not calculated since this involves the previously mentioned problem of current flowing out through an insulating electrode, although this can be done if it is assumed to be tapped only at the center of the channel.

The dashed lines in this plot indicate the efficiency of the Hartmann case at infinite aspect ratio. The curves for the finite difference calculations were made at low values of the aspect ratio to show more clearly the effects of the finite conductivity cases, which are naturally more pronounced in this limit. In all cases the load resistance is set at the optimum value predicted by the Hartmann approximation. It is tempting to assume that the effect of the decreased conductivity is to merely put an added resistance in series with the load resistance, thereby forcing the generator to run at a higher load factor than is its optimum. This is not entirely true, since not all the current flows through every part of the electrode, but enters and leaves at different places on the wall. Thus the change in conductivity is not simply a change in the load factor, but thinking about it in this way would suggest that it is necessary to determine a new optimum in the load factor that would be less than the Hartmann optimum when the increased resistance of the electrode is taken into account. Thus, each one of the curves

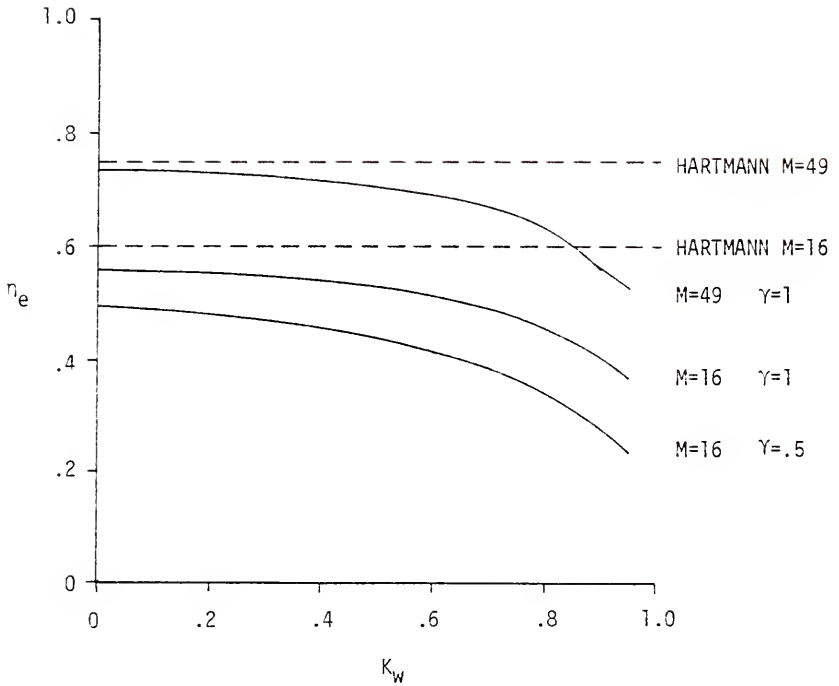

Figure 5-33. Efficiency versus Electrode Resistivity

in the figure could be raised somewhat by varying the load resistance along the curve to obtain the new optimum.

To give some idea of where real generator data would fall on curves in the plot, the electrode resistance factor can be calculated under the assumptions that the thickness of the electrode is one-tenth of its height, and the conducting fluid is an alloy of 22 percent sodium and 78 percent potassium (NaK). If the electrode material is copper, the resistance factor is 0.2, and if steel is used, it is 0.68. The curves would indicate a loss in efficiency for these cases from one to eight percentage points. Again, it should be noted that the curves given represent the worst case of both low aspect ratio and low Hartmann number. These are cases not likely to be found in practice, where even in the low aspect ratios found in the partitioned channels the walls can be assumed to be perfectly conducting for all but the end segments, since the current flows across the inner conducting walls and not along them. It should also be noted that the losses can always be diminished by using thicker electrodes and thereby going to lower electrode resistance factors, although it should be remembered that the boundary conditions of the finite difference calculations are based on the assumption of a "thin" electrode. In general, though, the loss of efficiency due to the finite conductivity of the electrode can be assumed negligible in a well-designed generator channel.

Average Velocity of the Fluid

Of great importance in the design of the generator is the average velocity of the working fluid moving through the channel. This gives the volumetric flow rate of the fluid and therefore determines the amount of fluid required to operate the generator. In general, low flow rates are desired since they indicate that the electromagnetic forces are retarding the flow and presumedly are generating the current for the output power.

In the normal case where the fluid properties are constant and the electrode conductivity is well approximated by the perfectly conducting case, the average velocity of the channel can be obtained from the efficiency of the generator given the Hartmann number and the load resistance factor. This relation is obtained from the equation (3-31) for the efficiency in terms of the average velocity and the magnetic flux density at the insulating wall.

$$\eta_e = \frac{RB_1^2}{\bar{V}}$$

Then from the calculations for the voltage of the generator, the average velocity and the magnetic flux density at the wall have been related for a given Hartmann number and load resistance ratio (3-28).

$$B_1 = - \frac{M}{1 + R} \bar{V}$$

The combination of these two relations gives the average velocity in terms of the efficiency.

$$\eta_e = \frac{M^2 R}{(1 + R)^2} \bar{V} \tag{5-8}$$

Although this relation makes the calculation of the average velocity possible, it is helpful for the interpretation of the results to plot curves of the average velocity itself. This is done in Figure 5-34, which shows the main features of the flow plotted as a function of aspect ratio. In this figure the average velocity is divided by the aspect ratio in order to change the nondimensionalization of the velocity from the square of the half-height of the channel, to the area of the cross section of the channel. This quantity then gives a comparison of the flow rates at the different aspect ratios, but at the same time maintains the cross-sectional area of the channel constant.

By modifying the program slightly it is possible to calculate the case with the Hartmann number equal to zero. In this case there are no electromagnetic forces so that the flow velocity is determined by the viscous forces alone. As can be seen in the figure, the curve as a function of the aspect ratio is symmetric about the case with aspect ratio of one. In the limit as the aspect ratio becomes large, the zero Hartmann number case becomes the one-dimensional Poiseuille flow between two infinite parallel plates, the curve of which is plotted in the figure. As the Hartmann number is increased and current is allowed to flow in the conducting fluid, the electromagnetic forces have a retarding effect on the flow velocity, so that the curve for the zero Hartmann number case is the maximum bound for all the other curves.

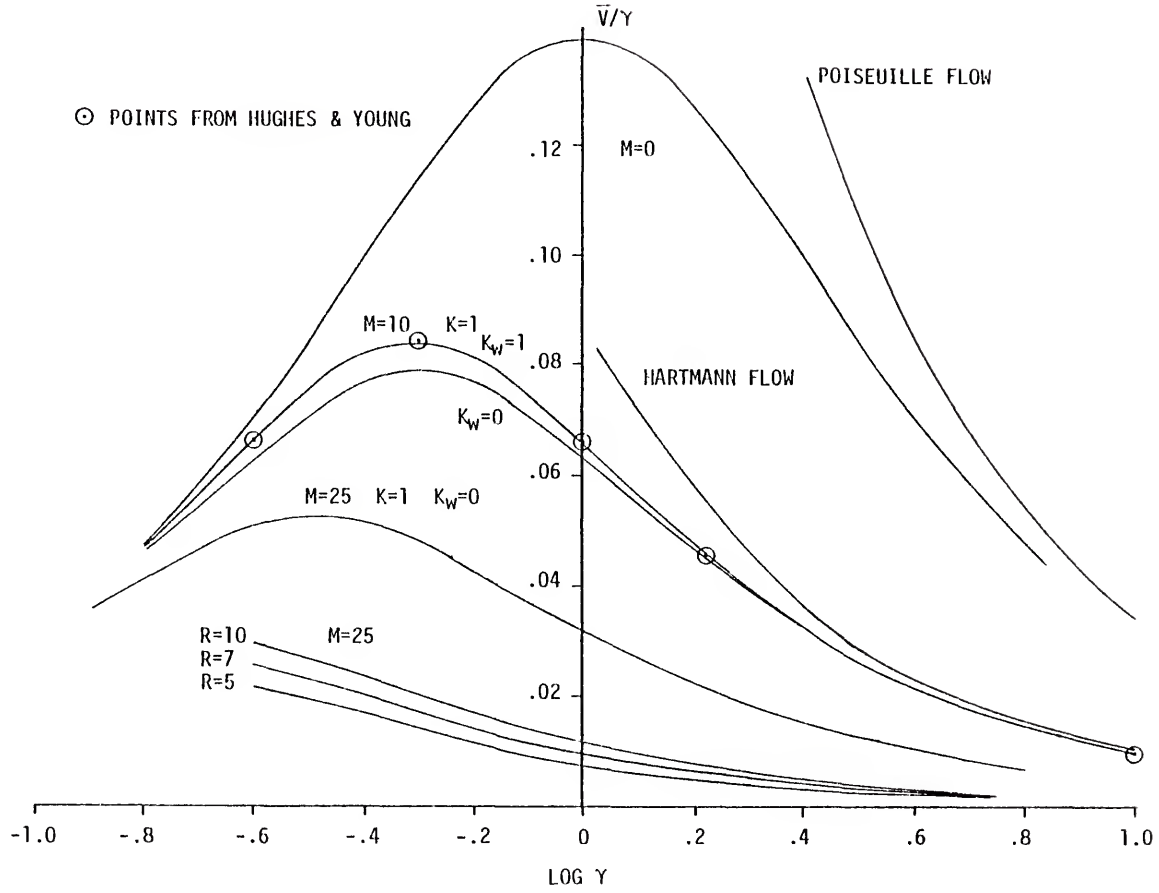

Figure 5-34. Flow Rate versus Aspect Ratio

The two curves for the Hartmann numbers of 10 and 25, each at a load factor of one, show the effect of the increasing Hartmann number on the average flow of the fluid. It is evident that the curve is no longer symmetric about the square channel case with aspect ratio of one. This follows from the fact that the boundary layers on the electrode wall are of much greater thickness than the Hartmann layers on the insulating walls. This plot also makes it graphically clear that when the pressure drop down the channel is held constant the velocity of the fluid will drop very rapidly as the Hartmann number is increased.

The effect of changing the resistance ratio is seen from the curves plotted at the Hartmann number of 25. When the load factor is one and the load resistance is infinite, the current in the channel is limited to that which can be returned in the Hartmann boundary layers. This minimum amount of current in the channel produces a minimum amount of retarding force on the flow, and therefore this curve represents a maximum bound on the velocity for a given Hartmann number no matter what the aspect ratio is. As the load resistance is lowered the current is allowed to increase, thus retarding the flow and lowering the velocity for a given pressure drop. The case of a load resistance of zero, which represents the short circuit case, would give the minimum velocity for a given Hartmann number at any aspect ratio.

The effect produced by the changes in the conductivity of the electrode is shown by the two curves at the Hartmann number of 10. By

decreasing the conductivity to the point where it is insulating, the current is further impeded so that the velocity is allowed to increase. It should be noted, though, that the effect is noticeable only at the low aspect ratios, where the electrode and its boundary layer become a major effect in the flow. As the aspect ratio becomes larger the effect vanishes with the two-dimensional aspects of the flow, and the curve approaches the one-dimensional Hartmann solution in the same manner as the perfectly conducting electrode case.

In calculations of this nature, where the flow rate or the efficiency of the generator is plotted as a function of the major parameters of the flow, it is difficult to find in the literature calculations of a similar nature that support the accuracy of these results. This is due mainly to the fact that the equations for the generator with the boundary conditions set for the generator case have not been solved by other analytical methods, such as the infinite series approach. For the insulating channel case where the load factor and the electrode resistance factor are both one, an analytical solution does exist for the flow rate and so can be compared to the finite difference calculations given here for this special case. A book by Hughes and Young (1966) gives values of the ratio of the flow rate at various Hartmann numbers and aspect ratios to the rate at zero Hartmann number. Using the value of the flow rate at zero Hartmann number given by the present calculations the points from the analytic method at a Hartmann number of 10 are plotted in the figure. It can be seen that the agreement between the two methods is excellent and confirms the accuracy of the present calculations.

Conductivity Variation

When the conductivity of the fluid is allowed to vary in the cross section, there are two main effects produced. One is the increase in the velocity of the fluid in the regions where the conductivity is lowered, and the other is the loss in efficiency of the generator. The loss in efficiency is almost entirely produced by the increase in the average velocity, since the need to supply a larger volume of fluid through the pressure drop for a given output of power means a greater input of power is required. A small additional loss in efficiency occurs when the conductivity variation produces a sufficiently large velocity gradient, that then dissipates more energy through viscous shear.

The effect of an increasingly peaked conductivity profile on the efficiency and average velocity of the channel is shown in Figure 5-35 for the case where the Hartmann number is 49. Here the generator is being operated near its maximum efficiency load resistance ratio of 7, and a large aspect ratio of 10 is used to facilitate a comparison with the results of the inviscid flow calculations.

Rather than use the hyperbolic tangent profile used previously for the plots of the contours with conductivity variation, a simpler parabolic conductivity variation in both the ξ and η directions is used, with the value at the walls maintained at one. The curve of efficiency and average velocity are then plotted against the value of the conductivity ratio at the center of the channel, which will be the point of minimum conductivity.

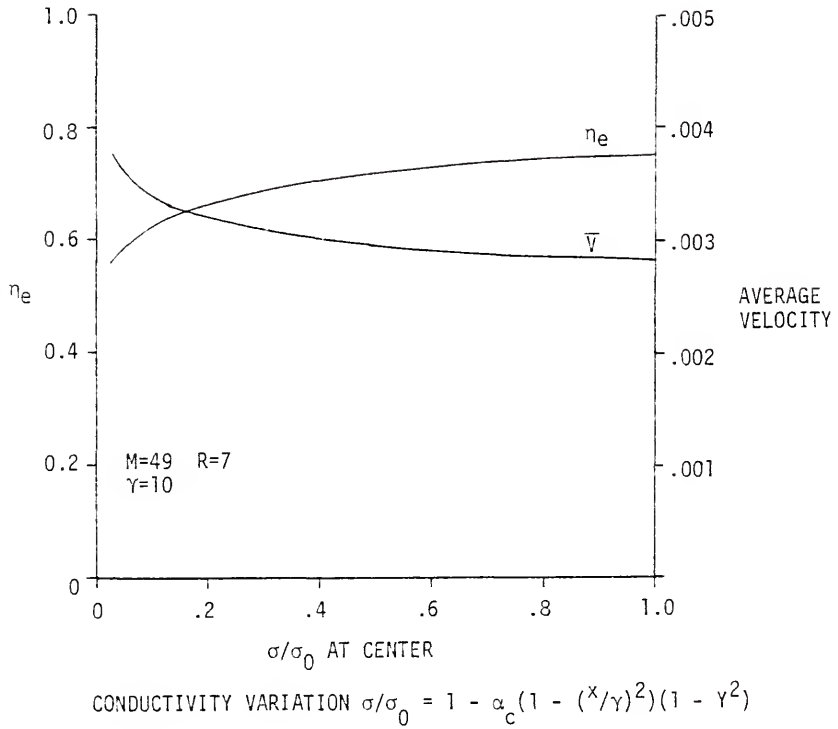

Figure 5-35. Flow Rate and Efficiency for Conductivity Variation

The figure shows clearly that as the conductivity profile becomes more and more peaked the efficiency drops off markedly, while at the same time the average velocity is increasing in like manner. The inverse symmetry of these two functions can be demonstrated by multiplying them together and noticing that the product is a constant value. This is an indication that the efficiency loss for the case here is due entirely to the increased flow rate requirements and any additional viscous shear losses are negligible.

Although the viscous shear in the core region of the flow is not significant enough to produce an effect on the overall efficiency of the channel, it does have an effect of reducing the maximum velocity point in the flow when the conductivity has become sufficiently low. This can be seen in Figure 5-36, where the velocity at the center of the channel, which is the maximum in the cross section, is plotted against the conductivity ratio at that point. The solid curve in this figure represents the velocity that would be calculated using the inviscid core flow model (3-46). Remember that the assumption in this model is that all the viscous effects of the flow are confined to the boundary layers on the walls of the channel, and the core can be assumed free of viscous effects. Under these assumptions the velocity becomes infinite as the conductivity approaches zero.

The symbols plotted represent the finite difference calculation with the viscous effects included. It can be seen that where the variation in the conductivity is small the inviscid core gives a

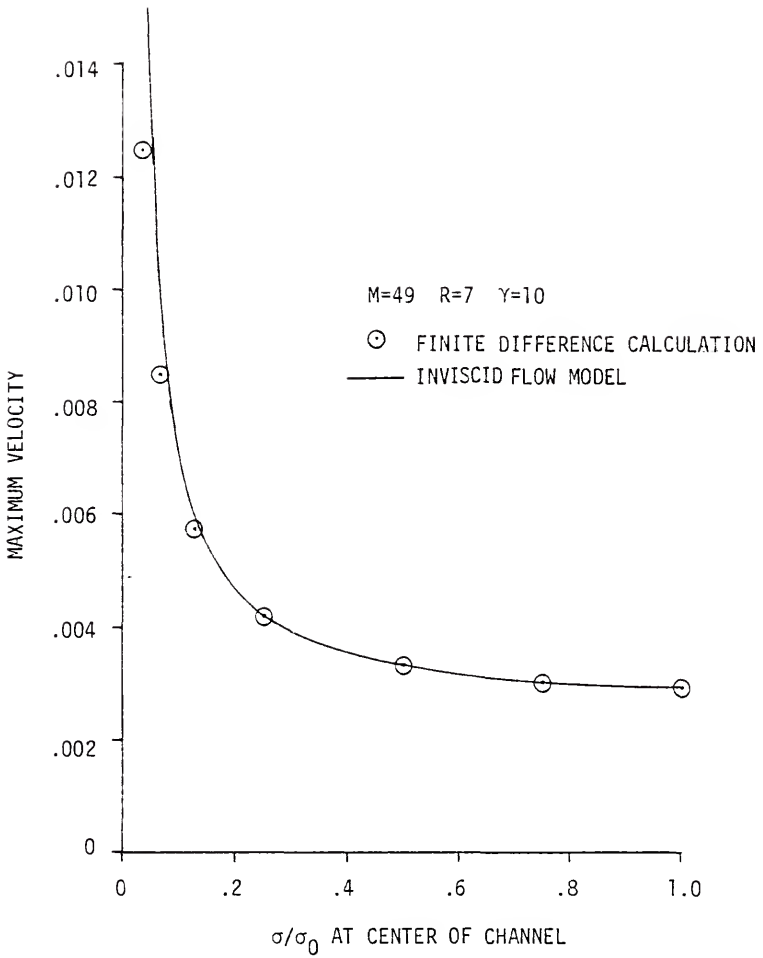

Figure 5-36. Maximum Velocity for Conductivity Variation

very accurate model of the flow, but as the conductivity becomes very low the velocity is prevented from diverging by the viscous forces present, so that the finite difference calculations drop well below the inviscid approximation. It can be expected that as the Hartmann number becomes larger the flow will be able to go to much lower conductivities before the solution deviates from the inviscid approximation, since all the velocities, and therefore the gradients, of the flow are very much reduced. Also, if the conductivity profile is allowed to vary in a smoother fashion, the approximation is more accurate, due to the reduced gradients in the flow.

Viscosity Variation

In the derivation of the governing equations for the flow, it is convenient to incorporate the possibility of a variation in the viscosity of the fluid in the cross section. The effect of a viscosity variation is shown in Figure 5-37, where the efficiency is plotted against the value of the viscosity ratio at the center of the channel. Here a parabolic profile is used in the same manner as for the conductivity variation described previously. Taking into account the possibility that the viscosity might increase, rather than decrease, toward the center of the channel, the efficiency is calculated for various peak values of the profile, for cases where the Hartmann number is very low and the resistance ratio is at its most efficient value. Doing the calculations for very low Hartmann numbers tends to accentuate any effect that may be present, since the viscous forces are then increased relative to the magnetic forces.

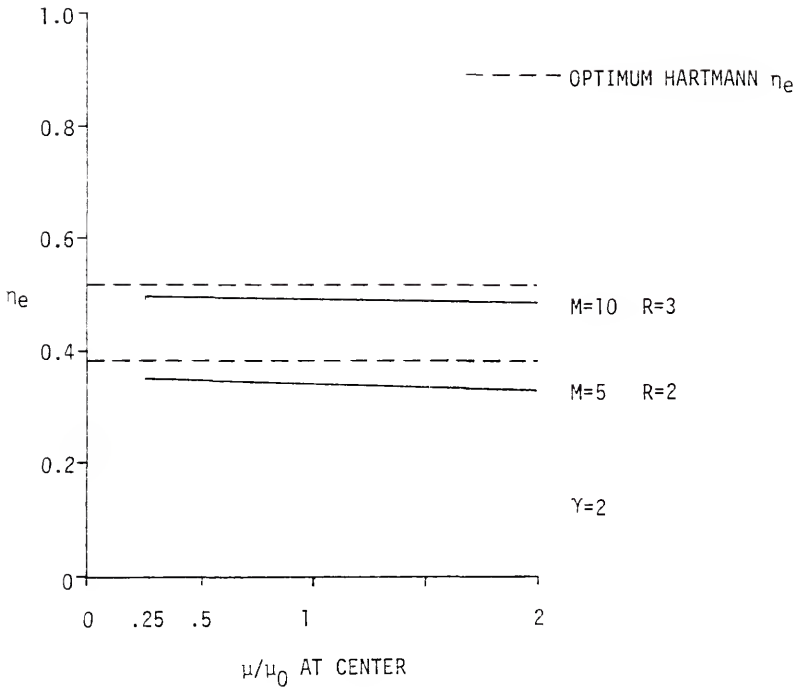

Figure 5-37. Efficiency for Viscosity Variation
$\mu/\mu_0 = 1 - \alpha_v(1 - (x/\gamma)^2)(1 - Y^2)$

From the plot it is clear that there is very little effect produced on the efficiency by the variation of the viscosity in the cross section. This once again shows that practically all the viscous effects are confined to the boundary layers on the wall and the effect of the viscosity variation in the core region of the flow is negligible. It should be noted that if the viscosity, or the conductivity, is allowed to vary along the wall, it produces an effect due to the apparent change in the Hartmann number of the channel. In this case, though, the specification of the Hartmann number of the generator becomes confused, and the results represent a case that is somewhat physically unrealistic.

CHAPTER VI
CONCLUSIONS

The main achievement of the work done in this study is the production of a computer program to solve the magnetohydrodynamic equations for laminar flow of a conducting fluid through a channel of rectangular cross section under the influence of a transversely applied magnetic field. Although these equations have been solved in an analytic form of an infinite series when the walls of the channel are either insulating or perfectly conducting, this is not possible for the more important case of the MHD generator where the walls perpendicular to the applied field are insulating and the walls parallel to the field are of arbitrary conductivity. The calculations presented in this report achieve a solution by breaking up the equations into their finite differences and solving them by a modified form of the Peaceman Rachford alternating direction implicit method. The equations presented are derived with the added possibility of varying the fluid properties of conductivity and viscosity from point to point over the cross section of the channel, thereby enabling the program to simulate in an average way the properties of a two-phase mixture of gas and liquid metal used as the working fluid of the generator. The program gives accurate solutions to these equations by relaxing the finite difference equations in a stable and rapidly converging manner for Hartmann numbers ranging from zero to

the relatively high value of 100, and an arbitrary value of the channel aspect ratio. This speed of calculation allows the generator parameters to be studied by calculating results for a large number of cases so that curves of efficiency and average velocity of the fluid can be plotted against Hartmann number, load factor and aspect ratio.

Contour plots of the magnetic flux density, which gives the streamlines of the current density, and contours of the velocity field are presented to indicate the main features to be encountered in the flow. The calculations confirm the results of previous investigators, that the thickness of the boundary layer on the insulating wall is proportional to the inverse of the Hartmann number and the thickness on the electrode wall is inversely proportional to the square root of the Hartmann number. The core region of the flow reported in the literature is found to be of uniform velocity only in the case where the conductivity of the fluid is constant. When it is allowed to vary, the velocity increases as the conductivity decreases, but the current streamlines are unaffected until the gradient of the velocity is enough to make the viscosity a significant retarding force on the flow.

The efficiency of the generator as a converter of pressure work of the fluid to electrical output is studied as a function of the general parameters. The main determinants of the efficiency are the Hartmann number and the load resistance of the external circuit. The effect of these parameters on the efficiency is well approximated

by the one-dimensional Hartmann solution. The peak of the efficiency versus load factor curve occurs when the resistance ratio equals the square root of the Hartmann number, and the maximum efficiency approaches one as the Hartmann number increases. Introducing the two-dimensional effects produced by a finite aspect ratio results in a decrease in efficiency due to losses in the electrode boundary layer, and a slight shift of the peak efficiency resistance ratio. For a given aspect ratio, this effect becomes smaller as the Hartmann number increases.

Another significant factor in the loss of efficiency is the conductivity decrease in the channel to be expected when a void fraction profile is introduced into the flow to simulate the two-phase condidions. This loss is produced by the requirement for a greater volumetric flow rate to sustain a given pressure drop. It is shown that if the conductivity gradients in the flow are not too great and the Hartmann number is high, then the flow at all points is well approximated by the inviscid core flow calculations. A small added loss of efficiency can be anticipated if the electrodes are less than perfectly conducting, and the losses for variations in the viscosity of the fluid are negligible.

The volumetric flow rate, being a significant design parameter of the generator, is studied for the effects produced by the changes in the generator conditions. Again as with the efficiency calculations, the Hartmann approximations are found to give good results for the effects of Hartmann number and load factor as long

as the aspect ratio is not too small. It is found that a good criterion for where the Hartmann approximation is accurate is that the product of the aspect ratio and the square root of the Hartmann number be greater than 10. A peak is found in the curve of flow rate versus aspect ratio at a low value of aspect ratio that decreases with increasing Hartmann number, but that this is not in any sense an optimum operating point. Again small variations are incurred for the cases when the conductivity of the electrodes is less than perfect. Also greater increases in the flow rate result as the conductivity decreases due to a peaking of the void fraction profile toward the center of the channel.

The computer program presented here is an effective tool for analyzing the magnetohydrodynamic generator under a wide variety of conditions. Although it is somewhat limited in only having rapid convergence for Hartmann numbers less than 100, this is the region of conditions under which it is most needed. For Hartmann numbers greater than this the approximate relations of the inviscid core flow calculations should be sufficiently accurate. But, in the case of low Hartmann number and low aspect ratio the two-dimensional solution is required and is effectively provided by the analysis done here.

For a number of practical situations the program can be seen as giving an effective means of determining whether a suggested change in the generator configuration is worthwhile. One such situation is the partitioned channel case analyzed previously. With the object of reducing the void fraction profile in the channel, the

partitions can only be determined to be effective in a trade-off between the improved efficiency of the flatter void fraction profile it provides, and the decreased efficiency due to the added walls and increased surface area of the channel. Since there are other reasons for breaking up the channel, such as decreasing the slip of the bubbles through the fluid, this analysis is not the only one that need be considered, but the program does indicate that the efficiency will not be seriously impaired if the Hartmann number of the entire channel is sufficiently high. In other situations where a change in the configuration is suggested, such as putting baffles in the Hartmann boundary layer to impede the return currents, the program can be helpful in determining its worth, but the internal parts of the program must first be modified slightly.

Although the program derived here is effective in analyzing the flow of the fluid at a given cross section, this is not the only area in which losses in efficiency occur, or in some cases even the most important one. Therefore, future work will concentrate on developing programs to analyze the end effects with the losses brought about by the three-dimensional aspects of the channel, and incorporating the more important two-phase aspects of the flow, such as the slip of the gas with respect to the liquid phase.

APPENDIX
COMPUTER PROGRAM

The program described here solves the magnetohydrodynamic equations in a rectangular duct with conductivity and viscosity variation within the cross section. The boundary conditions used are those appropriate for use with a Faraday generator configuration. The method of solution is by finite differences using the Peaceman Rachford Alternating Direction Implicit relaxation scheme.

The program listing follows this discussion. The program is broken up into a series of logical sections, each titled by a comment card. This description of the program proceeds along the lines of these divisions.

***** INITIALIZING STATEMENTS

These statements specify the dimensions of the arrays to be used. The indices specified as 20 represent the maximum number of nodes in the X direction. Indices of 50 represent the maximum number of nodes in the Y direction. To specify a grid beyond these limits requires a change of these statements.

***** START CASE ITERATION

Statement 100 is the start of a loop that includes the rest of the program. This section simply reads in the parameters for a given case and sets up the default values. All the data for a case is

found on one card. When no data card is found the program exits the loop by going to statement 999 and then stops.

Input Parameters:

Column	Symbol	Parameter	Format	Default	Range
1-5	H	Hartmann Number	F5.0	None	0-100
6-10	AR	Aspect Ratio	F5.0	None	.1-10
11-20	R	Relative Resistance	F10.0	None	.1-1000
21-30	WR	Electrode Resistance	F10.0	0	0-1000
31-35	ALPF	Conductivity Profile Parameter	F5.0	0	0-.999
36-40	ALPG	Viscosity Profile Parameter	F5.0	0	0-.999
41-42	NO	Time Step Parameter	I2	4	0-20
43-45	EMAX	Maximum Time Step	F3.0	15	1-50
46-50	TEST	Convergence Test Parameter	F5.0	.05	.001-.1
51-55	LLLMAX	Maximum Number of Iterations	I5	150	50-500
56-57	M	Number of Nodes in X Direction	I2	20	10-20
58-59	N	Number of Nodes in Y Direction	I2	30	10-50
60-61	NB	Number of Nodes in Hartmann Layer	I2	10	5-20
62	ITBF	Flag to Iterate on B1 Boundary Conditions	I1	0	0-1
63	IGF	Flag for Initial Guess	I1	0	0-1
64	IPLOT	Flag for Plot Routine	I1	0	0-1

Comments:

H, AR, and R must always be specified.

If R or WR are greater than 999, then they are assumed to be infinite as in the case of the insulating channel.

ALPF and ALPG are arbitrary parameters used in subroutine FFGG to specify the conductivity and viscosity profile. The present functional relation is a double parabola [$\sigma/\sigma_0=1-ALPF(1-(X/AR)^2)(1-Y^2)$] with values at the center of the channel related to ALPF and ALPG [$\sigma_c/\sigma_0=1-ALPF$; $\mu/\mu_0=1-ALPG$].

NO and EMAX relate to the calculation of the time step or iteration parameter. The value of the time step between each iteration starts at half the square of the spacing between nodes in the Y direction in the Hartmann boundary layer, and increases geometrically in NO steps to a maximum value of EMAX times the spacing squared.

The proper choice of EMAX for a given H and R relates to how fast the solution will converge, but the default of 15 is found to be fairly good in most cases.

TEST relates to the convergence criterion and the default gives four-place accuracy for Hartmann numbers 30 to 100. Smaller Hartmann numbers require TEST to be a little smaller to get four-place accuracy, while larger Hartmann numbers can use a larger value to stop the iterations sooner.

M and N specify the number of grid points. M is not critical and the default value is satisfactory. N of 20 is good for Hartmann numbers less than 30, but for Hartmann numbers 30 to 100 an N of 30 is necessary for accuracy. NB of 10 is a satisfactory number of nodes in the boundary layer for most cases.

If ITBF is one, the boundary condition B_1 is iterated on to give the specified value of R. If not the constant value given by the one-dimensional Hartmann solution is used, and the corresponding value of R is calculated. If the Hartmann number is greater than 50, the iteration on the boundary condition requires a large number of iterations so it is not used. The one-dimensional solution is sufficiently accurate in this case so that R is not far off the value specified.

If IGF is one, the program initially guesses all zeros for V and B, rather than the one-dimensional Hartmann solution. In the case of low aspect ratios the guess of zero was found to produce faster convergence.

If IPLOT is one, the program gives a GOULD plot of the velocity contours and current streamlines. This is presently set up to plot only for an asepct ratio of 2.

***** CALCULATE THE GRID POINTS

This is a simple routine to calculate the Y position of the horizontal rows and the X position of the vertical columns. X(1) and Y(1) are at the center of the channel, and X(M) at the electrode wall and Y(N) at the insulating wall. Rows Y(NH) to Y(N)are evenly spaced in the boundary layer of thickness DEL/H, where DEL is initialized to 5. Likewise, the columns X(MH) through X(M) are evenly spaced but to a thickness of $DEL/H^{\frac{1}{2}}$, unless the thickness of the boundary layer is greater than half the channel. X(1) through X(MN) are equally spaced Y(1) through Y(NH) have linearly increasing spacing from the value in the Hartmann layer to the center of the channel. The nodal locations are printed out.

***** INITIAL GUESS

Depending on the value of the flag IGF the initial values of the arrays V(I,J) and B(I,J) I=1,M; J=1,N are set equal to the one-dimensional Hartmann solution or zero. The value of the previous iteration VP(I,J) and BP(I,J), which are used for test purposes, are set equal to zero in the initializing statements.

***** CALCULATE THE CONDUCTIVITY AND VISCOSITY VARIATION

This is done in subroutine FFGG where σ_0/σ=F(I,J,1) and μ/μ_0=G(I,J,1) are calculated. The last indices of the arrays indicate these are the values of the functions. F(I,J,2) and G(I,J,2) are the derivatives of the functions in the X direction, and F(I,J,3) and G(I,J,3) are the derivatives in the Y direction at the node (I,J).

***** CALCULATE COEFFICIENTS FOR DIFFERENCE OPERATORS

The MHD equations to be solved for are given in terms of linear operators by

$$(L_X^B + L_Y^B)B + MP_Y V = 0$$

$$(L_X^V + L_Y^V)V + 1 + MP_Y B = 0$$

where the operators are defined as

$$L_X^B = F\frac{\partial^2}{\partial X^2} + \frac{\partial F}{\partial X}\frac{\partial}{\partial X} \qquad L_Y^B = F\frac{\partial^2}{\partial Y^2} + \frac{\partial F}{\partial Y}\frac{\partial}{\partial Y}$$

$$L_X^V = G\frac{\partial^2}{\partial X^2} + \frac{\partial G}{\partial X}\frac{\partial}{\partial X} \qquad L_Y^V = G\frac{\partial^2}{\partial Y^2} + \frac{\partial G}{\partial Y}\frac{\partial}{\partial Y}$$

$$P_Y = \frac{\partial}{\partial Y}$$

In this section these operators are calculated as the coefficients for a three-point finite difference approximation at each node in the grid assuming arbitrary spacings between nodes. For the operator

$BLX=\frac{1}{2}L_X^B$

BLX(I,J,1) is the coefficient multiplying the value of B(I,J)

BLX(I,J,2) is the coefficient multiplying the value of B(I+1,J)

BLX(I,J,3) is the coefficient multiplying the value of B(I-1,J)

The indices of the other finite difference operators are related in a similar manner to their linear operators and nodal locations. PY is also multiplied by the Hartmann number for convenience ($PY=\frac{1}{2}MP_Y$).

The coefficients SA, SB, SC, SD at the end are special four-point fits for calculating the slope of the functions at the insulating wall from the value of the functions at the first four points at the wall.

$$\left.\frac{\partial B}{\partial n}\right|_{WALL} = SA*B(I,N-3)+SB*B(I,N-2)+SC*B(I,N-1)+SD*B(I,N)$$

***** START ITERATION AND SET TIME STEP

This marks the start of the Peaceman Rachford Alternating Direction Implicit relaxation scheme. This point through statement 50 is in one DO loop that each time through makes one complete iteration step. The size in time of each step (E) is calculated here.

The PRADI relaxation scheme calculates the next iteration by the following equations

$$(1 - \tfrac{1}{2}EL_X^V)VS = (1 + \tfrac{1}{2}EL_Y^V)V^n + \tfrac{1}{2}E(1 + MP_Y B^n)$$

$$(1 - \tfrac{1}{2}EL_X^B)BS = (1 + \tfrac{1}{2}EL_Y^B)B^n + \tfrac{1}{2}EMP_Y V^n$$

$$(1 - \tfrac{1}{2}EL_Y^V)V^{n+1} - \tfrac{1}{2}EMP_Y B^{n+1} = \tfrac{1}{2}E + (1 + \tfrac{1}{2}EL_X^V)VS$$

$$(1 - \tfrac{1}{2}EL_Y^B)B^{n+1} - \tfrac{1}{2}EMP_Y V^{n+1} = (1 + \tfrac{1}{2}EL_X^B)BS$$

where V^n is the present value, VS is the intermediate value, and V^{n+1} is the value of the next iteration. Likewise for B^n, BS, and B^{n+1}.

***** CALCULATE V STAR

The value of VS is calculated from the first equation which is implicit only in the X direction and so is solved horizontally row by row. Using the finite difference coefficients calculated previously for the operators, the elements of the following tridiagonal matrix equation are evaluated.

$$\begin{bmatrix} AV(1) & BV(1) & & & & \\ CV(2) & AV(2) & BV(2) & & & \\ & \ddots & \ddots & \ddots & & \\ & & \ddots & \ddots & \ddots & BV(M-2) \\ & & & CV(M-1) & AV(M-1) & \end{bmatrix} \begin{Bmatrix} VS(1) \\ VS(2) \\ \vdots \\ VS(M-1) \end{Bmatrix} = \begin{Bmatrix} RV(1) \\ RV(2) \\ \vdots \\ RV(M-1) \end{Bmatrix}$$

The boundary conditions are then applied on the first equation and VS(M) is known to be zero.

***** SOLVE TRIDIAGONAL SYSTEM

This is a simple routine to solve the tridiagonal system of equations by Gaussian elimination. It is cut down to use the minimum amount of storage possible.

***** CALCULATE B STAR

The elements of the matrix equation for BS are then found in much the same manner. The following matrix equation is then solved once for each row in the grid.

$$\begin{bmatrix} DB(1) & EB(1) & & & \\ FB(2) & DB(2) & EB(2) & & \\ & \ddots & \ddots & \ddots & \\ & & & EB(M-1) & \\ & & FB(M) & DB(M) & \end{bmatrix} \begin{Bmatrix} BS(1) \\ BS(2) \\ \vdots \\ BS(M) \end{Bmatrix} = \begin{Bmatrix} RB(1) \\ RB(2) \\ \vdots \\ RB(M) \end{Bmatrix}$$

The boundary conditions are applied on the first and last equations with the conductivity of the electrode (WR) coming into play on the M^{th} term. If WR>999, it is set to infinity by replacing the M^{th} equation to give BS(M)=B1. The tridiagonal system is then solved using essentially the same routine as for the VS equation.

***** CALCULATE V AND B SIMULTANEOUSLY

The final two finite difference equations must be solved simultaneously for the value of the next iteration. The elements of the following matrix equation are then evaluated.

$$
\begin{bmatrix}
AV(1) & BV(1) & & & & & & DV(1) & EV(1) & & & \\
CV(2) & AV(2) & BV(2) & & & & & FV(2) & DV(2) & EV(2) & & \\
 & \ddots & \ddots & \ddots & & & & & \ddots & \ddots & \ddots & \\
 & & \ddots & \ddots & \ddots & BV(N-2) & & & & \ddots & \ddots & EV(N-2) \\
 & & & \ddots & \ddots & \ddots & & & & & \ddots & \ddots \\
 & & & & CV(N-1) & AV(N-1) & & & & & FV(N-1) & DV(N-1) \\
AB(1) & BB(1) & & & & & & DB(1) & EB(1) & & & \\
CB(2) & AB(2) & BB(2) & & & & & FB(2) & DB(2) & EB(2) & & \\
 & \ddots & \ddots & \ddots & & & & & \ddots & \ddots & \ddots & \\
 & & \ddots & \ddots & \ddots & BB(N-2) & & & & \ddots & \ddots & EB(N-2) \\
 & & & \ddots & \ddots & \ddots & & & & & \ddots & \ddots \\
 & & & & CB(N-1) & AB(N-1) & & & & & FB(N-1) & DB(N-1)
\end{bmatrix}
\begin{bmatrix} V(1) \\ V(2) \\ \vdots \\ V(N-1) \\ B(1) \\ B(2) \\ \vdots \\ B(N-1) \end{bmatrix}
=
\begin{bmatrix} RV(1) \\ RV(2) \\ \vdots \\ RV(N-1) \\ RB(1) \\ RB(2) \\ \vdots \\ RB(N-1) \end{bmatrix}
$$

These equations are implicit in the Y direction only and so are solved once along each vertical column of nodes. The boundary conditions are applied to the first and last equations in each half of the matrix, and the equation for B is modified to set B(1) equal to zero.

***** SOLVE THE MATRIX EQUATION

This section is an analogous relation to the previous equation of the tridiagonal system, although the routine is more complicated due to the matrix required for the simultaneous solution.

***** CALCULATE RIGHT COLUMN B

Since the far right column is on the electrode the velocity is zero, so that this column is solved separately for B alone. The first and last nodes in the column are known from the boundary conditions. The matrix equation is given by

$$\begin{bmatrix} DB(1) & EB(1) & & & \\ FB(2) & DB(2) & EB(2) & & \\ & \ddots & \ddots & \ddots & \\ & & \ddots & \ddots & EB(N-3) \\ & & & FB(N-2) & DB(N-2) \end{bmatrix} \begin{Bmatrix} B(2) \\ B(3) \\ \vdots \\ B(N-1) \end{Bmatrix} = \begin{Bmatrix} EB(1) \\ RB(2) \\ \vdots \\ RB(N-2) \end{Bmatrix}$$

The conductivity of the electrode again comes into play. If WR> 999, the whole step is bypassed, and B is set equal to the B_1 boundary condition. Otherwise the previously used routine for solving the tridiagonal system is applied.

***** TEST FOR CONVERGENCE

TESTV and TESTB are the test values for the increment in the values of V and B from their previous values, and are calculated based on the approximate maximum of V and B in the cross section, the size of the time step, and the TEST parameter input. Each node is tested for convergence and a zero or an asterisk is put in its position in arrays ICV and ICB depending on whether it is converged or not. If all the nodes are converged in each parameter, the DO loop is exited to statement 33. Otherwise the values of VP and BP are reset to the present iteration and the loop continues. If the scheme fails to converge by iteration LLLMAX, the loop exits at statement 50, and ICV and ICB are printed out showing the nodes that fail to converge.

***** CALCULATE B1 BOUNDARY CONDITION

The value of the boundary condition B1 is given in terms of the load resistance, electrode resistance, and the solution for B by

$$B_1 = \left(\frac{1}{1+WR/R*AR}\right)\left[\frac{WR}{R*AR}\int_0^1 B(AR,Y)dY - \frac{1}{R*AR}\int_0^Y F\left.\frac{\partial B}{\partial Y}\right|_{Y=1} dX\right]$$

This is calculated and set equal to B1S for later printout as the calculated value of B1. So that the boundary condition is not changed too fast, it is modified by the underrelaxation parameter W. W is calculated previously at the start of the case iteration and depends on R and WR in an empirically derived equation. It is kept less than one.

If ITBF is zero and B1 is not to be iterated on, this calculation is discarded and the one-dimensional value from the Hartmann

solution is used. If the load resistance is to be infinite (R>999), this is discarded and zero is used. The array values are set for the B1 and the loop returns for the next iteration.

***** END OF PRADI SOLUTION OF DIFFERENTIAL EQUATIONS

After the end of the PRADI solution the number of iterations it took, the time and relaxation parameters, and the test values are printed out. The calculated value of the load resistance (RS) that the solution corresponds to is then determined based on the calculated value of B1S and the set values. If the B1 is iterated on this should be very close to the set value. The load factor is then calculated from this.

***** CALCULATE AVERAGE VELOCITIES

The average velocity VAVE is obtained by averaging the values at the corners of each elemental rectangle of the grid and multiplying by its area and summing.

***** CALCULATION OF EFFICIENCIES

The efficiency ETA is calculated from the imposed value of B1, the correct load resistance RS, and the average velocity VAVE. ETAO is a calculation of the one-dimensional Hartmann efficiency at the specified value of R.

***** CALCULATE VELOCITY CONTOURS

The velocity array V is written out and then the contours of constant velocity are calculated using the subroutine CONTOR.

The inputs to CONTOR are the velocity array V, node location X,Y, the desired spacing between contours VSP, number of contours searched for (10), number of nodes M,N, the Hartmann number H, load factor RK, electrode resistance factor WK, and IPLOT.

***** CALCULATE CURRENT STREAMLINES

The magnetic flux density B is written out and the streamlines are calculated by a call to CONTOR similar to the previous case for the velocity. The velocity and the magnetic flux density are printed out in the order that the nodes would appear if they were in the fourth quadrant of the channel, with the insulating wall at the bottom row and the electrode wall at the right. The program then returns to statement 100 to read in the data for the next case. All the format statements are at the bottom of the program.

SUBROUTINE FFGG

This subroutine calculates the conductivity and viscosity variation through the common variable FG. The set up here is to calculate the functions and their derivatives using a double parabolic function with the parameters A and B. To use a different functional profile requires only changes to this subroutine and redefining the parameters A and B.

SUBROUTINE CONTOR

This subroutine calculates the contours of any field array by linear interpolation between nodes. These locations are put into arrays XX and YY up to 200 points per given contour. These linear

arrays are printed out one contour at a time. The routine is also set up to plot the contours on a GOULD plotter, but this set up is specifically designed to plot the quarter channel for the aspect ratio of 2:1. If another aspect ratio is desired, the plot is incorrectly drawn unless this routine is modified. The contours can be plotted by hand using the printed locations of the contour points. In this case the value of IPLOT should be left at zero.

```
C*****  MHD GENERATOR DUCT FLOW WITH CROSS STREAM DEPENDENT FLUID PROPERTIES
C*****  INITIALIZING STATEMENTS
      DIMENSION VLX(20,50,3),VLY(20,50,3),BLX(20,50,3),BLY(20,50,3)
      DIMENSION PY(50,3),AV(50),BV(50),CV(50),DV(50),EV(50),FV(50)
      DIMENSION AB(50),BB(50),CB(50),DB(50),EB(50),FB(50),RV(50),RB(50)
      DIMENSION V(20,50),VP(20,50),VS(20,50)
      DIMENSION B(20,50),BP(20,50),BS(20,50)
      DIMENSION X(20),Y(50)
      DIMENSION ICV(20,50),ICB(20,50)
      DIMENSION ER(10),VL(10),VL1(10),VL2(10),IVL(10)
      COMMON /FG/F(20,50,3),G(20,50,3)
      DATA LAST,IZER/1H*,1H0/
      DATA DEL,VP,BP/5.,2000*0.0/
      CALL PLOTS(-70,,20,)
      CALL LINEWT(-1)
      CALL PLOT(1.5,1.5,-3)
C*****  START CASE ITERATION
  100 READ(5,101,END=999)H,AR,R,WR,ALPF,ALPG,NO,EMAX,TEST,LLLMAX,M,N,NB,
     1 IIBF,IGF,IPLOT
  101 FORMAT(2F5.0,2F10.0,2F5.0,I2,F3.0,F5.0,I5,3I2,3I1)
      IF(M.EQ.0)M=20
      IF(N.EQ.0)N=30
      IF(NB.EQ.0)NB=10
      IF(NO.EQ.0)NO=4
      IF(EMAX.EQ.0.0)EMAX=15.
      IF(TEST.EQ.0.0)TEST=0.05
      IF(LLLMAX.EQ.0)LLLMAX=150
      MH=M/2
      NH=N-NB
      NM=N-1
      MM=M-1
      NMM=NM-1
      W=(R*WR/AR)/(1.75+7.*WR/AR)
      IF(W.GT.1.)W=1.0
      WK=WR/(1.+WR)
      RK=R/(1.+R)
      WRITE(6,47)H,RK,WK,AR,M,N
      IF(ALPF.NE.0.0)WRITE(6,89)ALPF
      IF(ALPG.NE.0.0)WRITE(6,88)ALPG
C*****  CALCULATE THE GRID POINTS
      A=(1.-DEL/H)/(NH-1.)
      D=0.5/H
      PA=-(A-D)/NH
      PB=2*A-C-PA
```

```
      PC=-2.*A+D
      HSR=H**0.5
      IF((DEL/H).GT.(1.-(1.*NH)/N))GO TO 3
      DO 1 I=1,NH
    1 Y(I)=PA*I*I+PB*I+PC
      DO 2 I=NH,N
    2 Y(I)=1.-DEL/H+DEL*(I-NH)/(H*(N-NH))
      GO TO 5
    3 DO 4 I=1,N
    4 Y(I)=(I-1.)/(N-1.)
    5 IF((DEL/HSR).GT.0.5*AR)GO TO 8
      DO 6 I=1,MH
    6 X(I)=(I-1)*(AR-DEL/HSR)/(MH-1.)
      DO 7 I=MH,M
    7 X(I)=AR-DEL/HSR+DEL*(I-MH)/(HSR*(M-MH))
      GO TO 10
    8 DO 9 I=1,M
    9 X(I)=AR*(I-1)/(M-1)
   10 CONTINUE
      WRITE(6,43)(X(I),I=1,M)
      WRITE(6,44)(Y(J),J=1,N)
      IF(IGF.EQ.1)GO TO 70
C*****  INITIALLY GUESS ONE DIMENSIONAL APPROXIMATION
      C=(R+1.)/(H*(H+R*TANH(H)))
      DO 11 J=1,N
      IF(Y(J).LT.(1.-14./H))GO TO 12
      V0=C*(1.-EXP(H*(Y(J)-1.)))
      B0=C*EXP(H*(Y(J)-1.))-Y(J)/H
      GO TO 13
   12 V0=C
      B0=-Y(J)/H
   13 DO 11 I=1,M
      V(I,J)=V0
   11 B(I,J)=B0
      GO TO 71
C***** INITIALIZE TO ZERO
   70 DO 72 J=1,N
      DO 72 I=1,M
      V(I,J)=0.0
   72 B(I,J)=0.0
   71 CONTINUE
C*****  CALCULATE THE CONDUCTIVITY AND VISCOSITY VARIATION
      CALL FFGG(M,N,X,Y,ALPF,ALPG)
C*****  CALCULATE COEFFICIENTS FOR DIFFERENCE OPERATORS
```

```
      DO 20 J=1,N
      IF(J.EQ.1.OR.J.EQ.N)GO TO 24
      YM=Y(J-1)-Y(J)
      YP=Y(J)-Y(J+1)
      YMP=Y(J-1)-Y(J+1)
      GO TO 25
   24 IF(J.EQ.N)GO TO 19
      YP=Y(J)-Y(J+1)
      YM=YP
      YMP=2.*YP
      GO TO 25
   19 YM=Y(J-1)-Y(J)
      YP=YM
      YMP=2.*YM
   25 PY(J,1)=0.5*H*(YM-YP)/(YM*YP)
      PY(J,2)=-0.5*H*YM/(YP*YMP)
      PY(J,3)=0.5*H*YP/(YM*YMP)
      DO 20 I=1,M
      IF(I.EQ.1.OR.I.EQ.M)GO TO 21
      XM=X(I-1)-X(I)
      XP=X(I)-X(I+1)
      XMP=X(I-1)-X(I+1)
      GO TO 22
   21 IF(I.EQ.M)GO TO 23
      XP=X(I)-X(I+1)
      XM=XP
      XMP=2.*XP
      GO TO 22
   23 XM=X(I-1)-X(I)
      XP=XM
      XMP=2.*XM
   22 VLX(I,J,1)=(-2.*G(I,J,1)+G(I,J,2)*(XM-XP))/(XM*XP*2.)
      VLX(I,J,2)=(2.*G(I,J,1)-G(I,J,2)*XM)/(XP*XMP*2.)
      VLX(I,J,3)=(2.*G(I,J,1)+G(I,J,2)*XP)/(XM*XMP*2.)
      VLY(I,J,1)=(-2.*G(I,J,1)+G(I,J,3)*(YM-YP))/(YM*YP*2.)
      VLY(I,J,2)=(2.*G(I,J,1)-G(I,J,3)*YM)/(YP*YMP*2.)
      VLY(I,J,3)=(2.*G(I,J,1)+G(I,J,3)*YP)/(YM*YMP*2.)
      BLX(I,J,1)=(-2.*F(I,J,1)+F(I,J,2)*(XM-XP))/(XM*XP*2.)
      BLX(I,J,2)=(2.*F(I,J,1)-F(I,J,2)*XM)/(XP*XMP*2.)
      BLX(I,J,3)=(2.*F(I,J,1)+F(I,J,2)*XP)/(XM*XMP*2.)
      BLY(I,J,1)=(-2.*F(I,J,1)+F(I,J,3)*(YM-YP))/(YM*YP*2.)
      BLY(I,J,2)=(2.*F(I,J,1)-F(I,J,3)*YM)/(YP*YMP*2.)
      BLY(I,J,3)=(2.*F(I,J,1)+F(I,J,3)*YP)/(YM*YMP*2.)
   20 CONTINUE
```

```
      SA=(Y(N-2)-Y(N))*(Y(N-1)-Y(N))/((Y(N-3)-Y(N-2))*(Y(N-3)-Y(N-1))*(Y
     1(N-3)-Y(N)))
      SB=-(Y(N-3)-Y(N))*(Y(N-1)-Y(N))/((Y(N-3)-Y(N-2))*(Y(N-2)-Y(N-1))*(
     1Y(N-2)-Y(N)))
      SC=(1.-SA*(Y(N-3)-Y(N))-SB*(Y(N-2)-Y(N)))/(Y(N-1)-Y(N))
      SD=-SA-SB-SC
C*****  START ITERATION AND SET TIME STEP (E)
      DO 50 LLL=1,LLLMAX
      IF((LLL-1).GT.NO)GO TO 57
      E=0.5*((Y(N)-Y(NM))**2.)*(EMAX*2.)**((LLL-1.)/NO)
   57 CONTINUE
C*****  CALCULATE V STAR
      DO 14 J=1,NM
      DO 15 I=1,MM
      AV(I)=1.-E*VLX(I,J,1)
      BV(I)=-E*VLX(I,J,2)
      CV(I)=-E*VLX(I,J,3)
      IF(J.EQ.1)GO TO 16
      RV(I)=V(I,J)+E*(VLY(I,J,1)*V(I,J)+VLY(I,J,2)*V(I,J+1)+VLY(I,J,3)*V
     1(I,J-1)+0.5*PY(J,1)*B(I,J)+PY(J,2)*B(I,J+1)+PY(J,3)*B(I,J-1))
      GO TO 15
   16 RV(I)=V(I,J)+E*(VLY(I,J,1)*V(I,J)+(VLY(I,J,2)+VLY(I,J,3))*V(I,J+1)
     1+0.5*(PY(J,1)+2.*PY(J,3))*B(I,J)+(PY(J,2)-PY(J,3))*B(I,J+1))
   15 CONTINUE
      BV(1)=BV(1)+CV(1)
C*****  SOLVE TRIDIAGONAL SYSTEM
      DO 17 I=2,MM
      AV(I)=AV(I)-CV(I)*BV(I-1)/AV(I-1)
   17 RV(I)=RV(I)-CV(I)*RV(I-1)/AV(I-1)
      VS(M,J)=0.0
      VS(MM,J)=RV(MM)/AV(MM)
      DO 14 K=2,MM
      I=MM+1-K
   14 VS(I,J)=(RV(I)-BV(I)*VS(I+1,J))/AV(I)
C*****  CALCULATE B STAR
      DO 27 J=2,NM
      DO 28 I=1,M
      DB(I)=1.-E*BLX(I,J,1)
      EB(I)=-E*BLX(I,J,2)
      FB(I)=-E*BLX(I,J,3)
   28 RB(I)=B(I,J)+E*(BLY(I,J,1)*B(I,J)+BLY(I,J,2)*B(I,J+1)+BLY(I,J,3)*B
     1(I,J-1)+PY(J,1)*V(I,J)+PY(J,2)*V(I,J+1)+PY(J,3)*V(I,J-1))
      EB(1)=EB(1)+FB(1)
      FB(M)=FB(M)+EB(M)
```

```
      RB(M)=RB(M)-EB(M)*2.*(X(M)-X(MM))*WR*(B(I,N)-B(M,J))/F(M,J,1)
      IF(WR.GT.999)RB(M)=B(1,N)*DB(M)
      IF(WR.GT.999.)FB(M)=0.0
C*****  SOLVE TRIDIAGONAL SYSTEM
      DO 26 I=2,M
      DB(I)=DB(I)-FB(I)*EB(I-1)/DB(I-1)
   26 RB(I)=RB(I)-FB(I)*RB(I-1)/DB(I-1)
      BS(M,J)=RB(M)/DB(M)
      DO 27 K=2,M
      I=M+1-K
   27 BS(I,J)=(RB(I)-EB(I)*BS(I+1,J))/DB(I)
C*****  CALCULATE V AND B SIMULTANEOUSLY
      DO 29 I=1,MM
      DO 30 J=1,NM
      AV(J)=1.-E*VLY(I,J,1)
      BV(J)=-E*VLY(I,J,2)
      CV(J)=-E*VLY(I,J,3)
      DV(J)=-E*PY(J,1)
      EV(J)=-E*PY(J,2)
      FV(J)=-E*PY(J,3)
      AB(J)=-E*PY(J,1)
      BB(J)=-E*PY(J,2)
      CB(J)=-E*PY(J,3)
      DB(J)=1.-E*BLY(I,J,1)
      EB(J)=-E*BLY(I,J,2)
      FB(J)=-E*BLY(I,J,3)
      IF(I.EQ.1)GO TO 31
      RV(J)=VS(I,J)+E*(0.5*VLX(I,J,1)*VS(I,J)+VLX(I,J,2)*VS(I+1,J)+VLX(I
     1,J,3)*VS(I-1,J))
      IF(J.EQ.1)GO TO 30
      RB(J)=BS(I,J)+E*(BLX(I,J,1)*BS(I,J)+BLX(I,J,2)*BS(I+1,J)+BLX(I,J,3
     1)*BS(I-1,J))
      GO TO 30
   31 RV(J)=VS(I,J)+E*(0.5*VLX(I,J,1)*VS(I,J)+(VLX(I,J,2)+VLX(I,J,3))*VS
     1(I+1,J))
      IF(J.EQ.1)GO TO 30
      RB(J)=BS(I,J)+E*(BLX(I,J,1)*BS(I,J)+(BLX(I,J,2)+BLX(I,J,3))*BS(I+1
     1,J))
   30 CONTINUE
      BV(1)=BV(1)+CV(1)
      DV(1)=DV(1)+2.*FV(1)
      EV(1)=EV(1)-FV(1)
      RV(NM)=RV(NM)-EV(NM)*B(1,N)
      RB(NM)=RB(NM)-EB(NM)*B(1,N)
```

```
      DB(1)=1.0
      EB(1)=0.0
      FB(1)=0.0
      AB(1)=0.0
      BB(1)=0.0
      CB(1)=0.0
      PB(1)=0.0
C*****  SOLVE THE MATRIX EQUATION
      DO 34 J=2,NM
      DI=AV(J-1)*DB(J-1)-AB(J-1)*DV(J-1)
      RV(J)=RV(J)-(CV(J)*(DB(J-1)*RV(J-1)-DV(J-1)*RB(J-1))-FV(J)*(AB(J-1
     1)*RV(J-1)-AV(J-1)*RB(J-1)))/DI
      RB(J)=RB(J)-(CB(J)*(DB(J-1)*RV(J-1)-DV(J-1)*RB(J-1))-FB(J)*(AB(J-1
     1)*RV(J-1)-AV(J-1)*RB(J-1)))/DI
      AV(J)=AV(J)+(CV(J)*(DV(J-1)*BB(J-1)-DB(J-1)*BV(J-1))-FV(J)*(AV(J-1
     1)*BB(J-1)-AB(J-1)*BV(J-1)))/DI
      AB(J)=AB(J)+(CB(J)*(DV(J-1)*BB(J-1)-DB(J-1)*BV(J-1))-FB(J)*(AV(J-1
     1)*BB(J-1)-AB(J-1)*BV(J-1)))/DI
      DV(J)=DV(J)+(CV(J)*(DV(J-1)*EB(J-1)-DB(J-1)*EV(J-1))-FV(J)*(AV(J-1
     1)*EB(J-1)-AB(J-1)*EV(J-1)))/DI
      DB(J)=DB(J)+(CB(J)*(DV(J-1)*EB(J-1)-DB(J-1)*EV(J-1))-FB(J)*(AV(J-1
     1)*EB(J-1)-AB(J-1)*EV(J-1)))/DI
   34 CONTINUE
      RV(NM)=(DB(NM)*RV(NM)-DV(NM)*RB(NM))/(DB(NM)*AV(NM)-DV(NM)*AB(NM))
      RB(NM)=(RB(NM)-AB(NM)*RV(NM))/DB(NM)
      DO 35 K=2,NM
      J=NM+1-K
      RV(J)=RV(J)-BV(J)*RV(J+1)-EV(J)*RB(J+1)
      RB(J)=RB(J)-EB(J)*RV(J+1)-EB(J)*RB(J+1)
      RV(J)=(DB(J)*RV(J)-DV(J)*RB(J))/(DB(J)*AV(J)-DV(J)*AB(J))
   35 RB(J)=(RB(J)-AB(J)*RV(J))/DB(J)
      DO 29 J=1,NM
      V(I,J)=RV(J)
   29 E(I,J)=RB(J)
C*****  CALCULATE RIGHT COLUME B
      IF(WR.GT.999.)GO TO 59
      DO 36 J=2,NM
      DB(J-1)=1.-E*BLY(I,J,1)
      DB(J-1)=DB(J-1)+F*BLX(M,J,2)*2.*(X(M)-X(MM))*WR/F(M,J,1)
      EB(J-1)=-E*BLY(I,J,2)
      FB(J-1)=-E*BLY(I,J,3)
   36 RB(J-1)=BS(M,J)+E*(BLX(M,J,1)*BS(M,J)+(BLX(M,J,2)+BLX(M,J,3))*BS(M
     1M,J)+BLX(M,J,2)*2.*(X(M)-X(MM))*WR*B(1,N)/F(M,J,1))
      RB(N-2)=RB(N-2)-FB(N-2)*B(1,N)
```

```
C*****  SOLVE TRIDIAGONAL SYSTEM
      DO 38 J=2,NMM
      DB(J)=DB(J)-FB(J)*EB(J-1)/DB(J-1)
   38 RB(J)=RB(J)-FB(J)*RB(J-1)/DB(J-1)
      B(M,NM)=RB(NMM)/DB(NMM)
      V(M,NM)=0.0
      B(M,1)=0.0
      V(M,1)=0.0
      DO 37 K=2,NMM
      J=NMM+1-K
      B(M,J+1)=(RB(J)-EB(J)*B(M,J+2))/DB(J)
   37 V(M,J+1)=0.0
      GO TO 58
   59 DO 60 J=2,N
      V(M,J)=0.0
   60 B(M,J)=B(1,N)
      V(M,1)=0.0
      B(M,1)=0.0
   58 CONTINUE
C*****  TEST FOR CONVERGENCE
      ITEST=0
      TESTV=TEST*V(1,NH)*E
      TESTB=TEST*ABS(B(1,NH))*E
      DO 18 I=1,M
      DO 18 J=1,N
      IF(ABS(V(I,J)-VP(I,J)).GT.TESTV)GO TO 52
      ITEST=ITEST+1
      ICV(I,J)=IZER
      GO TO 53
   52 ICV(I,J)=IAST
   53 IF(ABS(B(I,J)-BP(I,J)).GT.TESTB)GO TO 54
      ITEST=ITEST+1
      ICB(I,J)=IZER
      GO TO 18
   54 ICB(I,J)=IAST
   18 CONTINUE
      IF(ITEST.EQ.(2*M*N))GO TO 33
      DO 32 I=1,M
      DO 32 J=1,N
      VP(I,J)=V(I,J)
   32 BP(I,J)=B(I,J)
C*****  CALCULATE BI BOUNDARY CONDITION
      B1=0.0
      DO 39 I=1,M
```

```
   39 RB(I)=SA*B(I,N-3)+SB*B(I,N-2)+SC*B(I,N-1)+SD*B(I,N)
      DO 45 I=2,M
   45 B1=B1-0.5*(X(I)-X(I-1))*(F(I,N,1)*RB(I)+F(I-1,N,1)*RB(I-1))/(R*AR)
      DO 51 J=2,N
   51 B1=B1+(Y(J)-Y(J-1))*0.5*(B(M,J)+B(M,J-1))*WR/(R*AR)
      B1=B1/(1.+WR/(R*AR))
      E1S=B1
      B1=B(1,N)+W*(B1-E(1,N))
      IF(ITBF.EQ.0)B1=(1.+R)/(H*(H+R*TANH(H)))-1./H
      IF(R.GT.999.)B1=0.0
      DO 46 I=1,M
   46 B(I,N)=B1
   50 CONTINUE
C*****  END OF PRADI SOLUTION OF DIFFERENTIAL EQUATIONS
      WRITE(6,98)LLL,ITEST,((ICV(I,J),I=1,20),(ICB(K,J),K=1,20),J=1,N)
   33 CONTINUE
      WRITE(6,41)LLL,E,W,TEST,TESTV,TESTB
      IF(B1.EQ.0.0)B1=0.0000001
      RS=R*B1S/B1+(B1S/B1-1.)*WR/AR
      RKS=RS/(RS+1.)
      WRITE(6,97)B1S,RKS,RS
C*****  CALCULATE AVERAGE VELOCITIES
      VAVE=0.0
      DO 56 I=1,MM
      DO 56 J=1,NM
   56 VAVE=VAVE+0.25*(X(I+1)-X(I))*(Y(J+1)-Y(J))*(V(I,J)+V(I+1,J)+V(I,J+
     1 1)+V(I+1,J+1))/AR
      WRITE(6,42)VAVE
C*****  CALCULATION OF EFFICIENCIES
      ETA=RS*B1*B1/VAVE
      B10=-(1./H)+(1.+R)/(H*(H+R*TANH(H)))
      V0=(1.+R)*(1.-TANH(H)/H)/(H*(H+R*TANH(H)))
      ETA0=R*B10*B10/V0
      WRITE(6,92)ETA,ETA0
C*****  CALCULATE VELOCITY CONTOURS
      WRITE(6,99)
      WRITE(6,49)((V(I,J),I=1,10),J=1,N)
      IF(M.GT.10)WRITE(6,40)((V(I,J),I=11,20),J=1,N)
      VSP=(V(1,1)*1.001)/8.
      CALL CONTOR(V,X,Y,VSP,10,M,N,H,RK,WK,IPLOT)
      IF(IPLOT.EQ.1)CALL PLOT(0.,8.5,-3)
C*****  CALCULATE CURRENT STREAM LINES
      IF(M.GT.10)WRITE(6,99)
      WRITE(6,48)((B(I,J),I=1,10),J=1,N)
```

```
      IF(M.GT.10)WRITE(6,40)((B(I,J),I=11,20),J=1,N)
      BSP=(1.-H)/(10*H*H+0.000001)
      CALL CONTOR(B,X,Y,BSP,10,M,N,H,RK,WK,IPLOT)
      IF(IPLOT.EQ.1)CALL PLOT(11.,-8.5,-3)
      GO TO 100
  999 CONTINUE
      CALL PLOT(0.,0.,999)
      STOP
   40 FORMAT(//5(2X,10E12.4/))
   41 FORMAT(//9X,I3,' ITERATIONS',5X,'TIME STEP E=',F6.4,5X,'RELAXTION
     1W=',F7.4,5X,'TEST=',E7.1,5X,'V=',E8.2,5X,'B=',E8.2)
   42 FORMAT(10X,'AVERAGE VELOCITY=',E12.4)
   43 FORMAT(/10X,'X GRID POSITIONS'/2(2X,10E12.4/))
   44 FORMAT(10X,'Y GRID POSITIONS',/5(2X,10E12.4/))
   47 FORMAT('1',4X,'HARTMANN NUMBER',F8.2,5X,'LOAD FACTOR',F6.3,5X,'ELE
     1CTRODE RESISTIVITY ',F6.3,5X,'ASPECT RATIO',F6.2,5X,'GRID',I3,'X',
     2I2)
   48 FORMAT(/10X,'B FIELD'/50(2X,10E12.4/))
   49 FORMAT(/10X,'VELOCITY FIELD'/50(2X,10E12.4/))
   88 FORMAT(//10X,'VARIABLE VISCOSCITY G=PARABOLA  ALPHA=',F6.2)
   89 FORMAT(//10X,'VARIABLE CONDUCTIVITY F=RECIPROCAL PARABOLA  ALPHA='
     1,F6.2)
   92 FORMAT(/10X,'EFFICIENCY=',F6.3/10X,'ONE DIMENSIONAL EFFICIENCY=',F
     16.3)
   95 FORMAT(/10X,'VISCOSITY RATIO AT NODES OUTSIDE BOUNDARY LAYER'/10(1
     1X,3(10F4.0,2X)/))
   96 FORMAT(/10X,'CONDUCTIVITY RATIO AT NODES OUTSIDE BOUNDARY LAYER'/1
     10(1X,3(10F4.0,2X)/))
   97 FORMAT(/10X,'CALCULATED B1=',E12.4,5X,'ACTUAL LOAD FACTOR=',F6.3,5
     1X,'ACTUAL RELATIVE RESISTANCE=',F7.3)
      END
```

```
      SUBROUTINE FFGG(M,N,X,Y,A,B)
C*****  THIS SUBROUTINE SETS THE CONDUCTIVITY AND VISCOSITY OF THE FLUID
      DIMENSION X(20),Y(50)
      COMMON /FG/F(20,50,3),G(20,50,3)
      DATA ICASE,PI/0,3.141592654/
      DO 1 I=1,M
      DO 1 J=1,N
      G(I,J,1)=1.-B*(1.-(X(I)/X(M))**2.)*(1.-Y(J)*Y(J))
      G(I,J,2)=B*2.*X(I)*(1.-Y(J)*Y(J))/X(M)
      G(I,J,3)=B*2.*Y(J)*(1.-(X(I)/X(M))**2.)
      F(I,J,1)=1./(1.-A*(1.-(X(I)/X(M))**2.)*(1.-Y(J)*Y(J)))
      F(I,J,2)=-F(I,J,1)*F(I,J,1)*2.*A*X(I)*(1.-Y(J)*Y(J))/X(M)
      F(I,J,3)=-F(I,J,1)*F(1,J,1)*2.*A*Y(J)*(1.-(X(I)/X(M))**2.)
    1 CONTINUE
      RETURN
      END
```

```
      SUBROUTINE CONTOR(B,X,Y,DD,NLL,M,N,H,RK,WK,IPLOT)
C*****  THIS SUBROUTINE FINDS, ORDERS AND PLOTS THE CONTOURS
      DIMENSION B(20,50),X(20),Y(50),XX(200),YY(200)
      DATA IP/0/
      IF(IPLOT.EQ.0)GO TO 58
C*****  DRAW AXIS AND LIST TITLE
      IF(IP.EQ.1)GO TO 56
      IP=1
      CALL SYMBOL(4.,-.75,0.25,'VELOCITY CONTOURS',0.,17,0.25,1)
      GO TO 57
   56 CALL SYMBOL(4.,-.75,0.25,'CURRENT STREAMLINES',0.,19,0.25,1)
      IP=0
   57 CALL SYMBOL(2.,-1.,0.1875,'M=      K=       K =     ',0.,22)
      CALL SYMBOL(5.,-1,1071,0.1313,'W',0.,1)
      CALL NUMBER(2.375,-1.,0.1875,H,0.,-1)
      CALL NUMBER(3.6875,-1.,0.1875,RK,0.,2)
      CALL NUMBER(5.375,-1.,0.1875,WK,0.,2)
      CALL AXIS(0.,0.,'CENTER OF CHANNEL',-17,8.,0.,0.,0.25)
      CALL AXIS(0.,0.,'CENTER OF ELECTRODES',20,4.,90.,0.,0.25)
      CALL AXIS(8.,0.,'ELECTRODE',-9,4.,90.,0.,0.25)
      CALL AXIS(0.,4.,'INSULATING WALL',15,8.,0.,0.,0.25)
   58 MM=M-1
      NM=N-1
      DX=(X(2)-X(1))*1.0001
      A=0.0
C*****  SELECT CONTOUR VALUE
      DO 51 LL=1,NLL
      A=A+DD
      K=0
C*****  INTERPOLATE TO FIND CONTOUR LOCATIONS (XX,YY)
      DO 52 I=1,M
      DO 52 J=1,NM
      IF(.NOT.(A.LE.B(I,J+1).AND.A.GT.B(I,J).OR.A.GE.B(I,J+1).AND.A.LT.B
     1(I,J)))GO TO 52
      K=K+1
      XX(K)=X(I)
      YY(K)=Y(J)+(Y(J+1)-Y(J))*(A-B(I,J))/(B(I,J+1)-B(I,J))
      IF(K.EQ.100)GO TO 55
   52 CONTINUE
      DO 53 I=1,MM
      DO 53 J=1,NM
      IF(.NOT.(A.LE.B(I+1,J).AND.A.GT.B(I,J).OR.A.GE.B(I+1,J).AND.A.LT.B
     1(I,J)))GO TO 53
      K=K+1
```

```
      XX(K)=X(I)+(X(I+1)-X(I))*(A-B(I,J))/(B(I+1,J)-B(I,J))
      YY(K)=Y(J)
      IF(K.EQ.100)GO TO 55
   53 CONTINUE
      IF(K.EQ.0)GO TO 51
   55 IF(K.EQ.100)WRITE(6,97)
C*****  ORDER CONTOUR LOCATIONS IN LINE (XX,YY)
      KM=K-1
      DO 54 L=2,KM
      LP=L+1
      DO 54 I=LP,K
      IF(ABS(XX(L)-XX(L-1)).GT.DX)GO TO 50
      IF(ABS(XX(I)-XX(L-1)).GT.DX)GO TO 54
      IF(ABS(YY(I)-YY(L-1)).GE.ABS(YY(L)-YY(L-1)))GO TO 54
   50 CONTINUE
      XS=XX(I)
      YS=YY(I)
      XX(I)=XX(L)
      YY(I)=YY(L)
      XX(L)=XS
      YY(L)=YS
   54 CONTINUE
      WRITE(6,99)A,(XX(I),I=1,K)
      WRITE(6,98)(YY(I),I=1,K)
C*****  PLOT CONTOUR
      IF(IPLOT.EQ.0)GO TO 51
      XX(K+1)=0.0
      YY(K+1)=0.0
      XX(K+2)=0.25
      YY(K+2)=0.25
      CALL LINE(XX,YY,K,1,0,0)
   51 CONTINUE
      RETURN
   97 FORMAT(10X,'CONTOUR POINTS EXCEEDED 100 ABOVE')
   98 FORMAT(4(2X,25F5.2/))
   99 FORMAT(10X,'CONTOUR VALUE=',E12.4/4(2X,25F5.2/))
      END
```

BIBLIOGRAPHY

Branover, H. and Gershon, P., 1976a, An Experimental MHD-facility for the Investigation of Some Important Features of Turbulence Suppression, Proceedings of the Bat-Sheva Seminar on MHD-Flows and Turbulence, J. Wiley-Keter, Jerusalem.

Branover, H. and Gershon, P., 1976b, MHD Turbulence Study Part II, Ben-Gurion University of the Negev, Beer Sheva, Israel, Dept. of Mechanical Engineering, Report ME 6-76.

Branover, H., Gershon, P. and Yakhot, A., 1977, MHD Turbulence and Two Phase Flow, Ben-Gurion University of the Negev, Beer Sheva, Israel, Dept. of Mechaincal Engineering, Report ME 5-77.

Chang, C. C. and Lundgren, T. S., 1961, Duct Flow Magnetohydrodynamics, Z. Angew. Math. Phys., 12, 100-114.

Chiang, D. and Lundgren, T. S., 1967, Magnetohydrodynamic Flow in a Rectangular Duct with Perfectly Conducting Electrodes, Z. Angew. Math. Phys., 18, 92-105.

Douglas, J., 1962, Alternating Direction Methods for Three Space Variables, Numer. Math., 4, 41-63.

Einstein, A., 1906, Eine neue Bestimmung der Molekül dimensionen, Ann. Physics, 19, 289-306.

Elkins, R. E., Lindgren, E. R., Trovillion, T. A. and Kurzweg, U. H., 1978, Two Phase Magnetohydrodynamic Channel Flow, The Second Bat-Sheva Seminar on MHD-Flows and Turbulence, Ben-Gurion University of the Negev.

Elliott, D. G., 1962, Two Fluid Magnetohydrodynamic Cycle for Nuclear-Electric Power Conversion, ARS J., 32, 924.

Faraday, M., 1832, Bakerian Lecture Series, Philosophical Transactions of the Royal Society of London, 15, 125-128.

Hamming, R. W., 1973, Numerical Methods for Scientists and Engineers, McGraw-Hill, New York.

Hantman, R. G., Cole, R. L., Fabris, G. and Cutting, J.C., 1975, Peformance of a Constant Velocity Variable-Area Two-Phase Liquid-Metal MHD Generator, Sixth International Conference on MHD Power Generation, Paris.

Hartmann, J., 1937, Hg-Dynamics I, Math.-fys. Medd., 15, 6.

Hartmann, J., and Lazarus, F., 1937, Hg-Dynamics II, Math.-fys. Medd., 15, 7.

Hua, H. M. and Lykoudis, P. S., 1974, Turbulence Measurements in a Magneto-Fluid-Mechanic Channel, Nuclear Science and Engineering, 54, 445.

Hughes, W. F. and Young, F. J., 1966, The Electromagnetodynamics of Fluids, John Wiley and Sons, New York.

Hunt, J. C. R., 1965, Magnetohydrodynamic Flow in Rectangular Ducts, J. Fluid Mech., 21, 577-590.

Jackson, W. D., 1963, Liquid-Metal Faraday-Type MHD Generators, IEEE Trans. Power Apparatus and Systems, 82, 904-907.

Lafferty, J. F. and Hammitt, F. F., 1967, Nucl. Appl., 3, 5, 317-323.

Maxwell, J. C., 1904, A Treatise on Electricity and Magnetism, Oxford University Press, 435-441.

McAdams, W. H., Woods, W. K. and Heroman, L. C., 1942, Vaporisation inside Horizontal Tubes II. Benzene-Oil Mixtures, Trans. ASME, 64, 193.

Mitchell, A. R., 1969, Computational Methods in Partial Differential Equations, John Wiley and Sons, London.

Mitchell, A. R. and Fairweather, G., 1964, Improved Forms of the Alternating Direction Methods of Douglas, Peaceman and Rachford for Solving Parabolic and Elliptic Equations, Numer. Math., 6, 285-292.

Murgatroyd, W., 1953, Experiments on Magneto-Hydrodynamic Channel Flow, Phil. Mag., 44, 1348-1354.

Peaceman, D. W., and Rachford, H. H., 1955, The Numerical Solution of Parabolic and Elliptic Differential Equations, J. Soc. Indust. App. Math., 3, 28-41.

Petrick, M., 1965, Liquid Metal Magnetohydrodynamics, IEEE Spectrum, 2, 137-151.

Petrick, M., Fabris, G., Pierson, E. S., Carl, D. A., Fischer, A. K. and Johnson, C. E., 1977, Experimental Two-Phase Liquid-Metal Magnetohydrodynamic Generator Program, Argonne National Laboratory, Engin. Division Report, ANL/MHD-77-3.

Petrick, M. and Lee, K. Y., 1964a, Performance Characteristics of a Liquid Metal MHD Generator, Argonne National Laboratory, ANL-6870.

Petrick, M. and Lee, K. Y., 1964b, Proc. Second Int. Symp. MHD Elect. Power Gen., Paris.

Petrick, M. and Roberts, J. J., 1967, Performance of Space-Power Liquid Metal MHD Cycles Utilizing a Two-Phase Flow Generator, J. Spacecraft and Rockets, 4, 8, 967-973.

Prem, L. L. and Parkins, W. E., 1964, A New Method of MHD Power Conversion Employing a Fluid Metal, International Symposium on MHD Elect. Power Gen., Paris.

Shercliff, J. A., 1953, Steady Motion of Conducting Fluids in Pipes under Transverse Magnetic Fields, Proc. Cambridge Phil. Soc., 49, 136-144.

Shercliff, J. A., 1956, The Flow of Conducting Fluids in Circular Pipes under Transverse Magnetic Fields, J. Fluid Mech., 1, 644-665.

Sutton, G. W., Hurwitz, H. and Poritsky, H., 1962, Electrical and Pressure Losses in a Magnetohydrodynamic Channel Due to End Current Loops, IEEE Trans. on Communications, 80, 687-695.

Tanatugu, N., Fujii-E, Y. and Suita, T., 1971, Decrease in Power Density Due to Finite Electrode Conductivity in LM-MHD Generator, J. Nuclear Sci. and Tech., 8, 10, 588-596.

Tanatugu, N., Fujii-E, Y. and Suita, T., 1972, Electrical Conductivity of Liquid Metal Two-Phase Mixture in Bubbly and Slug Flow Regime, J. Nuclear Sci. and Tech., 9, 12, 753-755.

Tanatugu, N., Fujii-E., Y. and Suita, T., 1973, Frictional Pressure Drop for NaK-N_2 Two-Phase Flow in Rectangular Cross Section Channel of Large Aspect Ratio, J. Nuclear Sci. and Tech., 10, 4, 219-226.

Taylor, G. I., 1932, Viscosity of a Fluid Containing Small Drops of Another Fluid, Proc. Roy. Soc., A138, 41-48.

Trovillion, T. A., Kurzweg, U. H., Elkins, R. E., and Lindgren, E. R., 1978, Hydromagnetic Channel Flows of Fluids with Cross Stream Dependent Electrical Conductivity, The Second Bat-Sheva Seminar on MHD-Flows and Turbulence, Ben-Gurion University of the Negev.

Uflyand, Y. S., 1961, Flow Stability of a Conducting Fluid in a Rectangular Channel in a Transverse Magnetic Field, Sov. Phys.-Tech. Phys., 5, 1194.

Varga, R. S., 1962, Matrix Iterative Analysis, Prentice-Hall, Englewood Cliffs, New Jersey.

Wachspress, E. L., 1957, A Generalized Two-Space Dimension Multigroup Coding for the IBM 704, General Electric Co., CURE Report KAPL-1724.

Wachspress, E. L., 1966, Iterative Solution of Elliptic Systems, Prentice-Hall, Englewood Cliffs, New Jersey.

Wallis, G. B., 1969, One-Dimension Two-Phase Flow, McGraw-Hill, New York.

Wissmiller, J. C., 1964, Velocity Profiles for Magnetohydrodynamic Flow in Rectangular Ducts, M.S. Thesis, Dept. Electrical Eng., M.I.T.

BIOGRAPHICAL SKETCH

Thomas A. Trovillion, Jr. was born May 10, 1949, in Winter Park, Florida, and grew up in the Orlando area. Graduating from Winter Park High School in 1967 he entered the University of Florida, where he received the degrees of Bachelor of Science in Aerospace Engineering in August 1971 and Master of Science in December 1972. His Master's thesis was entitled "Experimental Investigation of the Velocity Field of a Jet in a Crossflow." While at the university he enrolled in the Air Force Reserve Officer Training Corps, and received a commission as a Second Lieutenant in the United States Air Force on March 18, 1972. After graduation he spent three months on active duty at Eglin AFB, Florida. On completion of his active duty he went to work for the Pratt and Whitney Aircraft Research and Development Center in West Palm Beach, Florida, where he was employed as an analytical design engineer working on combustor development for jet engines. He returned to the University of Florida to work toward receiving the degree of Doctor of Philosophy.

I certify that I have read this study and that in my opinion it conforms to acceptable standards of scholarly presentation and is fully adequate, in scope and quality, as a dissertation for the degree of Doctor of Philosophy.

U. H. Kurzweg

Ulrich H. Kurzweg, Chairman
Professor of Engineering Sciences

I certify that I have read this study and that in my opinion it conforms to acceptable standards of scholarly presentation and is fully adequate, in scope and quality, as a dissertation for the degree of Doctor of Philosophy.

E. Rune Lindgren
Professor of Engineering Sciences

I certify that I have read this study and that in my opinion it conforms to acceptable standards of scholarly presentation and is fully adequate, in scope and quality, as a dissertation for the degree of Doctor of Philosophy.

Martin A. Eisenberg
Professor of Engineering Sciences

I certify that I have read this study and that in my opinion it conforms to acceptable standards of scholarly presentation and is fully adequate, in scope and quality, as a dissertation for the degree of Doctor of Philosophy.

Bernard M. Leadon, Jr.
Professor of Engineering Sciences

I certify that I have read this study and that in my opinion it conforms to acceptable standards of scholarly presentation and is fully adequate, in scope and quality, as a dissertation for the degree of Doctor of Philosophy.

Charles P. Luehr
Associate Professor of Mathematics

This dissertation was submitted to the Graduate Faculty of the College of Engineering and to the Graduate Council, and was accepted as partial fulfillment of the requirements for the degree of Doctor of Philosophy.

June 1978

Hubert A. Lewis
Dean, College of Engineering

Dean, Graduate School

UNIVERSITY OF FLORIDA
3 1262 08553 2835